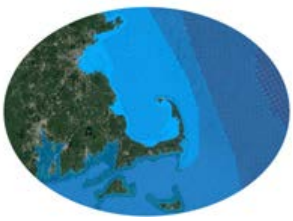

Simulations of 2021 Hydrodynamics and Water Quality in the Massachusetts Bay System using the Bays Eutrophication Model

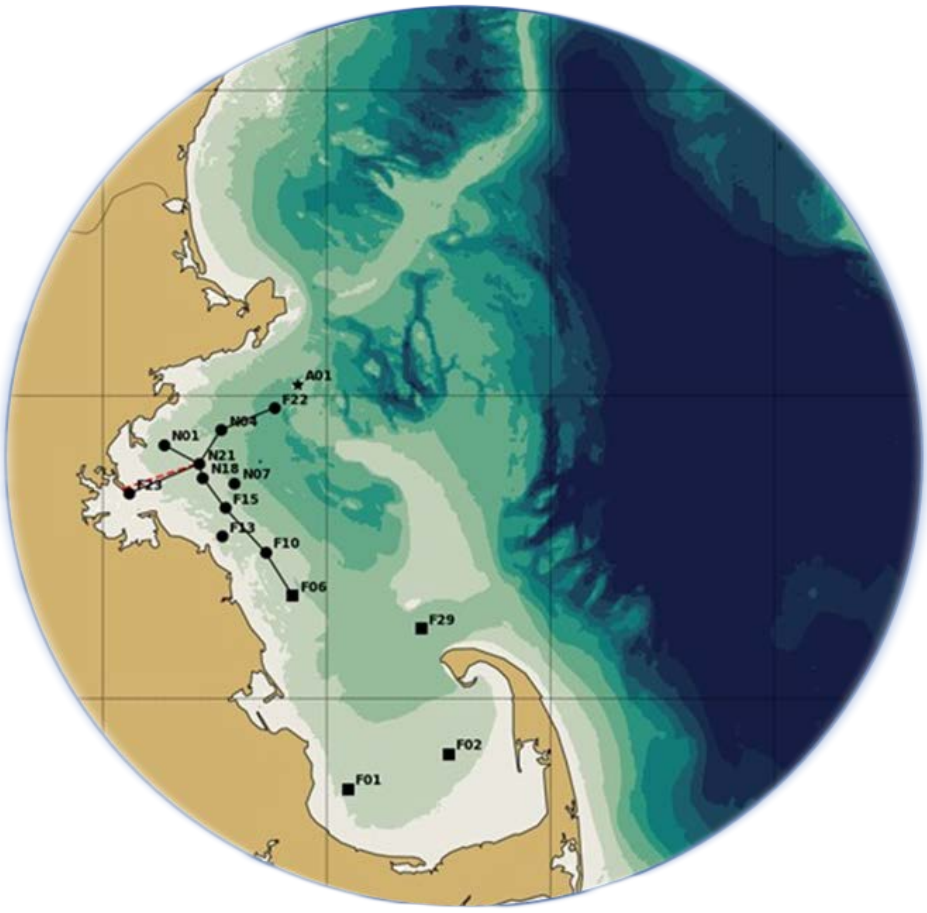

Massachusetts Water Resources Authority
Environmental Quality Department
Report 2023-07

Citation:

Deltares, 2023**. Simulations of 2021 Hydrodynamics and Water Quality in the Massachusetts Bay System using the Bays Eutrophication Model.** Boston: Massachusetts Water Resources Authority. Report 2023-07. 83 p.

MWRA Environmental Quality Department reports can be downloaded from http://www.mwra.com/harbor/enquad/trlist.html.

Deltares USA

Simulations of 2021 Hydrodynamics and Water Quality in the Massachusetts Bay System using the Bays Eutrophication Model

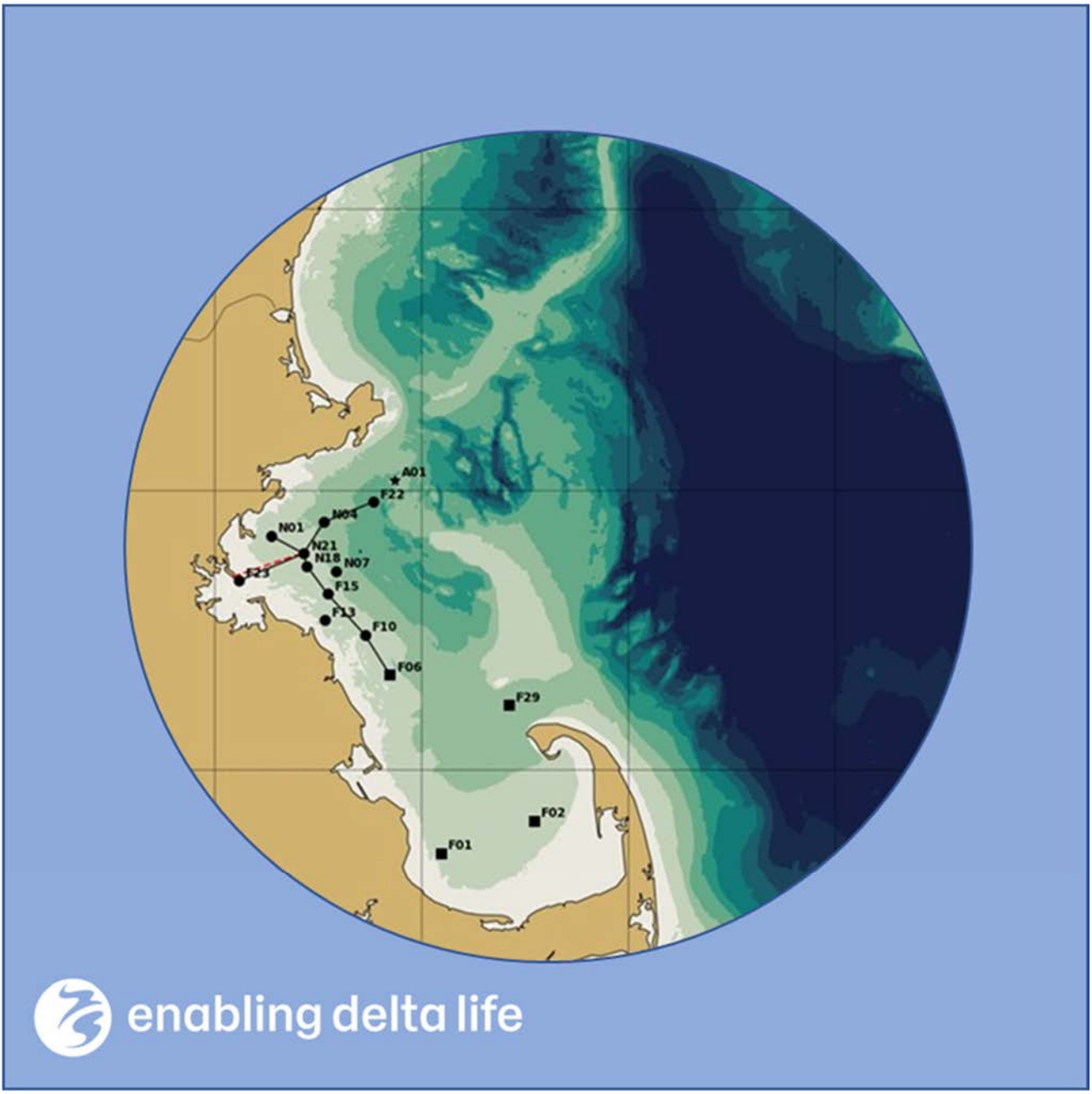

Simulations of 2021 Hydrodynamics and Water Quality in the Massachusetts Bay System using the Bays Eutrophication Model

Author(s)
Binglei Gong[1]
Benjamin Munster[1]
Lauriane Vilmin[2]
Stendert Laan[2]
Pradeep Mugunthan[1]

Partners
[1] Four Peaks Environmental and Data Solutions, AMHERST MA 01002, United States of America
[2] Deltares, Delft, The Netherlands

Simulations of 2021 Hydrodynamics and Water Quality in the Massachusetts Bay System using the Bays Eutrophication Model

Client	MA Water Resources Authority - Massachusetts Water Resources Authority
Contact	Mr Wu
Reference	
Keywords	updated BEM, 2021 simulations, hydrodynamics, water quality

Document control	
Version	1.2
Date	July 18, 2023
Project nr.	2243
Document ID	DNL 11208511-002-ZKS-0001
Pages	82
Status	final

Doc. version	Author	Reviewer	Approver
1.2	Binglei Gong[1] Benjamin Munster[1] Stendert Laan[2] Lauriane Vilmin[2] Pradeep Mugunthan[1]	Jos van Gils[2]	Toon Segeren[2] Edwin Welles

Partners

[1] Four Peaks Environmental and Data Solutions, AMHERST MA 01002, United States of America
[2] Deltares, Delft, The Netherlands

Deltares, 2023. Simulations of 2021 Hydrodynamics and Water Quality in the Massachusetts Bay System using the Bays Eutrophication Model, Deltares Ref. Nr. 11208511-002-ZKS-0001

Cover image: MWRA observation locations in Massachusetts Bay

Summary

This report presents hydrodynamic and water quality model results for the Massachusetts Bays system (Massachusetts Bay, Cape Cod Bay, and Boston Harbor) during 2021. Treated effluent sent from the Massachusetts Water Resources Authority (MWRA) treatment plant through a 15 km (9.5 mi) long tunnel and released at an outfall offshore in Massachusetts Bay contains nutrients. Nutrients are necessary and important to support healthy and diverse marine ecosystems. However, excess nutrients can cause eutrophication, the overgrowth of phytoplankton (microscopic marine algae) which degrades water quality and can harm marine life by depleting oxygen when it decays. To address potential eutrophication and other concerns, MWRA maintains an extensive bay and harbor field monitoring program, which this modelling complements.

The hydrodynamic model simulates temperature, salinity, and currents, and is the foundation for the water quality model, which simulates key eutrophication parameters including nutrients, chlorophyll a (a measure of phytoplankton), and oxygen. Deltares (2021) explains the methods. Hydrodynamic results for 2021 agree well with available observations and capture the geographic and vertical structure, and temporal variability, of temperature and salinity distributions and density stratification, as well as tidal and non-tidal currents. As in observations, stratification in the 2021 simulation peaked in July and August, corresponding with record-high summer river flows. River flow in 2021 was lower than normal during winter and spring, but July, August, and September saw the highest flows of the 30-year monitoring program. Owing to this higher than typical summer river flow, observed and modeled salinity at the water surface was low.

The 2021 water quality simulation captured general patterns in observed seasonal variations, geographic distributions, and vertical structure for many variables. This included the late spring reduction in near-surface dissolved inorganic nitrogen (DIN) due to phytoplankton uptake, and its replenishment after mixing in fall due to cooling and storms. It also included seasonal dissolved oxygen variations, with peak values in spring at shallow depths due to colder water and phytoplankton growth, and late summer minima at depth where stratification inhibits reaeration by air-sea exchange. Modeled dissolved oxygen levels at the seafloor dropped to low levels at the end of the summer and beginning of fall, similar to observations, which were low from February to June with historic minima at many stations by May. Observations suggested there was a spring *Phaeocystis* bloom and in the model *Phaeocystis* appeared during this period; a summer dinoflagellate (*A. catenella*) bloom was observed in 2021 and was similarly predicted by the model; however, the model predicted chlorophyll a levels were lower than observed. In addition to those more bay-wide patterns, in the model as in observations, DIN was elevated persistently within about 10 km (6 mi) of the outfall and intermittently as far as about 20 km (12 mi) away, mainly due to nitrogen from ammonium in the treated effluent. The model captured the observed vertical structure of this effluent influence, which reached the surface through the winter months and remained at depth from about May through October when the bay was stratified. Consistent with field observations, the model did not show indications of eutrophication as evidenced by the relatively low chlorophyll a levels. The outfall did not appear to be influencing nearshore chlorophyll a or dissolved oxygen. Overall, the 2021 simulation supports the conclusions from field monitoring, that eutrophication was not a concern.

Contents

List of Figures

1 Introduction

The Massachusetts Water Resources Authority (MWRA) has established a long-term monitoring program to evaluate the impact of its sewage treatment plant effluent on the water quality and ecosystem function of Massachusetts Bay, Cape Cod Bay, and Boston Harbor. The monitoring program primarily consists of a series of ongoing field observation surveys and includes complementary water quality modeling as required by the discharge permit (No. MA0103284). The water quality simulations are carried out using the Bays Eutrophication Model (BEM, Deltares, 2021). This report presents simulation results for the 2021 calendar year.

1.1 Background on oceanographic processes influencing water quality

Massachusetts Bay and Cape Cod Bay (Figure 1-1) comprise a temperate coastal embayment system. Readers unfamiliar with the geography and/or the current understanding of the physical and biological oceanographic processes characterizing the system are referred to the introductory summaries found in sections 1.2 and 1.3 of MWRA Technical Report 2011-13 (Zhao et al., 2012), in the annual MWRA water column monitoring reports (e.g., for calendar year 2021, Libby et al., 2022), and in references cited by them. (All MWRA Technical Reports, including those just cited, are available online at http://www.mwra.state.ma.us/harbor/enquad/trlist.html.) A brief summary follows here. In this subsection the focus is on processes and influences other than effluent from the MWRA outfall, which has been shown in past studies to have a minor system-wide effect.

System hydrodynamics are characterized by a persistent general circulation pattern driving the flow of offshore Gulf of Maine waters into Massachusetts Bay via the Western Maine Coastal Current off Cape Ann, then southward before returning offshore just to the north of Cape Cod, with a portion of the flow first passing through Cape Cod Bay to the south (Figure 1-1). Rough estimates of the water residence time are about a month based on the surface currents, somewhat longer at mid-depth or deeper, where currents are weaker, and also longer in Cape Cod Bay than in Massachusetts Bay. While this slow general circulation is important in determining long-term average transport pathways, superposed on it are stronger and more variable wind-driven currents, and oscillatory tidal motions. Temperatures follow the characteristic temperate seasonal pattern of minima in late winter and peaks in late summer. Salinities are freshest inshore and in the upper several meters; in addition to the influence of offshore oceanographic conditions, they vary mainly in response to riverine inputs including primarily those brought by the Western Maine Coastal Current and the Merrimack River outflow to the north, and to a lesser extent the smaller amounts delivered via Boston Harbor. There is a seasonal cycle in vertical structure that includes transitions between well-mixed conditions, present from fall through early spring due to higher winds and atmospheric cooling, and strong density stratification during the late spring and summer due mainly to increased surface temperatures resulting from atmospheric heating.

The biology of the system is plankton-based and exhibits clear seasonal cycles that are tied closely to those hydrodynamic features, but with more pronounced spatial and interannual variability. Phytoplankton abundance typically peaks most strongly during bloom-favorable conditions in the late winter and early spring, as temperatures rise, light increases, and nutrients remain plentiful near the surface due to the active vertical mixing. Following the transition from spring to summer, near-surface nutrient concentrations become depleted as density stratification impedes the vertical mixing that replenishes them. Zooplankton abundance and biomass generally peak in late summer, following the

spring increase in phytoplankton prey levels. Primary productivity is commonly sustained at modest levels through summer and typically there is a second increase in phytoplankton during fall, when vertical mixing increases again and delivers nutrients to the surface while temperature and light conditions are still favorable before winter. Dissolved oxygen (DO) concentrations are influenced by a combination of biological and physical processes; the net result is a seasonal peak in late spring, due to phytoplankton production increasing winter levels already high due to strong reaeration, then steady decreases to a late summer minimum due to respiration and reduced reaeration. The summer oxygen minimum is lower at depth, where stratification limits reaeration.

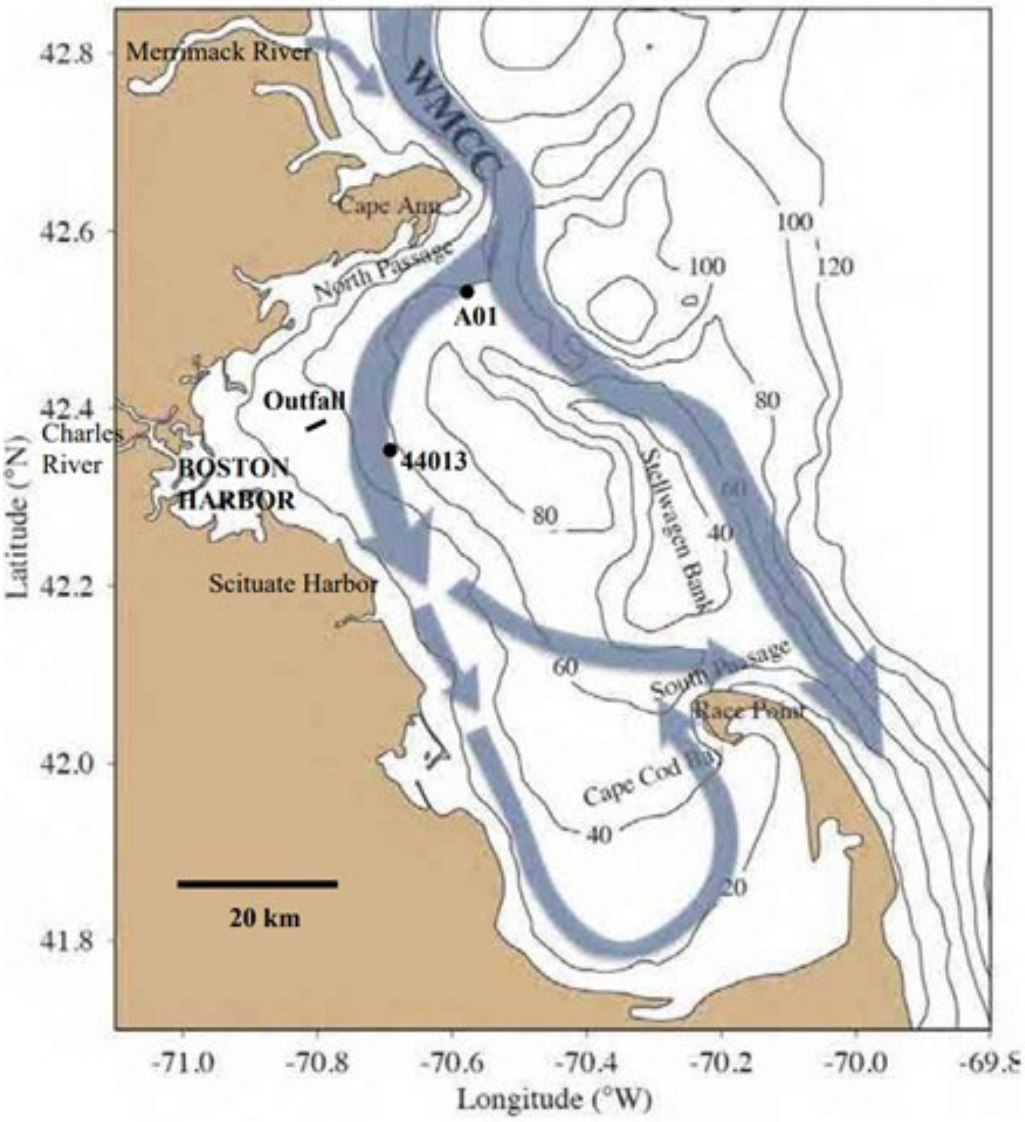

Figure 1-1 Geography, bathymetry, schematic long-term mean circulation.

WMCC = Western Maine Coastal Current. A01 = Oceanographic mooring (Northeastern Regional Association of Coastal and Ocean Observing Systems). 44013 = Weather buoy (National Data Buoy Center). Contours = water depth in meters. Figure from Zhao et al. (2017), adapted from Xue et al. (2014).

1.2 Summary of observed 2021 conditions

To provide context for descriptions of model simulations of 2021 throughout this report, a brief summary of 2021 observations (Libby et al., 2022) is provided here. From February through May, monitoring was disrupted and fewer measurements were collected than usual due to the COVID pandemic. River flow in 2021 was lower than normal during winter and spring, but July, August, and September saw the highest flows of the 30-year monitoring program and caused unusually low surface salinities and unusually high stratification. Both surface and deep water temperatures were unusually warm. Total phytoplankton abundances were lower than typical, mainly due to low abundances of centric diatoms, *Phaeocystis*, and the usually numerically dominant microflagellates. Dinoflagellates, mainly *Karenia mikimotoi,* are the only phytoplankton functional group that appears to be increasing in recent years. Chlorophyll concentrations were generally lower than typically observed but increased during the March and July surveys in Massachusetts Bay and the February, April, June, August, and September surveys in Cape Cod Bay. Winter/spring diatom and *Phaeocystis* blooms were inferred from indirect information including mooring measurements of fluorescence, changes in nutrient concentrations, and satellite images of ocean color. A large *Alexandrium catenella* bloom occurred in late June and July. Bottom water DO concentrations were low, and below historic minima, at many stations by May. Wind-driven mixing events in late May through July contributed to downwelling favorable conditions that kept the normal seasonal decrease in bottom water DO concentrations in June and July less severe than would otherwise have occurred. Nonetheless, the strong stratification in late July and August contributed to a sharp decrease in bottom water DO concentrations in late summer, to low values bay-wide, and the lowest in the 30-year monitoring period at the Stellwagen Basin station.

2 Methods

A complete model description is documented in MWRA's technical report 2021-02 and its appendices (Deltares, 2021). The model is set up in the Delft3D Flexible Mesh Suite, developed by Deltares. Technical details on the model set-up, its grid and forcing is presented in Appendix A of Deltares (2021). A description of the software package and underlying hydrodynamic and water quality equations are available in Section A1 of Deltares (2021), and in Deltares (2019a, b). The model was calibrated using the years 2012-2016, as described in Appendix B of Deltares (2021). The results of the model validation are given in the main report body of Deltares (2021).

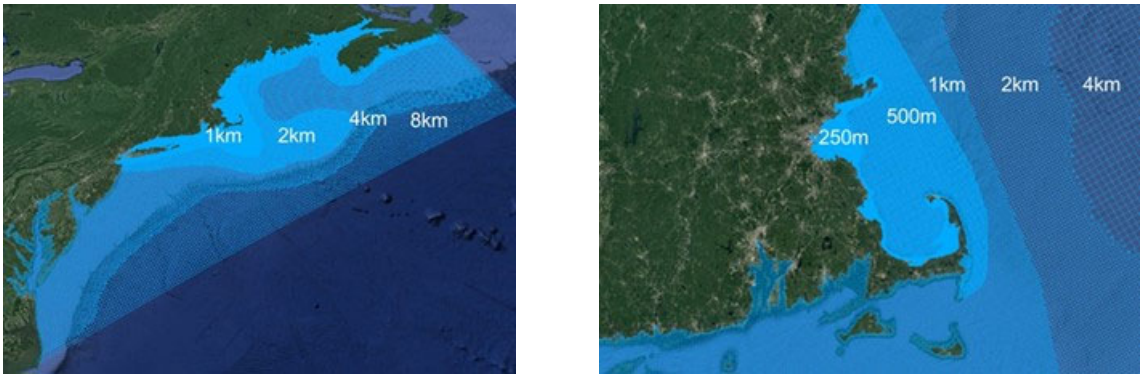

Figure 2-1 Model grid of the entire model domain (left) and zoomed-in for Massachusetts Bay (right)

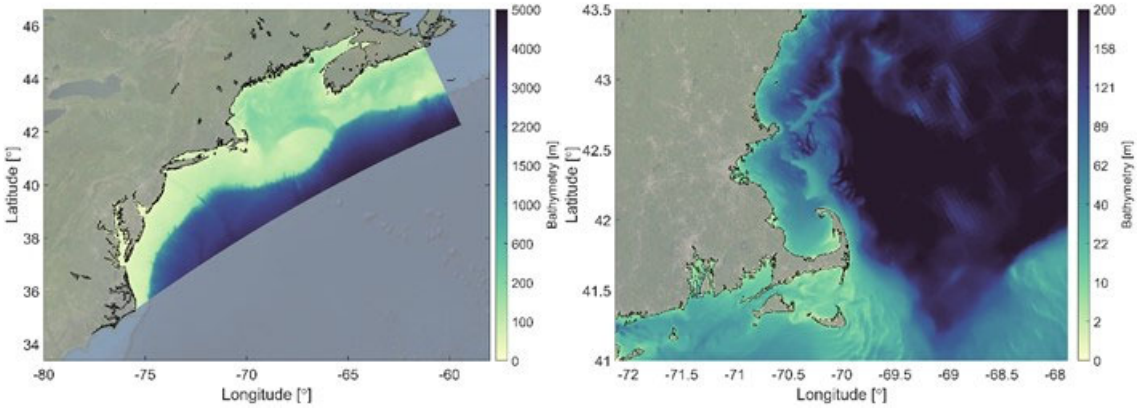

Figure 2-2 Model bathymetry of the entire model domain (left) and zoomed-in for Massachusetts Bay (right)

The model domain is large in order to best handle influences of offshore boundaries, as explained in Deltares (2021); it covers the entire Gulf of Maine region as well as the coastal region to the south, down to and including Chesapeake Bay (Figure 2-1 and Figure 2-2). Model performance in comparison to field measurements has been demonstrated most carefully in the area of Massachusetts Bay nearest the outfall, using MWRA observations (Deltares, 2021). The horizontal resolution is roughly 8 km at the open ocean and is gradually refined toward the coast, with a maximum resolution of 250 m in Boston Harbor and along the surrounding coastline, including at the outfall location.

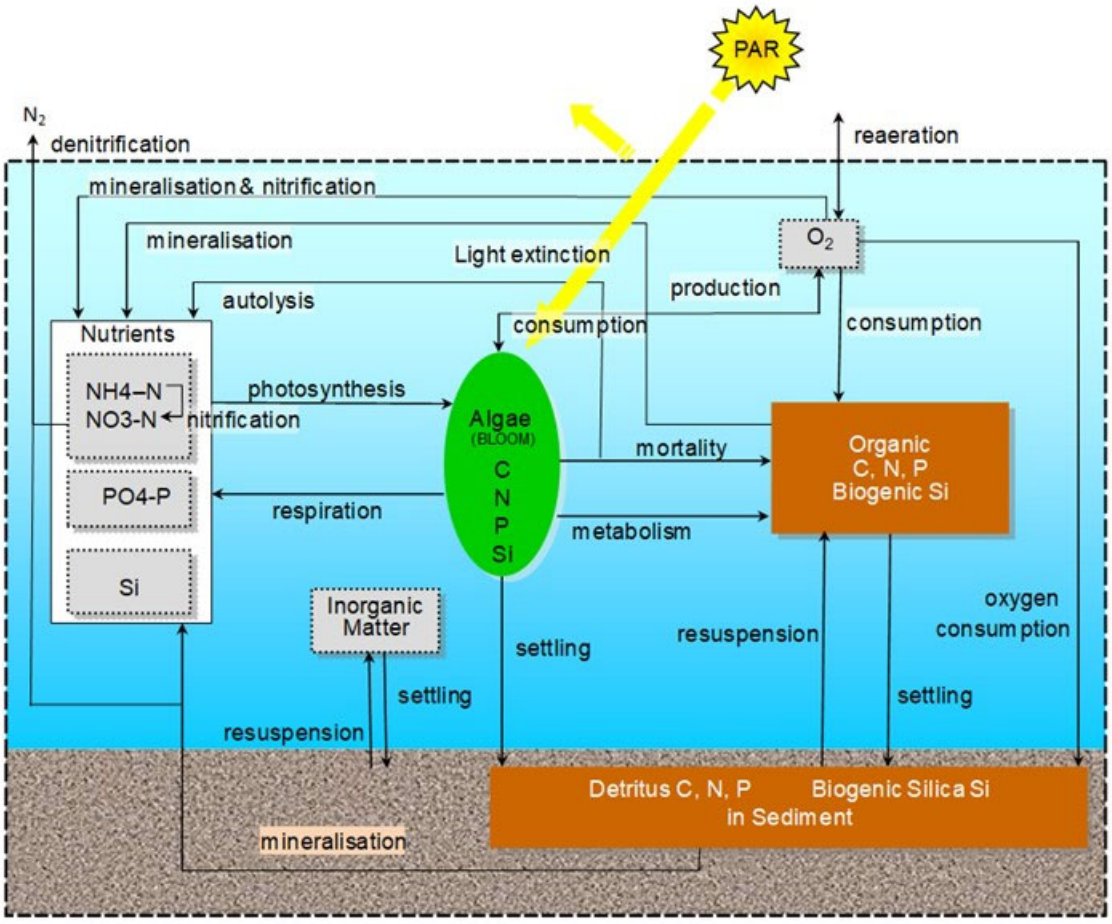

Figure 2-3 Schematic overview of all state variables and processes. Reproduced from Deltares (2021). Note that Inorganic Matter, Algae and Detritus affect light extinction in the water column.

Figure 2-3 provides an overview of the simulated state variables and processes for the water quality component. Four functional groups of pelagic phytoplankton are simulated ("Algae" in the figure): diatoms, dinoflagellates, other flagellates, and *Phaeocystis*.

The monitoring stations used to assess model performance and the transects along which water quality variables are examined are mapped in Figure 2-4. Model-observation comparison time-series are plotted for a representative selection of eight stations: N01 in the Northern Mass Bay, F22 with a greater oceanic influence, F23 near the outlet of Boston Harbor, N18 close to the MWRA outfall, N07 southeast of the outfall, F13 and F06 toward the south shore, and F02 in Cape Cod Bay.

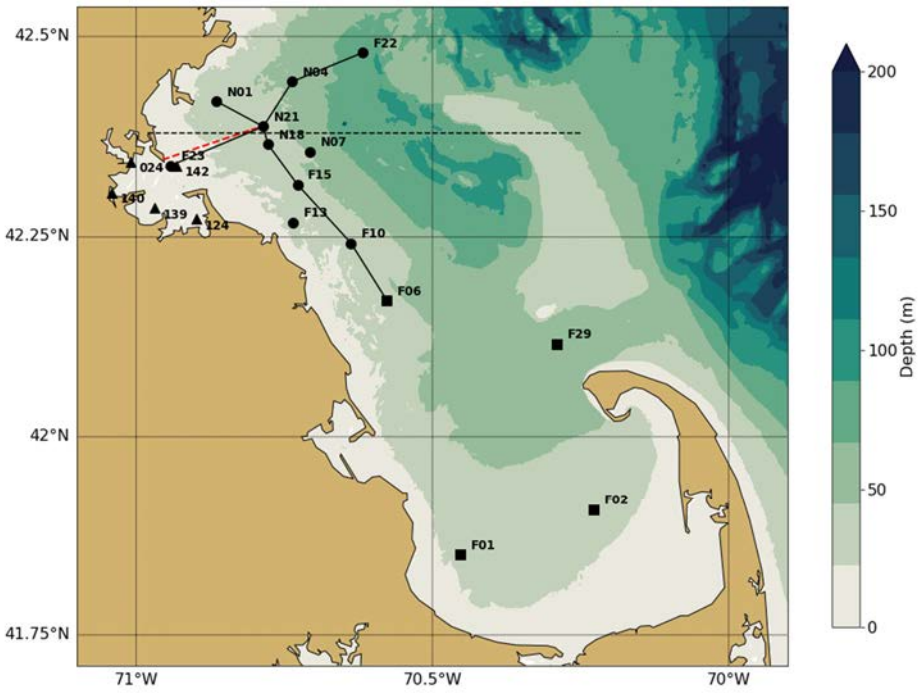

Figure 2-4 Location of MWRA monitoring locations (circles=Northern stations, squares=Southern stations, triangles=Harbor stations). The red dashed line indicates the tunnel to the outfall diffusers. The black lines are the West-East and North-South transects used for model-observation comparisons. The horizontal black dashed line represents the transect through the outfall on which model results are presented in later figures.

2.1 Updated methods

In the 2021 BEM run, no changes to the methods as used for the 2020 BEM run (Deltares, 2022b) were implemented.

3 Forcing

3.1 Wind, heat flux, solar radiation and rivers

3.1.1 Wind

In Figure 3-1, the main characteristics of the monthly-mean wind forcing for the simulated year 2021 are compared to the means of the previous 20 years (2000-2020) for the A01 mooring location off Cape Ann (Figure 1-1). Ranges of the standard deviation and of the minimum and maximum values are also shown.

The seasonal pattern of the vector-averaged velocities (top frame) largely followed the long-term mean. Notable differences were visible in the months of January, February, April, May, and September. In January and February, winds were directed further towards the south rather than the long-term average direction of south-east. In both April and May winds were directed more eastward compared to long-term average direction of north-northeast. In September, the winds were largely oriented north-east, which is a nearly 180 degree reversal from the usual south-west winds during that time of the year.

Wind speeds (second frame) were lower than the long-term mean in January, April, August, and December. In February, July, September, and November, the wind speeds were higher than the long-term mean. Monthly-mean wind stress magnitudes (third frame) show a similar pattern. The mean wind stresses were weaker than the long-term average in January, March, April, August, and December, with the December wind stress comparable to the 20-year minimum. North-south wind stresses (bottom frame) are an indicator for upwelling. North-south wind stress was weaker than normal in February and September, which is in agreement with 2021 observations of weaker summer upwelling than typical.

3.1.2 Heat flux

A comparison between time series of the calculated net air-sea heat flux (including solar radiation) for 2021 and for the previous years is given in Figure 3-2. A moving average with a window of 3 days is applied to visualize the instantaneous values. A positive net flux value indicates the net heat exchange is from air to sea, and vice versa. The time series of the net flux includes ranges of the standard deviation from the mean and of the minimum and maximum values. The cumulative flux (middle frame) is presented without any filtering.

The seasonal pattern in 2021 (top frame) showed an overall negative heat flux in winter (loss of heat from the surface, cooling of the ocean) and an overall positive heat flux in summer (heating of the ocean). The 2021 net flux was generally comparable to the long-term patterns and within one standard deviation of the long-term mean for most of the year except for portions of late spring, mid-summer, and short periods in February and December.

The cumulative flux (middle frame) in 2021 was slightly higher than the long-term mean throughout the year. At the end of 2021, the cumulative flux has a similar value as the long-term mean. The same pattern was visible in the cumulative anomaly of the heat flux (bottom frame).

3.1.3 Solar radiation

The solar radiation from the meteorological forcing product is given in Figure 3-3. The solar radiation was similar to the long-term mean in most months. However, it fell below average in February, causing a brief decrease in the cumulative flux, and was above average in March and May, causing an increase in the cumulative flux, which remained at about +0.05 GJ m^{-2} until the end of the year. So, on an annual-mean basis, 2021 had slightly more incident surface solar radiation than a typical year.

The slightly higher than average net surface heat flux in 2021 was consistent with the slightly higher than average incident radiation in 2021. Every year there is a net influx of solar radiation of about 5.5 GJ m^{-2}. Since the net air-surface heat flux was about 0.5 GJ m^{-2} in 2021, around 5.0 GJ m^{-2} was lost through other air-sea heat fluxes. These fluxes consist of evaporative and convective turbulent fluxes or long wave radiation.

3.1.4 Rivers

In Figure 3-4 the volume transport for Merrimack River is presented. The figures include the daily-averaged discharges (top frame) for the simulated year 2021 and for the previous 20 years (2000-2020). Ranges of the standard deviation and of the minimum and maximum values are also given.

The discharge in the Merrimack River was mostly lower than the long-term mean in the first 6 months of the year. After that, it was mostly higher than average with runoff events in July, August, and November, including summer events that exceeded the long-term maximum flows. This was visible in the total discharged volume (middle frame), which was lower than the long-term mean from February to the end of year. The deviation (from the long-term mean) gradually reduced starting in July due to the discharge events. The largest anomaly of the discharged volume (bottom frame) in 2021 was negative with a value of about -2.0 km^3 in early July and returned closer to the long-term mean by the end of the year with a negative anomaly of about -0.4 km^3, due to the high flow events in summer.

The combined volume transport for the rivers discharging directly to Massachusetts Bay and Cape Cod Bay is presented in Figure 3-5. These rivers are Saugus, Mystic, Charles, Neponset, North, and Jones. The pattern of the combined discharge was similar to the pattern of discharge of the Merrimack River. The discharged volume was lower than the long-term mean until July with multiple events from July to November. This resulted in a positive anomaly of the discharged volume (bottom frame) of 1.4 km^3 at the end of the year.

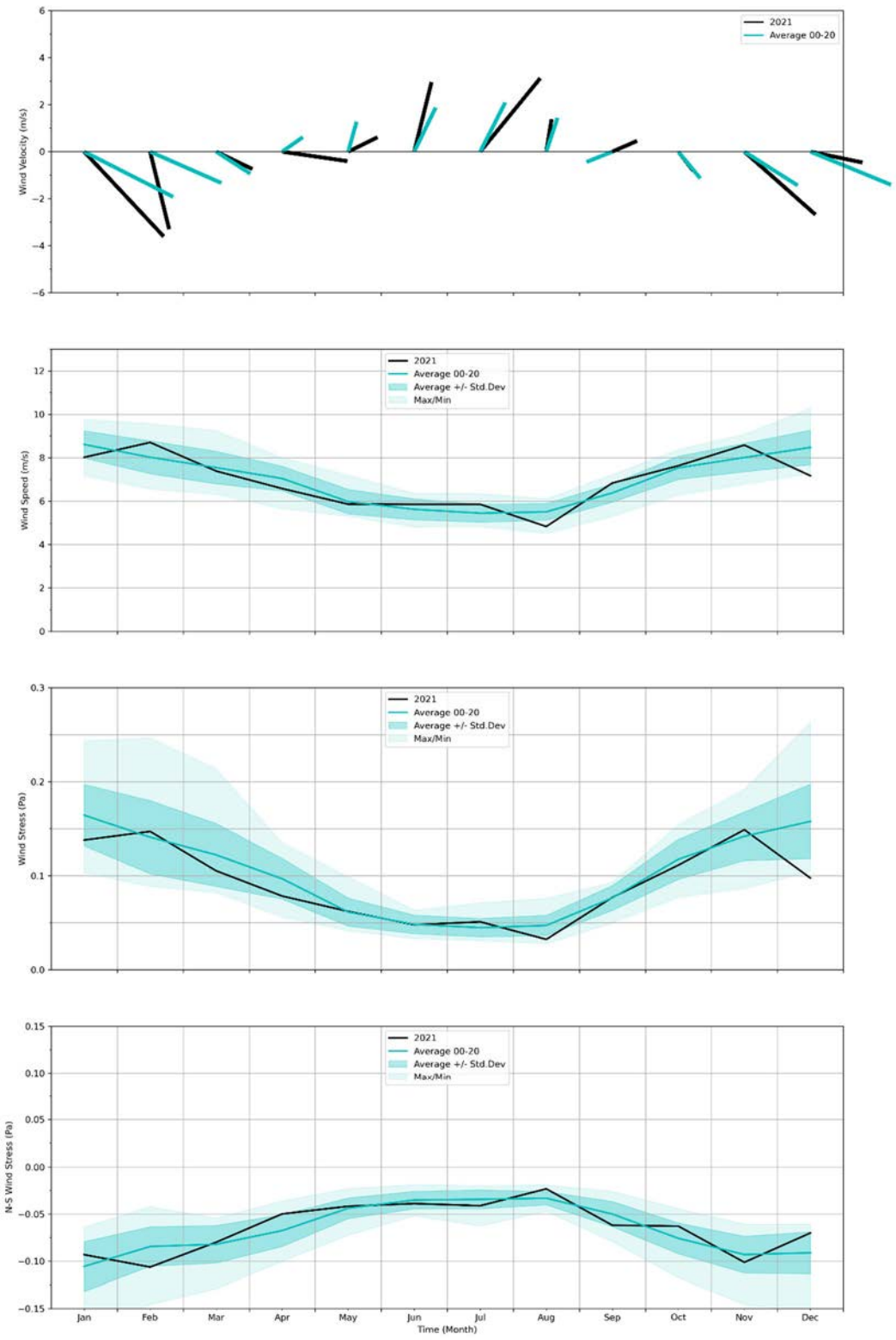

Figure 3-1 Surface wind forcing, monthly averages, compared to prior 20-year period.

Top frame: Vector-averaged wind velocities. Second frame: Wind speed. Third frame: Wind stress magnitude. Bottom frame: North-south component of wind stress, an indicator for wind-driven upwelling.

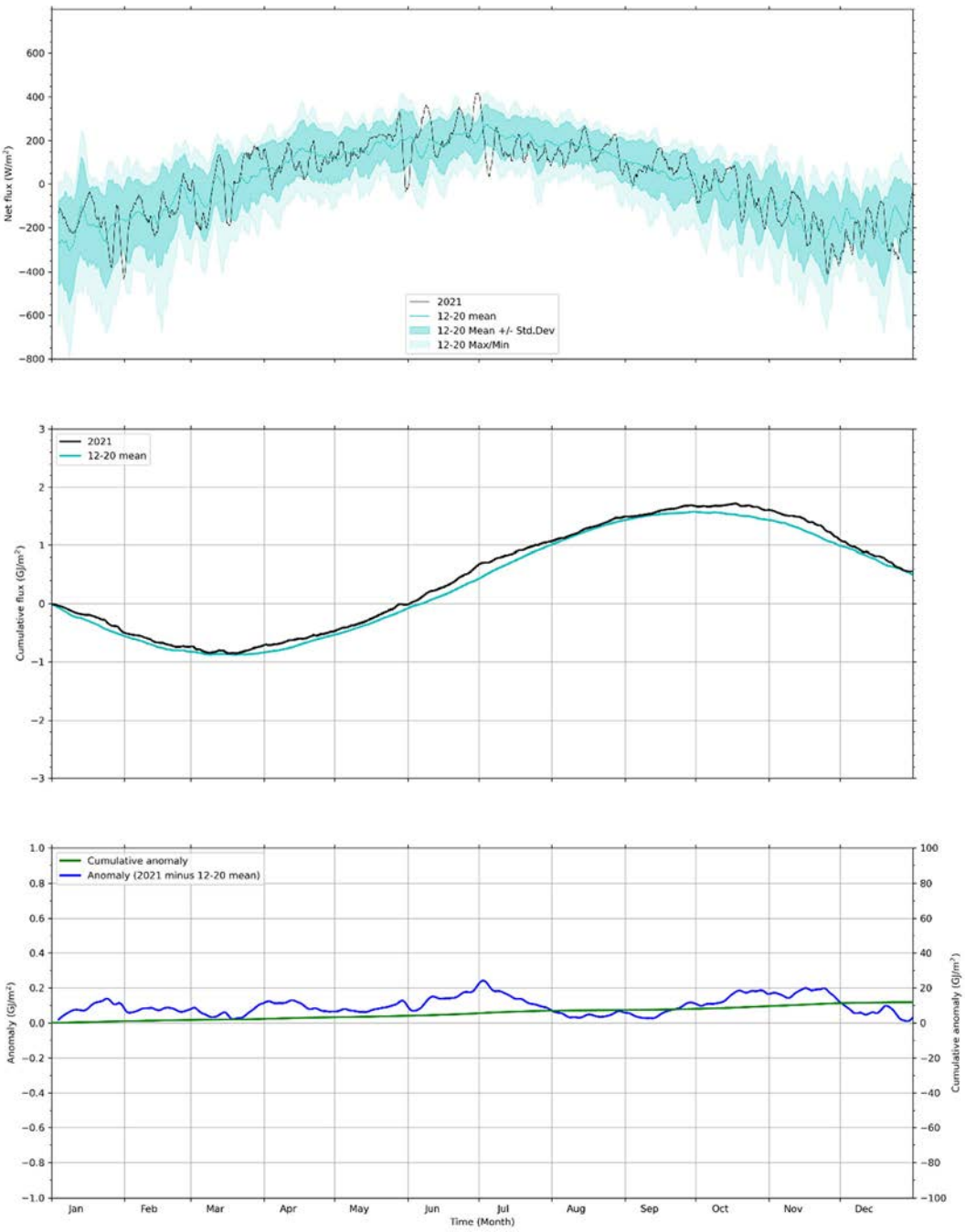

Figure 3-2 Surface heat flux, compared to prior 8-year period.

Top frame: Net heat flux into ocean. Middle frame: Cumulative net heat flux starting from January 1. Bottom frame: Anomaly (blue, left axis) and cumulative anomaly (cumulative sum of daily mean anomaly; green, right axis) of 2021 net cumulative heat flux relative to 2012-2020 average. The 2012-2020 reference period has been used because direct simulation output is available; it is shorter than the 20 years used for the long-term mean.

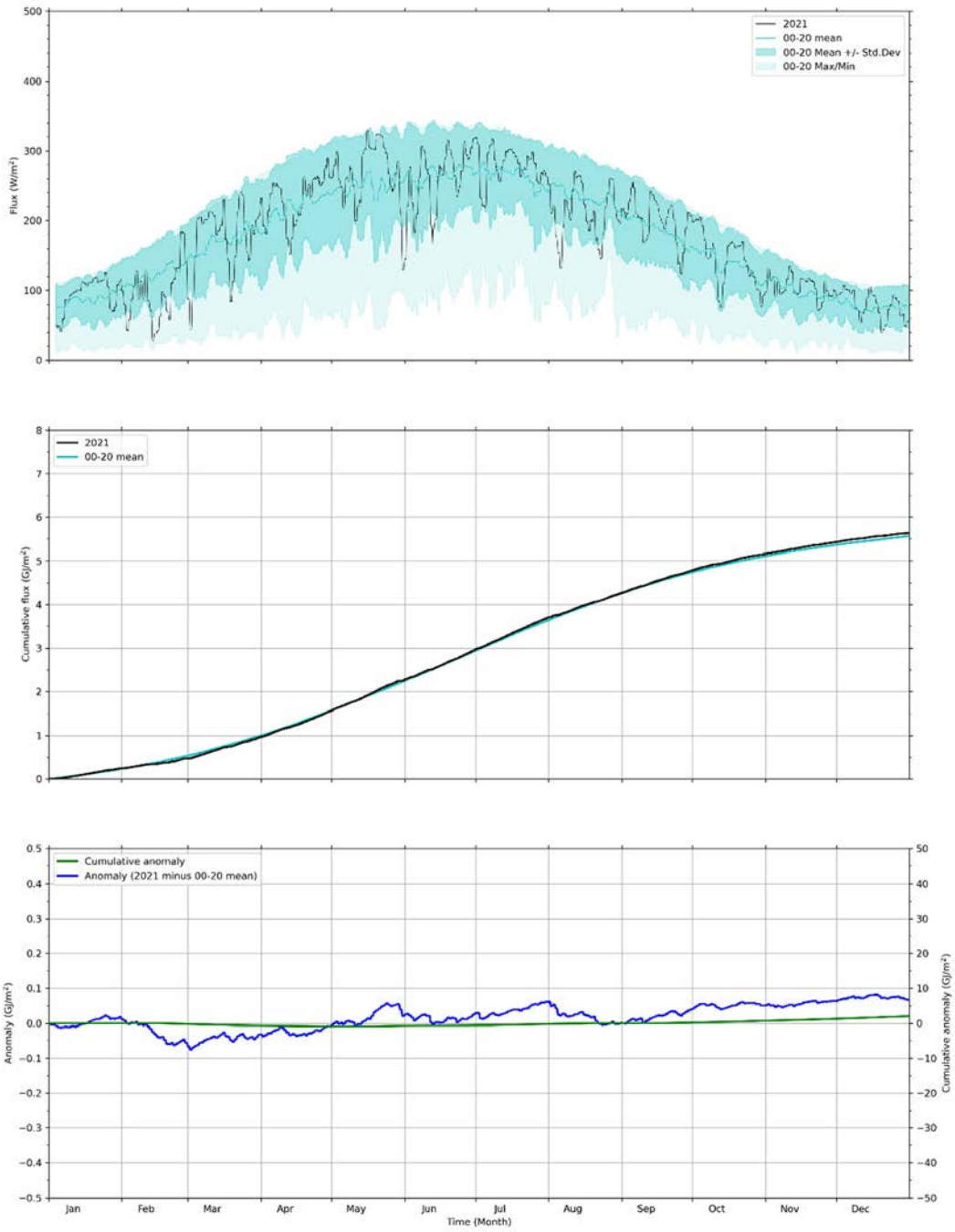

Figure 3-3 Solar radiation, compared to prior 20-year period.

Top frame: Solar radiation into ocean. Middle frame: Cumulative solar radiation starting from January 1. Bottom frame: Anomaly and cumulative anomaly (cumulative sum of daily mean anomaly) of 2021 cumulative solar radiation relative to 2000-2020 average.

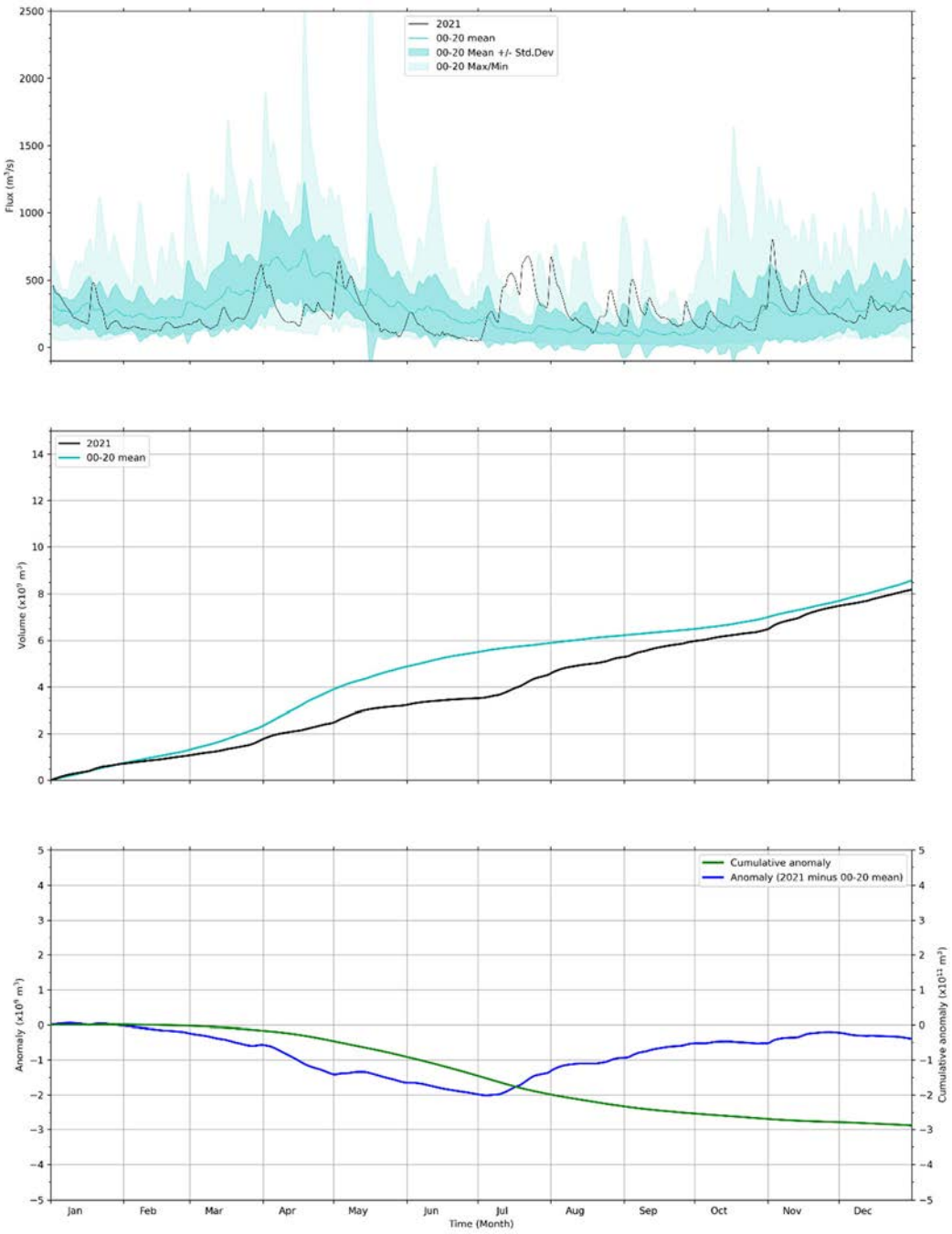

Figure 3-4 Merrimack River daily/cumulative flux and anomaly relative to previous 20 years.

Top frame: Merrimack River volume flux. Middle frame: Cumulative flux relative to January 1. Bottom frame: Anomaly and cumulative anomaly (cumulative sum of daily mean anomaly) of flux in 2021 relative to 2000-2020 average.

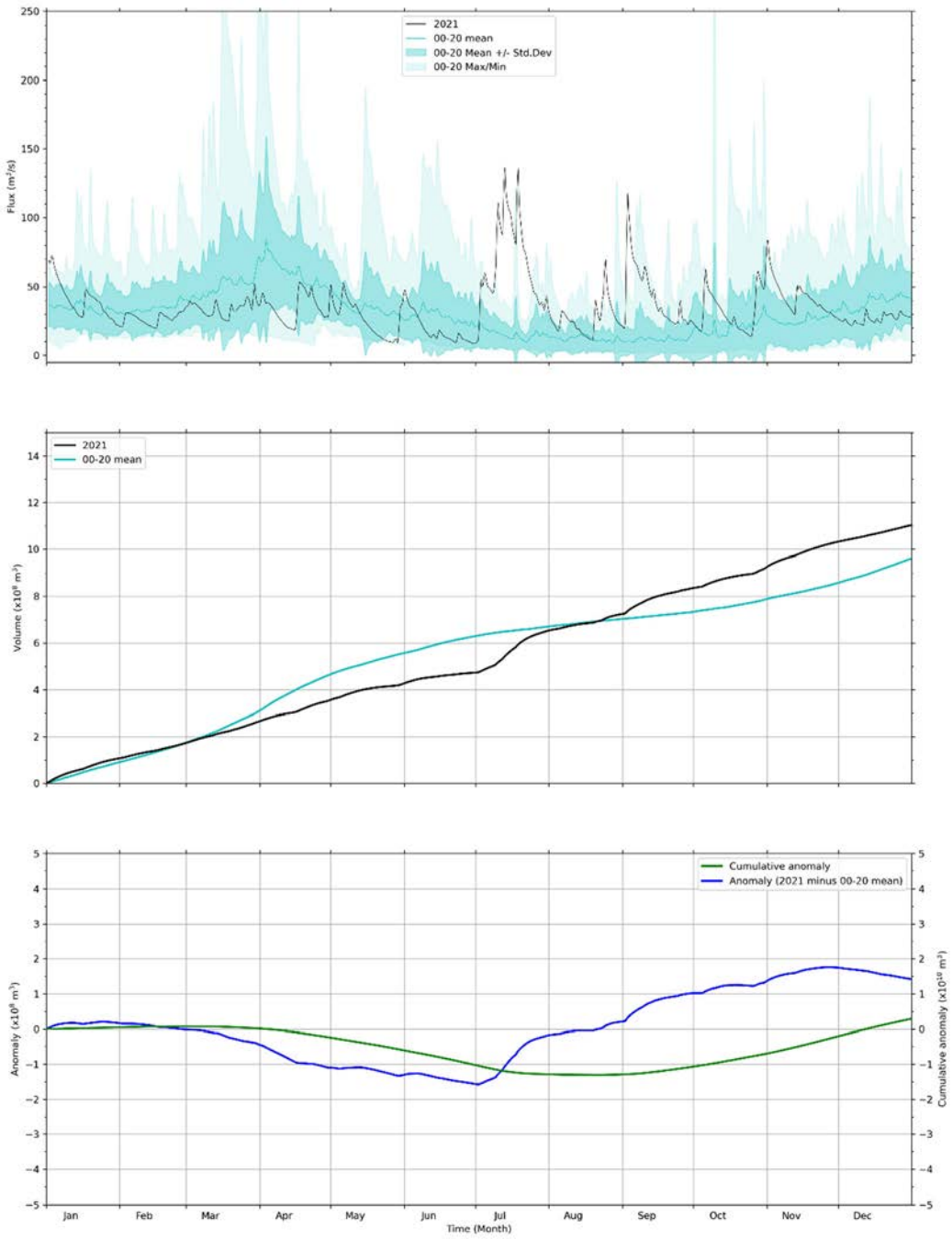

Figure 3-5 Summed discharge of all modeled rivers (Saugus, Mystic, Charles, Neponset, North, and Jones) flowing directly in to Massachusetts and Cape Cod Bays.

Presented as in Figure 3-4.

3.2 Loading of organic carbon, nitrogen, and phosphorous

Loads directly entering Massachusetts and Cape Cod Bays from rivers, the Deer Island treatment plant, and the atmosphere are shown in Figure 3-6. Loads entering the system through its offshore boundary are marked “oceanic input”, for example originating from rivers to the north including the Merrimack.

Model results show that oceanic input was the dominant source of organic carbon (OC), nitrogen, and phosphorus (both in organic and inorganic forms), accounting for 99%, 93%, and 97% of their total inputs, respectively (Figure 3-6). The simulated oceanic inputs of total nitrogen (TN) and total phosphorus (TP) were comparable to years 2017-2019 (within ~1 percentage points). TN input was comparable to the estimates based on the simulation of 1992 conditions from Hunt et al. (1999), reported by Zhao et al. (2017). Hunt et al. (1999) indicated that 93% of the TN entering the Massachusetts Bay originated from the Gulf of Maine.

Rivers were the second largest source of OC, accounting for 84% of the non-oceanic input. MWRA loads constitute the main non-oceanic source of TN and total phosphorus (TP). These occur mainly in the inorganic form. Atmospheric deposition accounted for approximately 11% of the non-oceanic TN inputs. Finally, rivers are the smallest source of TN and TP to Massachusetts and Cape Cod bays, representing 8% and 6% of their non-oceanic inputs, respectively. The contributions of river inputs to total OC, TN, and TP loads in 2021 were on the high side of the ranges of those from previous years (2017-2020). This is most likely due to the higher-than-average river discharges in the second half of the year.

The 2021 OC loads from the MWRA effluent were in the middle of the range of loads from the preceding years 2016-2020. The 2021 TN and TP effluent loads were on the low side compared to 2016-2020. The organic fraction of TN effluent loads was relatively high compared to the years 2015-2018 but slightly lower than 2019 and 2020.

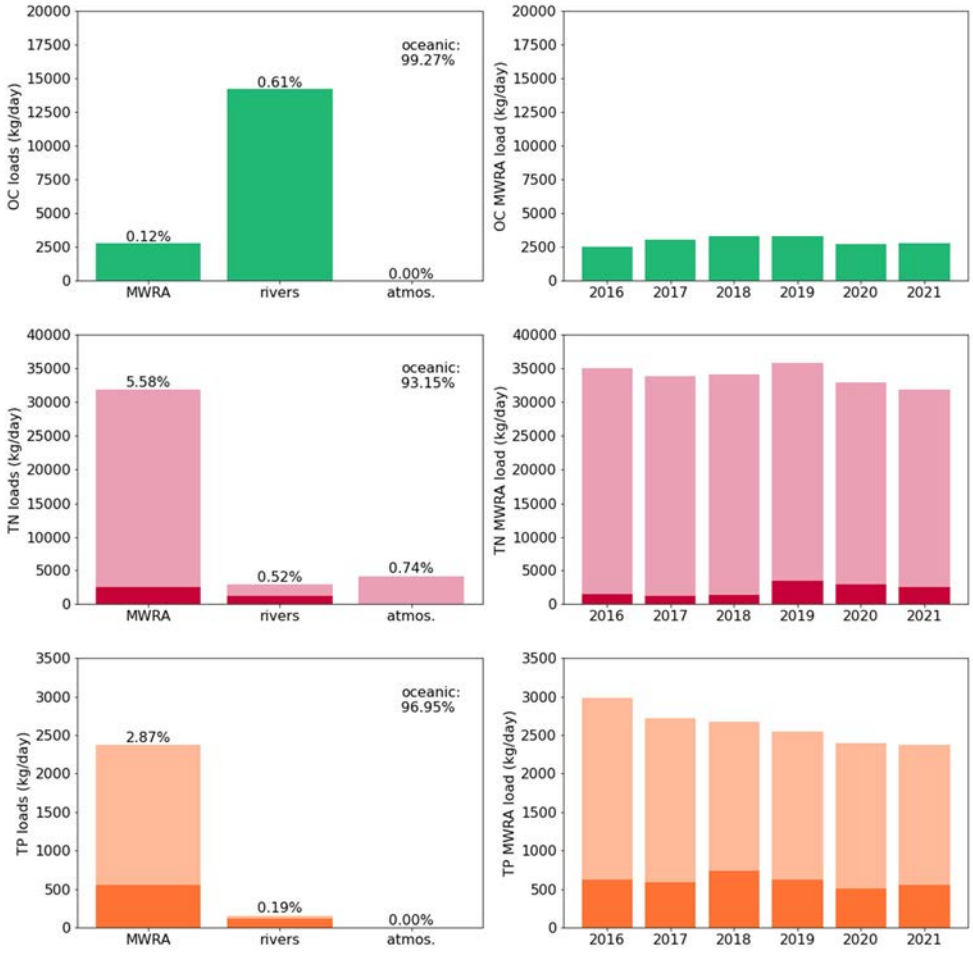

Figure 3-6 Organic Carbon (OC), Total Nitrogen (TN) and Total Phosphorus (TP) loads to Massachusetts and Cape Cod Bays in 2021. In the TN and TP plots, the darker sections of the bars represent the organic fractions. Left: loads from non-oceanic sources; percent of total is shown at top of each bar, and percent oceanic input (offshore boundary) shown at upper right. (Percentages correspond to summed organic and inorganic fractions.) Right: Deer Island Treatment Plant loads since 2016. OC=organic carbon; TN=total nitrogen; TP=total phosphorus.

4 Hydrodynamic Model

In this section the performance of the hydrodynamic model is discussed, and model results are compared to measurements.

4.1 Verification of model performance

The model skill was assessed for surface and bottom temperature and salinity by means of a statistical analysis. Three quantitative skill measures (correlation, normalized standard deviation Std*, and normalized unbiased root mean square error uRMSE*) were determined, based on simulation results and vessel-based observations by MWRA surveys. The result is presented in four sets of Taylor diagrams in Figure 4-1. The left column shows the 2012-2016 validation period (Deltares, 2021) and the right column shows the 2021 simulation. See also the box below for further details and an explanation of the statistics in the diagrams.

Temperatures had correlation of over 0.96 and 0.97, Std* of 0.95-1.10 and 0.90-1.30, and uRMSE* of under 0.30 and 0.41, at the surface and bottom respectively. The performance at the surface was slightly improved compared to the validation result, while at the bottom the performance was similar to the validation result.

The skill of simulated salinity varied more per observation station, compared to temperature. The performance at the surface and at the bottom is mostly similar to the validation result. The correlations are slightly improved compared to the validation results for both the surface and bottom salinity.

Overall, the figures presented here serve to verify that the performance of the hydrodynamic model in the simulations of 2021 did not deviate substantially from its performance during the 5-year validation period. For completeness, Taylor diagrams broken out for individual years 2012-2016, are presented in Appendix A of the Annual BEM Report on 2017 (Deltares, 2022a).

How to read a Taylor diagram

A Taylor diagram consists of a combination of three quantitative skill measures:

- Correlation Coefficient, represented in the plot by the azimuthal angle or blue lines.
- Normalized Standard Deviation (Std*), the Standard Deviation of the model results, normalized (*) by the standard deviation of the corresponding measurements. This ratio represents the relative amplitude of the modeled and observed variations, with a value of less than one indicating less modeled variability. It is represented in the plot by the radial distance from the origin (0,0).
- Unbiased Root-Mean-Square Error or standard deviation of the error, normalized with the standard deviation of the corresponding measurements (uRMSE*). It is represented in the plot by the grey contours, whose values are proportional to the radial distance from the target (black star).

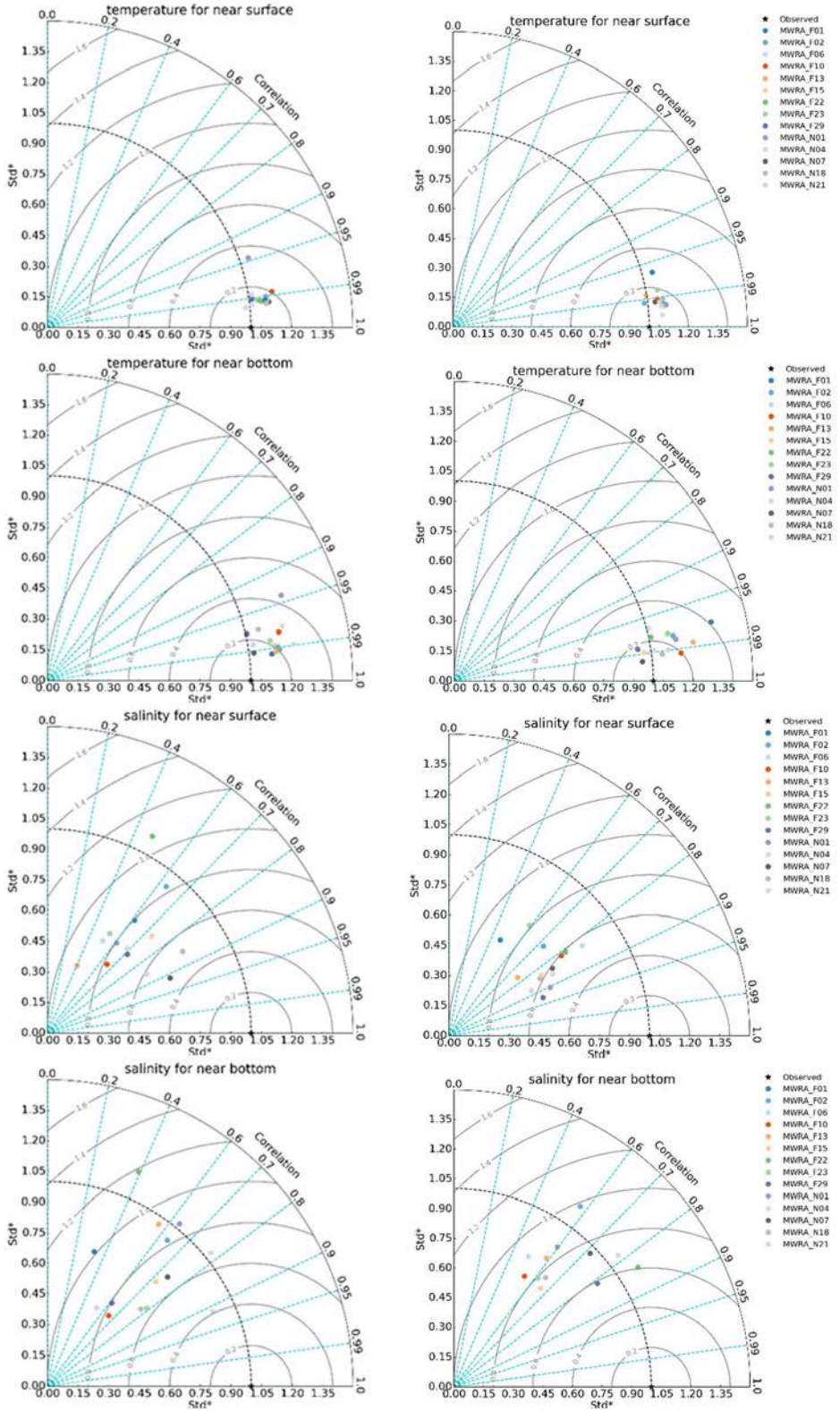

Figure 4-1 Taylor diagrams of model quality for MWRA vessel-based survey observations.

Temperature (upper frames), salinity (lower frames); 2012-2016 validation period (left column) and 2021 simulation (right column)

4.2 Model-observation comparisons

The simulation for 2021 was compared to observations to assess the level of agreement between them for temperature and salinity, both in time and space.

4.2.1 Time series of temperature and salinity

For eight observation stations in the Massachusetts Bay and Cape Cod Bay, simulation timeseries of the surface (less than 5 m deep) and bottom (within 5 m of seafloor) temperature and salinity are presented in Figure 4-2 and Figure 4-4, respectively. Additionally, a comparison at three levels within the water column, between the surface and seafloor, is given for temperature and salinity in Figure 4-3 and Figure 4-5 (described below), respectively.

In these figures, vessel-based observations by MWRA surveys are included as individual symbols. The locations of the observation stations are given on a bathymetric map in the upper left frame. They include four stations generally surrounding the outfall (N01, N07, N18, and F13), one to the south (F06), one farther offshore (F22), one at the mouth of Boston Harbor (F23), and one in central Cape Cod Bay (F02).

In Figure 4-3 and Figure 4-5. showing results from within the water column, the depths vary from station to station and survey to survey but are nominally at 25%, 50%, and 75% of the water depth. The model output between surveys is not shown on these figures because the depths used, set by the observations, differ from survey to survey.

Overall, the seasonal cycle and most events were well captured by the model. Simulated stratification was in line with observations. At most stations, the onset of temperature stratification was in April with a maximum in July and August. The water column started to become mixed again over the course of October. The seasonal variations in salinity and salinity stratification in 2021 were largely limited, especially in spring. However, at most stations, particularly those to the north or closer to the shoreline (e.g., F22, N01, N18, and F13), surface salinities were unusually low in July and August based on the observed data (Libby et al., 2022; Figure 4-4). This can be attributed to the unusually high river flows observed in summer 2021, visible in the timeseries of river discharges in Figures 3-4 and 3-5. A drop in surface and bottom temperature was observed in late-June in the observations (N01, N18, F22, and F23), which was also reproduced by the model (Figure 4-2). In most cases model-observation differences for temperature were less than 1°C at the surface and seafloor and slightly larger within the water column. An exception is that the model overestimated an anomalously low temperature observation in late-July at F23, which indicated a temperature drop of approximately 5°C at all depths from near-surface to near-seafloor compared to observations immediately preceding this measurement in mid-July (Figure 4-3). This is due to the runoff event that potentially brought cooler water to the nearshore location, which is not accurately reflected in the model simulations because the temperature boundary condition for the freshwater inflows is based on NWIS data that were typically collected monthly and did not have the temperature data from this event. Simulated salinity showed a bias similar to previous years throughout the water column for most samples in 2021. This bias increased for July and August when the 2021 surface salinity observations were unusually low due to freshwater inflow.

4.2.2 Spatial representation of temperature and salinity

To assess the simulation spatially, maps have been plotted for surface and seafloor conditions, with the mean of the modeled results averaged over a period of 5 days centered on the observation dates. The five presented periods span the seasonal cycle of stratification. This is given in Figure 4-6 and Figure 4-7 for temperature and in Figure 4-8 and Figure 4-9 for salinity. For the model-observation

comparison, the available observations are plotted over the simulation fields as colored symbols. Note that the presented simulation fields are the average over 5 days, where the observations are instantaneous values, usually measured in the morning. This might introduce a bias.

These figures show a good agreement between the simulation and observations. The spatial variation at both the surface and bottom was comparable, with near-shore temperatures warmer in summer and colder in winter. At both depths, salinities were generally fresher near the coast. Similar to 2020 and 2018 (and in contrast with other years), no large freshwater plume was present in the spring or early summer of 2021. This can be explained by the low discharge from the Merrimack River in the first 6 months of 2021 (Figure 3-4). Model-observation differences for salinity were the largest in August when surface salinity observations are lower in response to the river flow runoff events in July and August, while the simulated surface salinities did not exhibit the pronounced decline evident in the observations. At the seafloor, the maximum overestimation of the salinity was 0.5 PSU. Model-observation differences for surface and seafloor temperatures were at most 1°C.

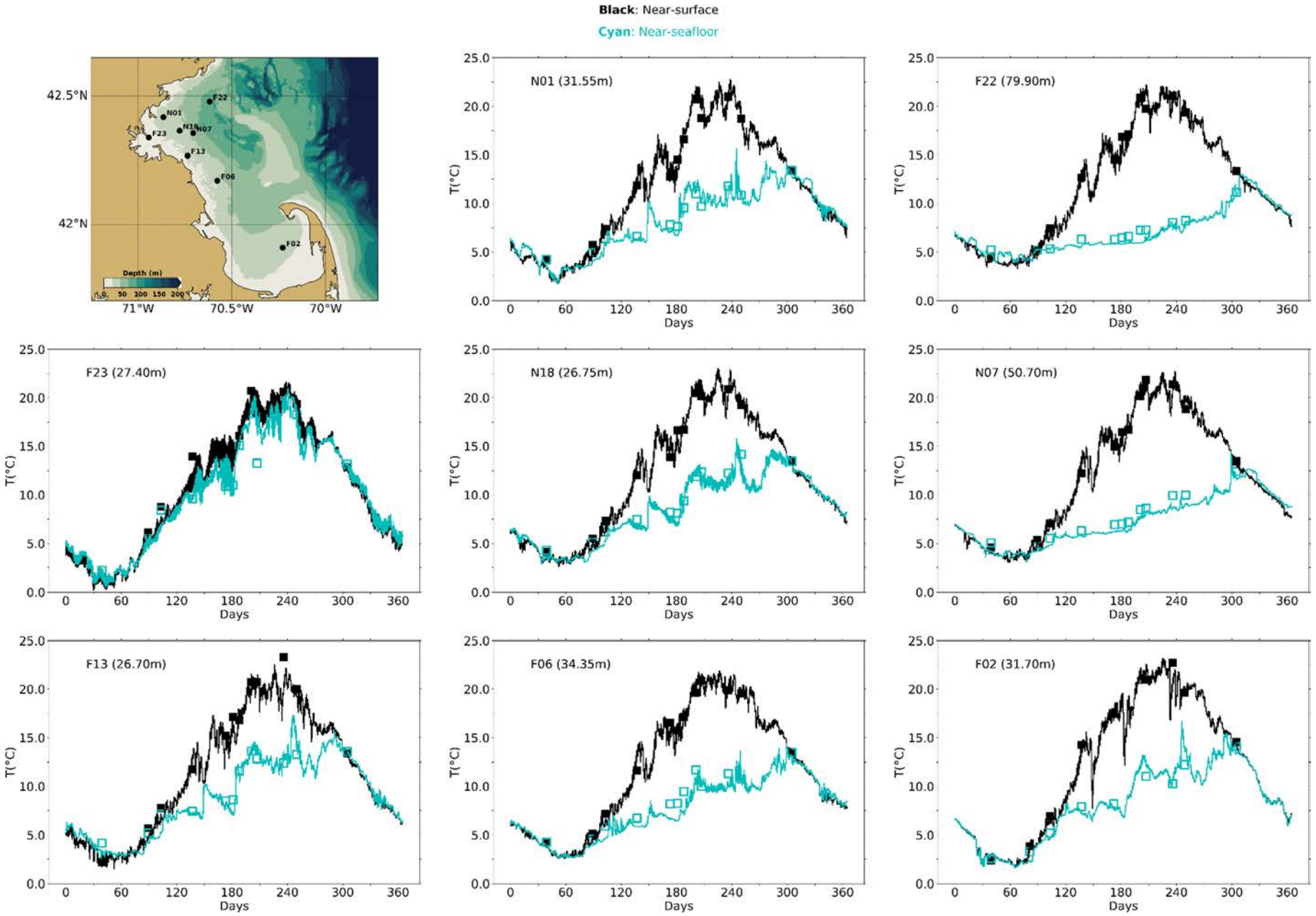

Figure 4-2 Temperature time series, model-observation comparison near surface (black) and seafloor (cyan).

Model results: lines. MWRA vessel-based survey observations: symbols.

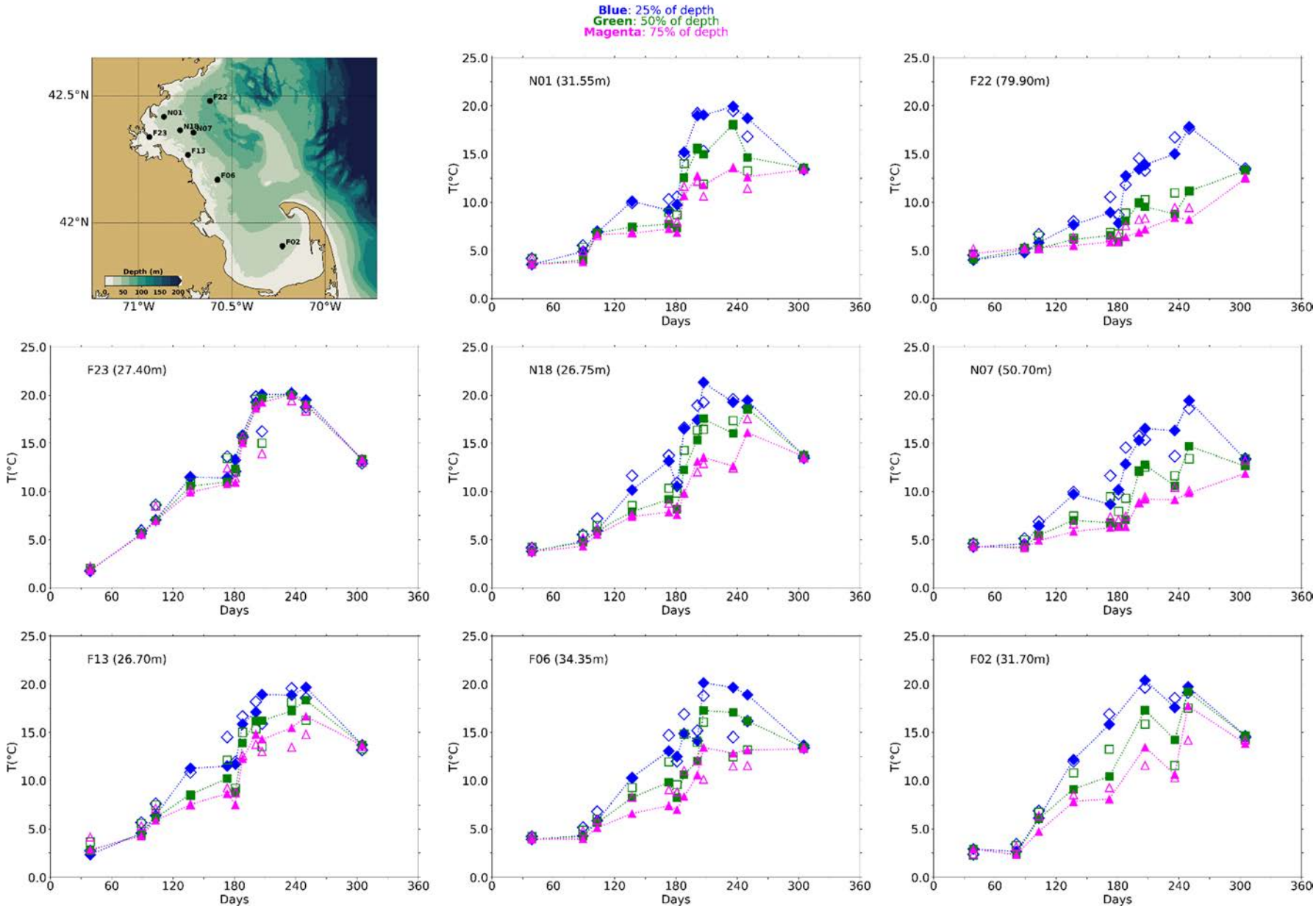

Figure 4-3 Temperature time series, model-observation comparison in water column (between surface and seafloor).

Model results: lines with filled symbols. MWRA vessel-based survey observations: open symbols.

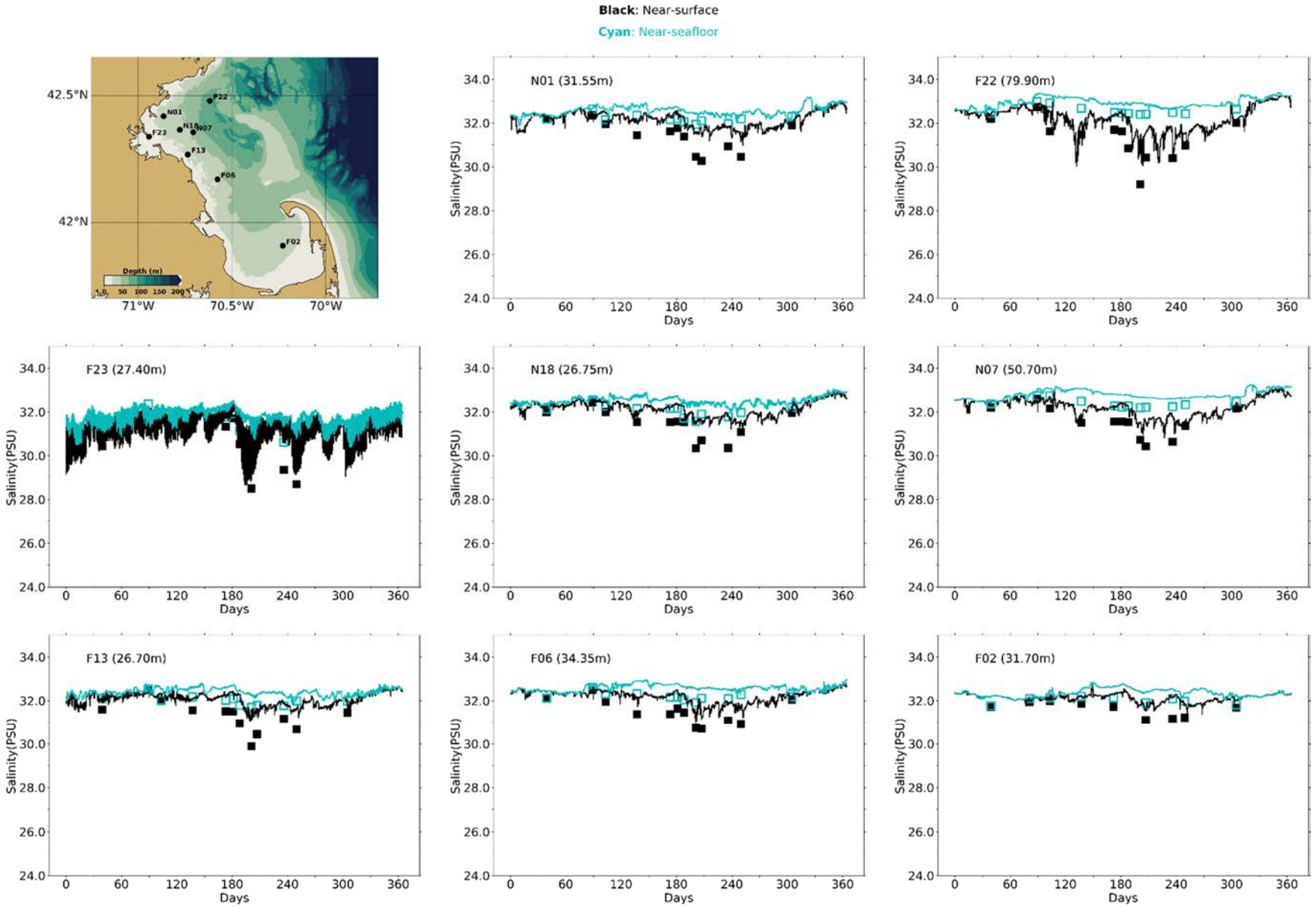

Figure 4-4 Salinity time series, model-observation comparison near surface (black) and seafloor (cyan).

Model results: lines. MWRA vessel-based survey observations: symbols.

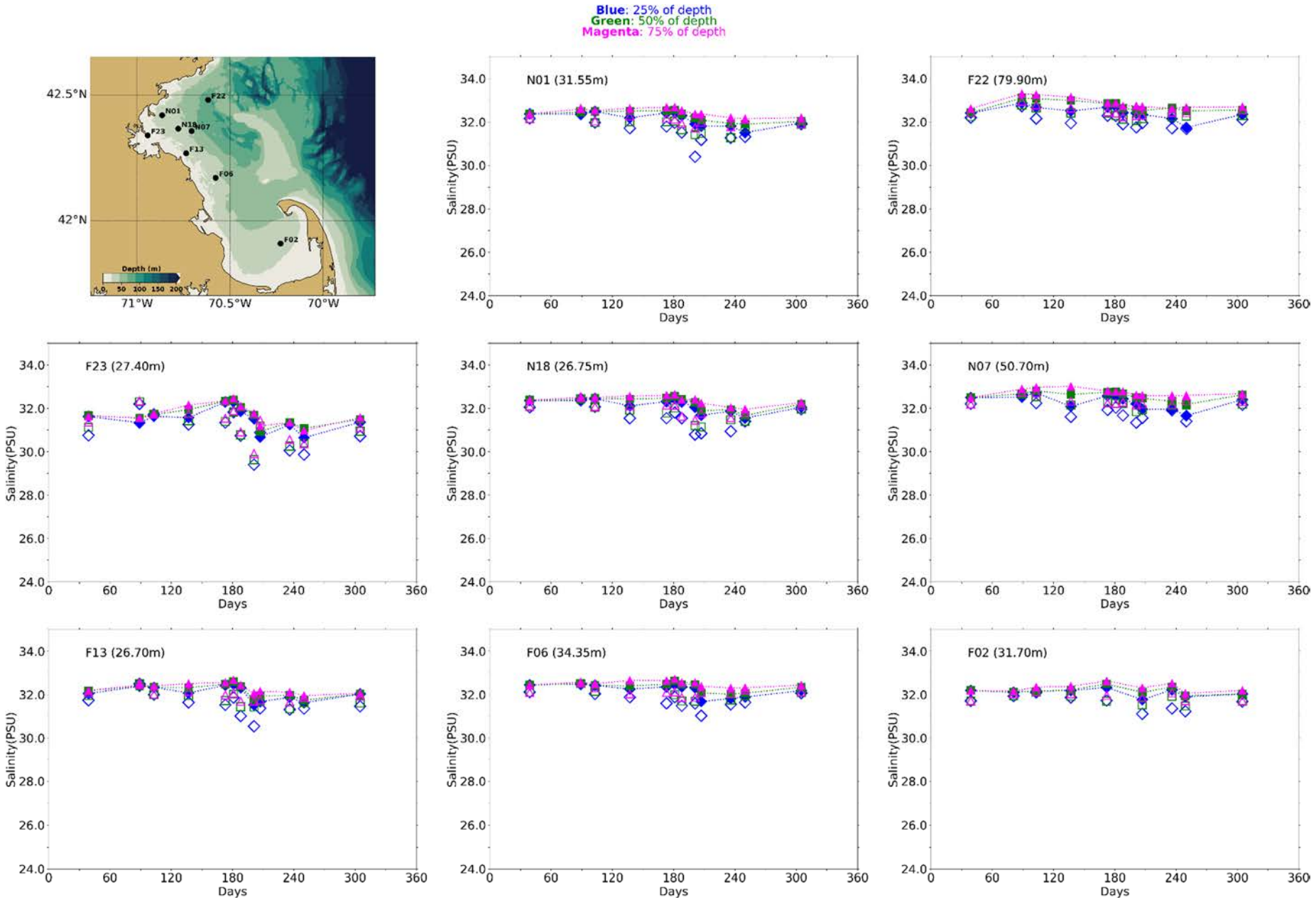

Figure 4-5 Salinity time series, model-observation comparison in water column (between surface and seafloor).

Model results: lines with filled symbols. MWRA vessel-based survey observations: open symbols.

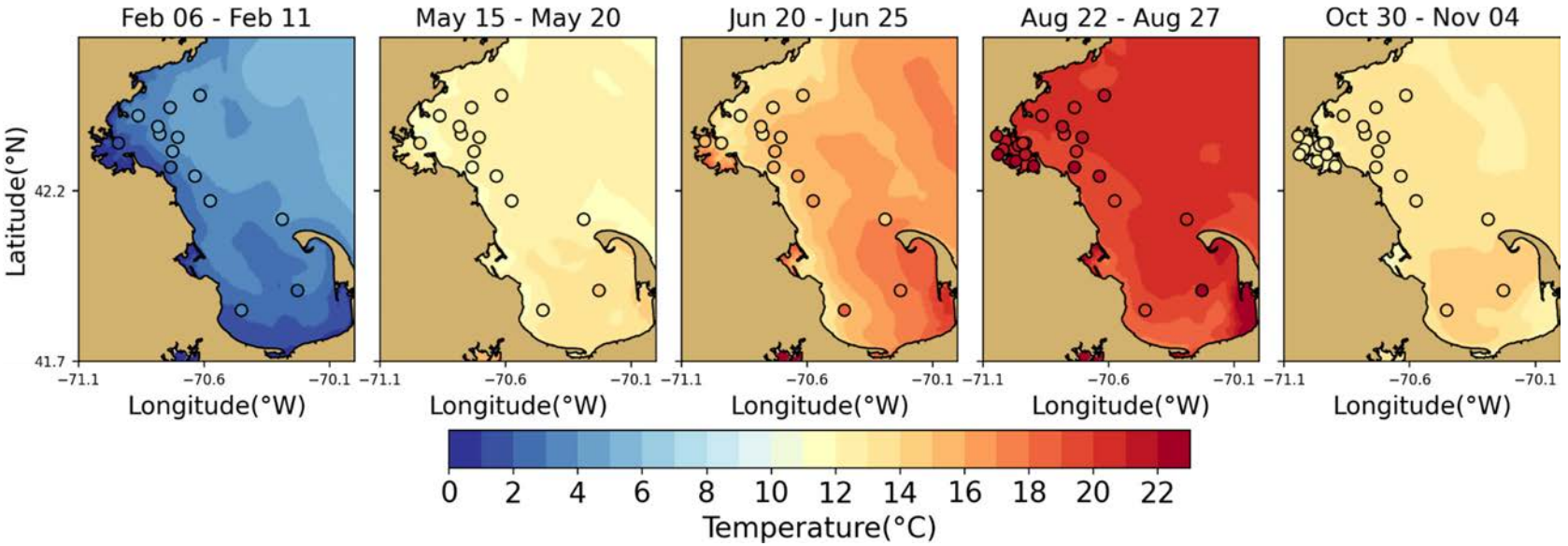

Figure 4-6 Temperature spatial structure, at/near sea surface, model-observation comparison.

Model results: background. MWRA vessel-based survey observations: symbols. Model results are averaged over the 5-day period centered on the measurement date.

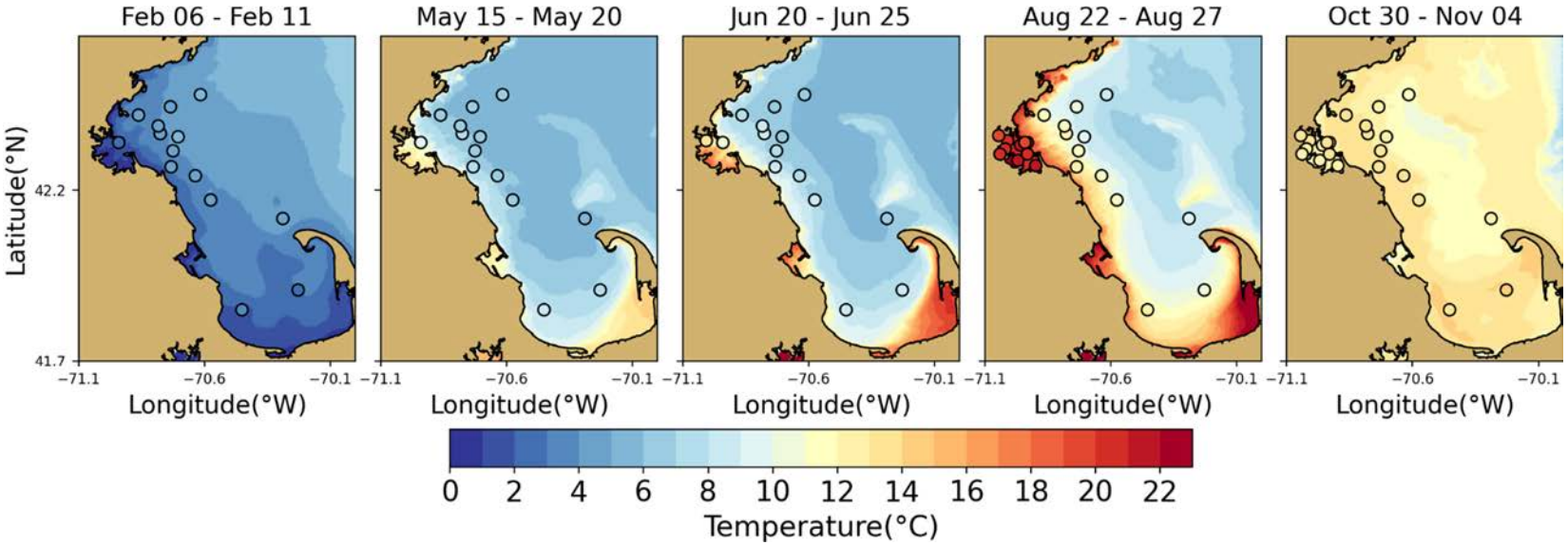

Figure 4-7 Temperature spatial structure, at/near seafloor, model-observation comparison.

Model results: background. MWRA vessel-based survey observations: symbols. Model results are averaged over the 5-day period centered on the measurement date.

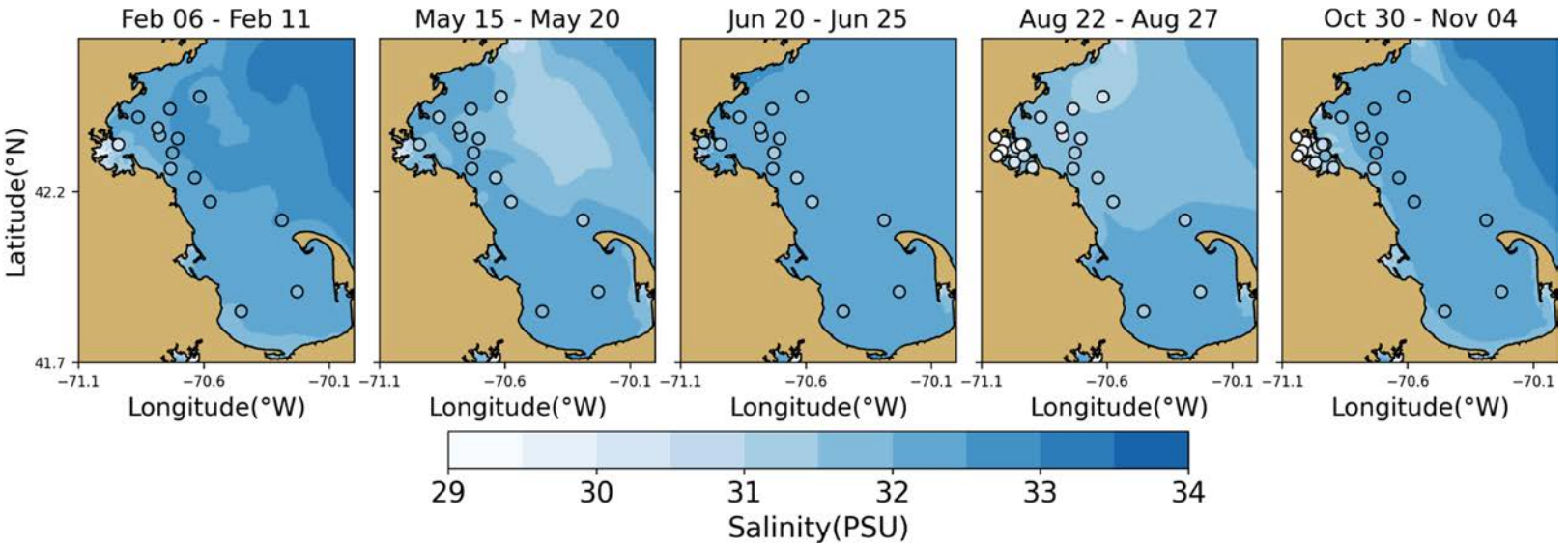

Figure 4-8 Salinity spatial structure, at/near sea surface, model-observation comparison.

Model results: background. MWRA vessel-based survey observations: symbols. Model results are averaged over the 5-day period centered on the measurement date.

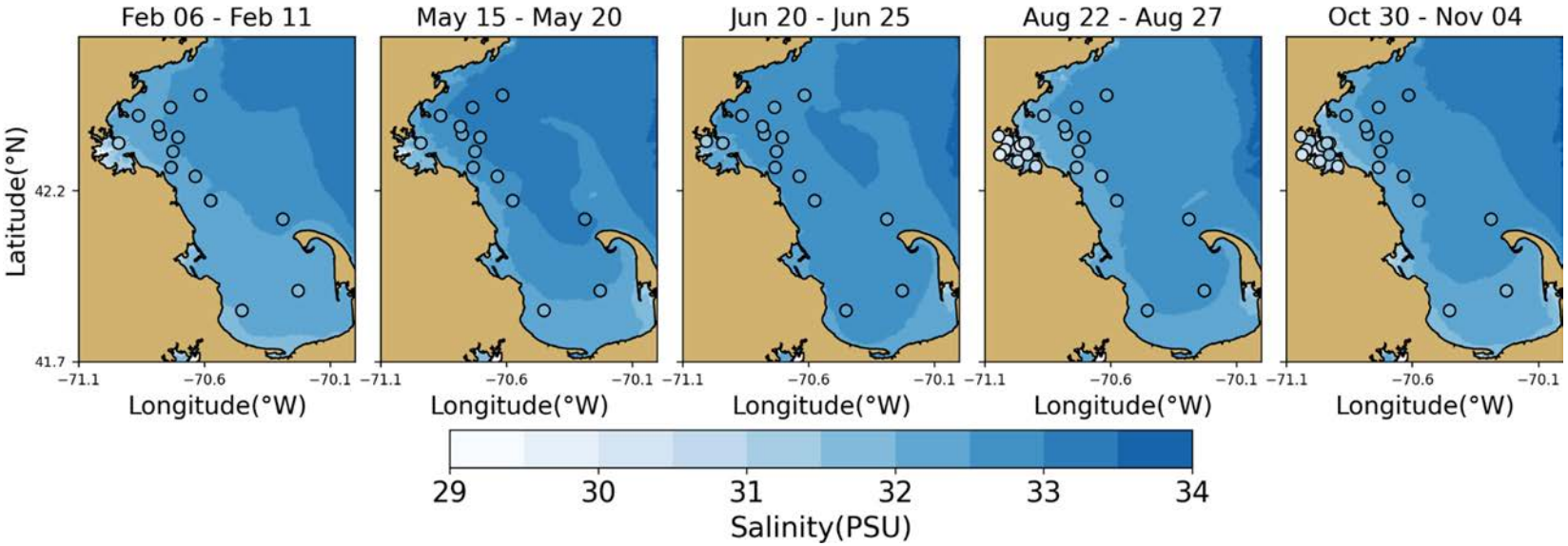

Figure 4-9 Salinity spatial structure, at/near seafloor, model-observation comparison.

Model results: background. MWRA vessel-based survey observations: symbols. Model results are averaged over the 5-day period centered on the measurement date.

4.2.3 Continuous measurements of temperature and salinity

Hourly measurements were available from Mooring A01 at multiple depths. This station is located south of Cape Ann, northeast from MWRA station F22. To provide a more complete assessment of the model-observation comparison in time, timeseries for this station are presented in Figure 4-10. This figure shows the simulated and observed temperature and salinity at three depths (1m, 20m, and 50m; top panels of Figure 4-10) and the salinity and temperature differences between the 1m and 20m depths and 1m and 50m depths (bottom panels of Figure 4-10), as an indication of the stratification within the water column. Observation data at the surface were only available during the summer months and from November onward. Consequently, large gaps are present in the 1m time series and vertical difference time series of both temperature and salinity.

The available data showed a good result of the model-observation comparison for temperature and salinity and different depths. The bias of about 0.50-0.75 PSU throughout the water column, as explained in Deltares (2021), is clear in the second frame of the figure. The typical seasonal cycle of less saline near-surface waters occurred in July and August of 2021 instead of early summer due to the lower-than-average discharge from Merrimack River until mid-July of 2021. In the summer months, simulated surface temperature showed good agreement with data and was slightly underestimated at 20m and 50m. In 2021, it was observed that both the 20m and 50m water temperatures were unusually warm, so this represents an extreme situation for the model. Temperature stratification was, however, well represented in the model. Individual events were captured, but in summer months, an underestimation of up to 2°C occurred at the 50m depth. The salinity stratification showed a good comparison between model and observations. Overall, the model captures features of observed stratification well, as is important for the water quality simulation because stratification is a main influence on vertical transport.

4.2.4 Continuous measurements of non-tidal currents

For Mooring A01 observed currents were available as well, although surface currents from mid-June up to and including October of 2021 were missing. In Figure 4-11 and Figure 4-12 a model-observations comparison is presented for the first and second halves of the year, respectively. In the top frame, time series of wind from the meteorological product used to force the model is given for context. In the frames below, simulated and observed time series of non-tidal currents at four depths (2m, 10m, 22m and 50m) are given alternately. To remove the tidal variability, timeseries have been filtered using a low-pass filter with a 33h filter half amplitude (Alessi, 1985). The resulting signal consists mainly of weather-related and seasonal changes. For plotting this has been subsampled to a 6h resolution.

The time series of the filtered wind showed wind in all directions. Winds were generally changing on timescales of multiple days. In general, the wind speeds were lower during the calmer summer months. Winds included a dominantly eastward component year-round, with a dominant southward component in winter and a dominant northward component in summer.

Simulated and observed non-tidal currents showed a similar pattern with a prevailing direction to the south and west. The simulated currents showed less variability in direction than observed, but the order of magnitude of their amplitudes was similar. Strong currents occurred in April and at the end of May and October due to a strong south-westward wind. Throughout the year, some small events occurred, but these were not persistent. These events were well represented in the model. This model-observation comparison at a specific location is a challenging test of the hydrodynamic simulation performance. The agreement between the two was sufficient to conclude that the

representation of processes in the hydrodynamic model was adequate to support water quality modelling.

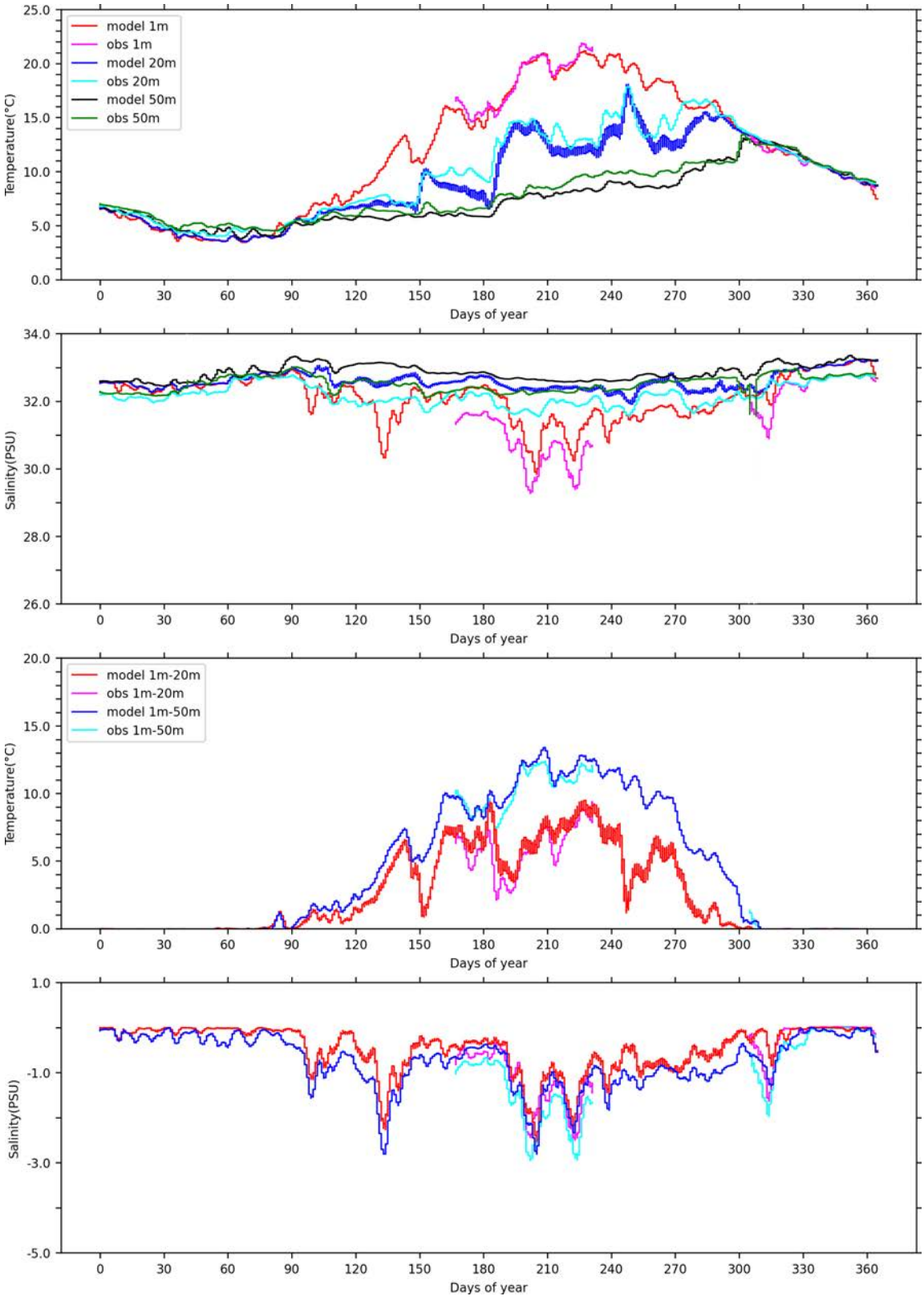

Figure 4-10 Time series Mooring A01 temperature/salinity model-observation comparison (3-day means), three depths and two stratification levels.

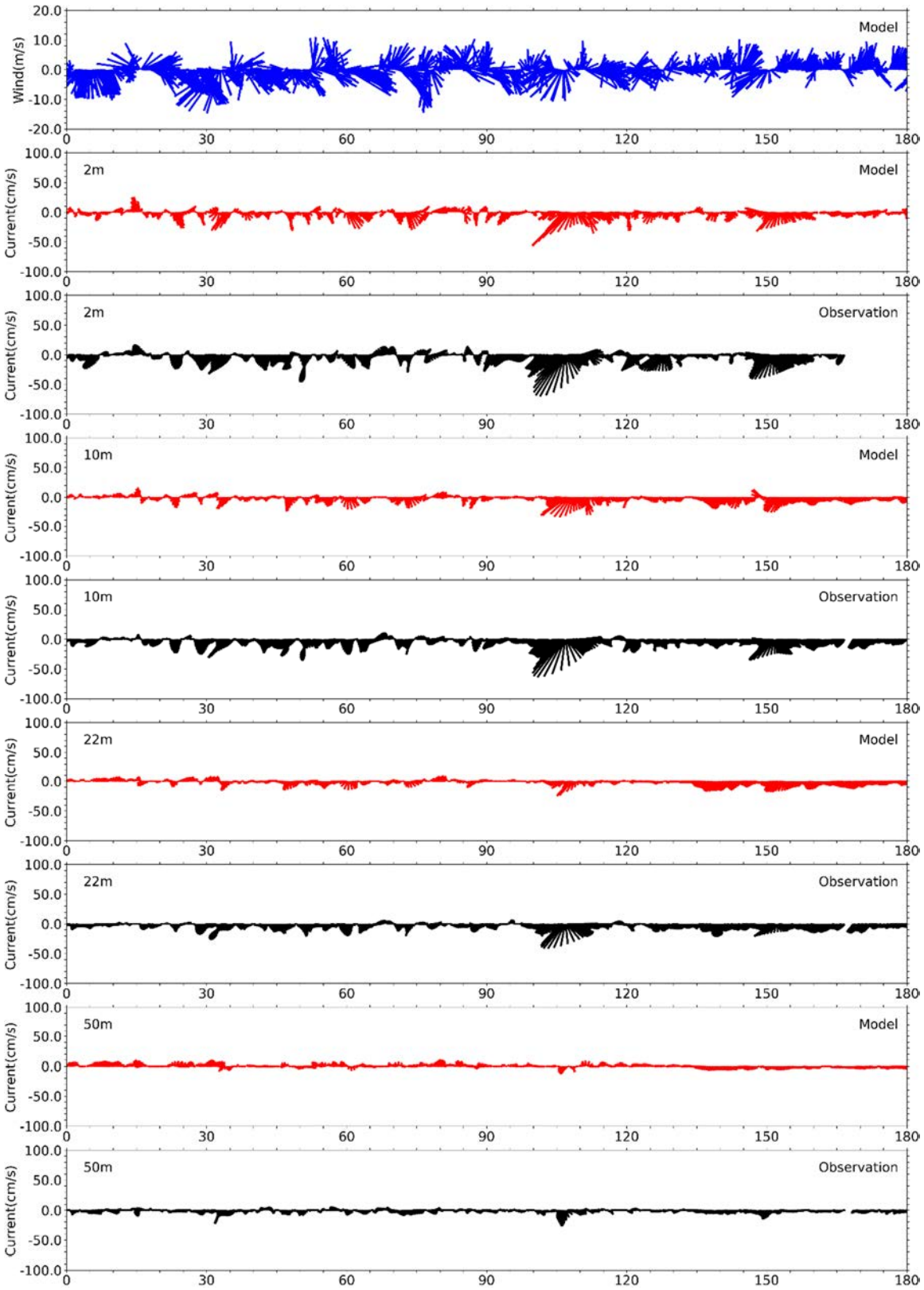

Figure 4-11 Currents time series model-observation comparison, Jan – Jun.

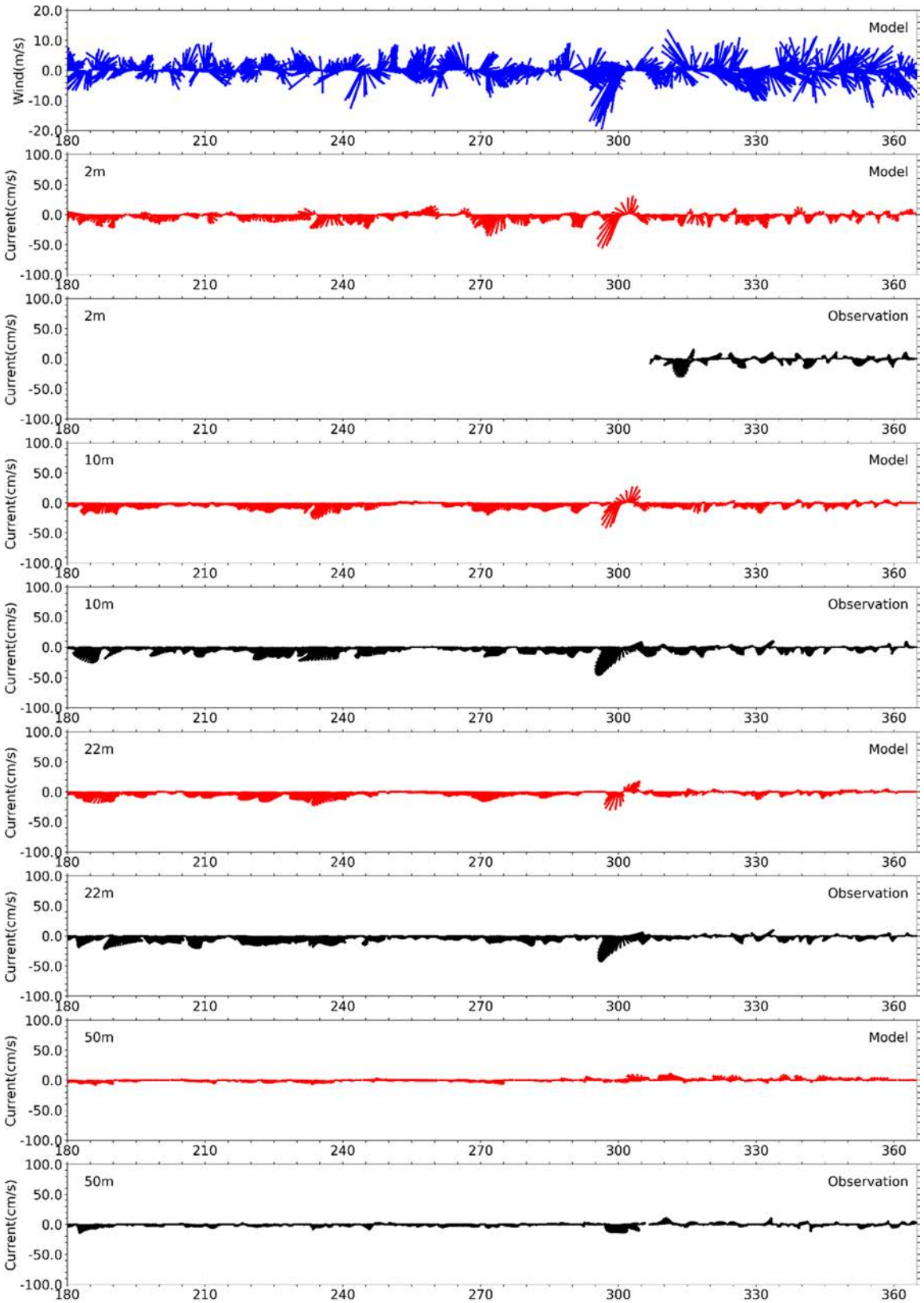

Figure 4-12 Currents time series model-observation comparison, Jul – Dec.

4.3 Model monthly-mean circulation

Figure 4-13 and Figure 4-14 present the simulated monthly-mean currents at the surface and at a depth of 15 m. Flow was largely consistent with the general circulation pattern recognized to hold (Figure 1-1).

This schematic pattern was most apparent in the residual surface currents between January and August and between October and November. In September the circulation was partially reversed in the northern half of Massachusetts Bay. In December the direction of the currents was the same, but the magnitude was very low. Surface currents near the Massachusetts Bay were strongest off Cape Ann and Cape Cod with the largest magnitudes in April and July respectively, reaching up to 0.20-0.25 m s^{-1}. This was lower than the maximum in other years. Residual currents within Massachusetts Bay were strongest in June with magnitudes up to 0.15 m s^{-1} near North Passage and in the center of the bay (see Figure 4-13) and in January with similar magnitudes nearshore near Scituate Harbor. During the rest of the year surface currents were calmer and did not exceed 0.10 m s^{-1}. The strongest north-eastward currents in North Passage occurred in November, reaching up to 0.15 m s^{-1}.

In general, the circulation pattern at 15 m depth (Figure 4-14) was somewhat similar to the general circulation pattern of Figure 1-1, including a flow directed into northern Massachusetts Bay from offshore, and changed little from month to month. Current magnitudes were lower than at the surface, with maxima in July of up to 0.25 m s^{-1} at Cape Cod. Within Massachusetts Bay, residual currents were smaller than at the surface, reaching up to 0.2 m s^{-1} at North Passage in August. In Cape Cod Bay, residual current magnitudes at this level were weaker, due to its limited depth and sheltered geometry.

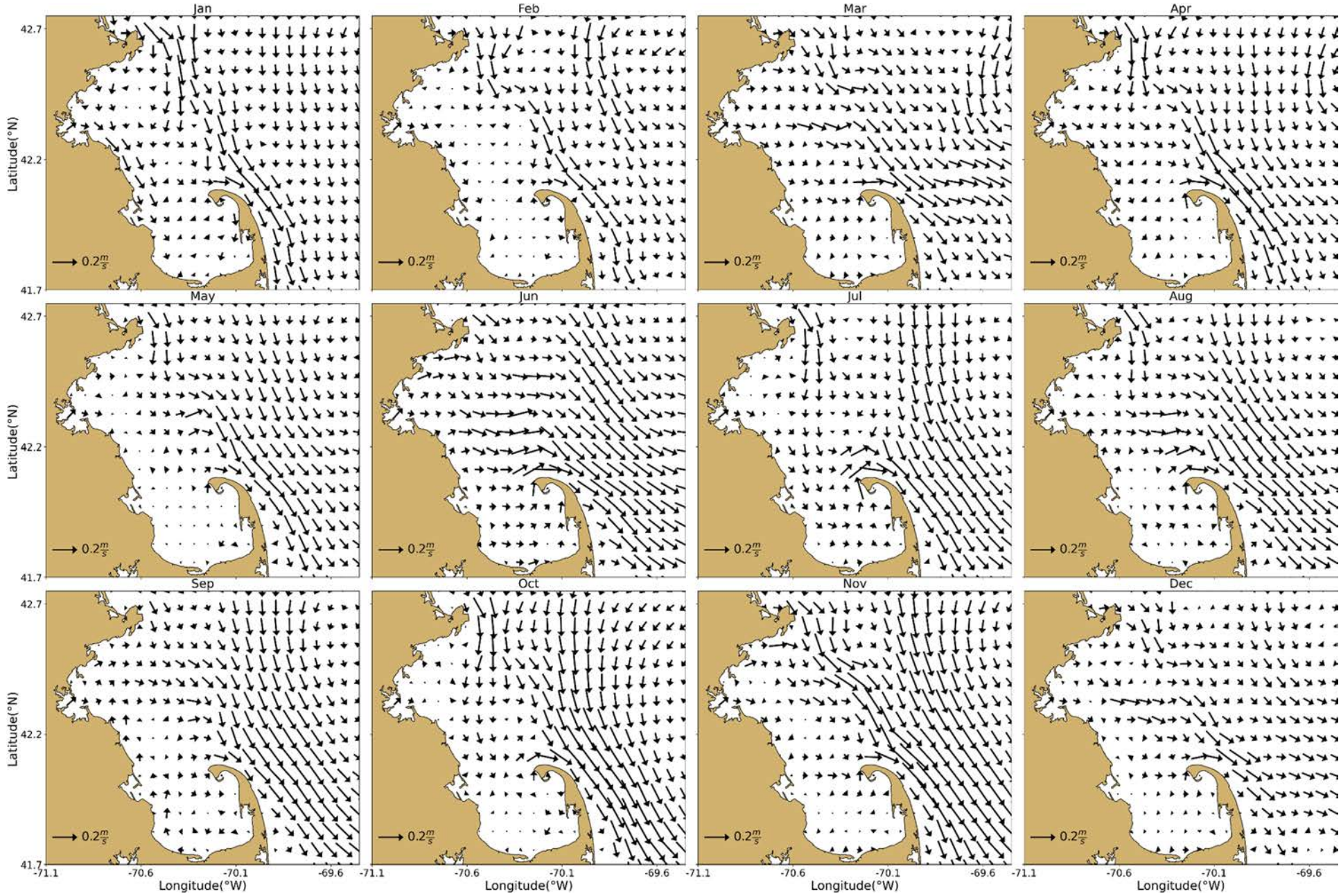

Figure 4-13 Model currents, monthly-mean spatial structure, at sea surface.

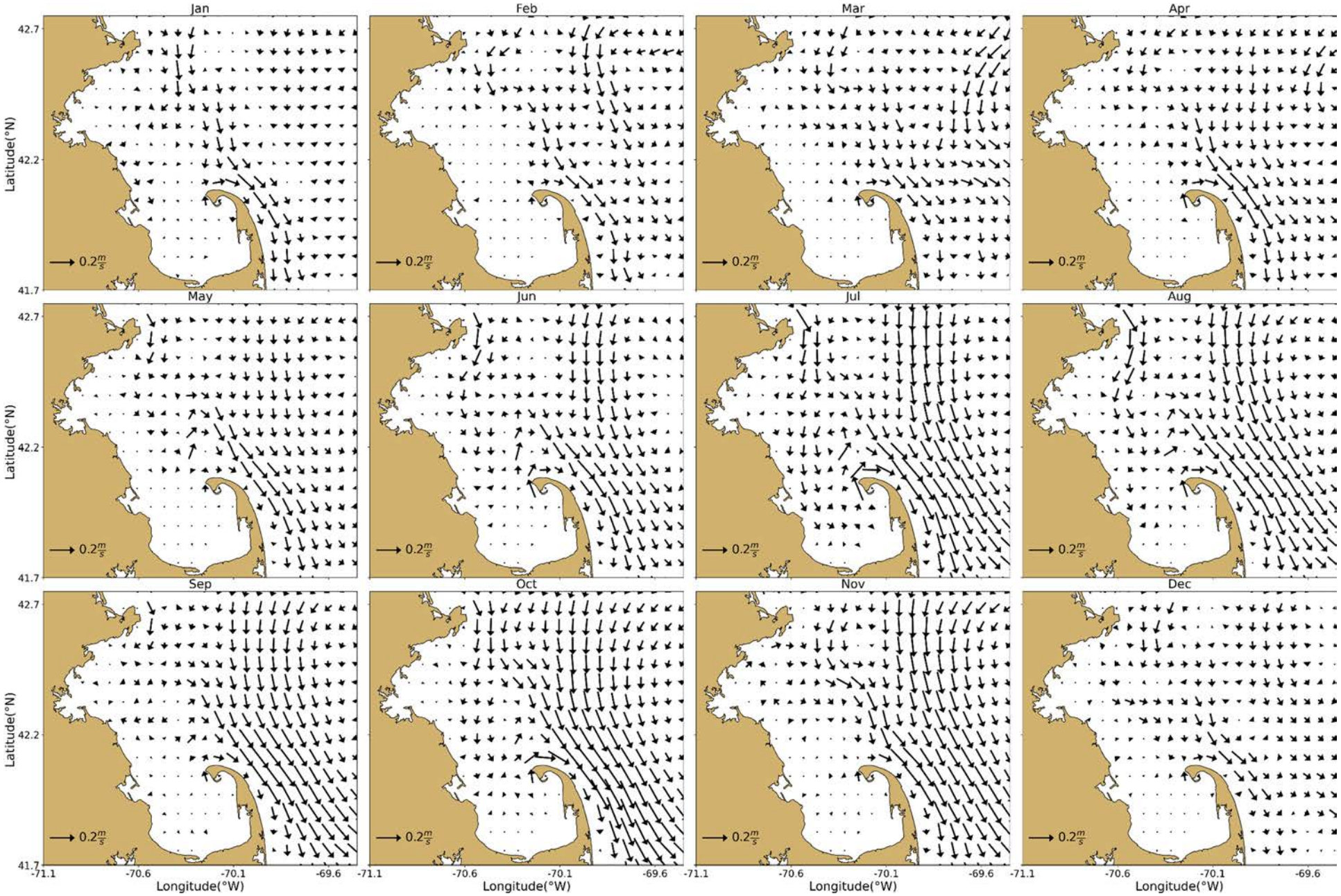

Figure 4-14 Model currents, monthly-mean spatial structure, 15 m deep.

5 Water Quality Model

5.1 Verification of model performance

To demonstrate that the water quality model performance during 2021 was comparable to the performance for the calibration and validation period 2012-2016, skill metrics were calculated and plotted on Taylor diagrams as in Section 4. Station N21 directly on top of the outfall was excluded, as a comparison to field data is of limited value for this station, as discussed by Deltares (2021). Information on how to interpret Taylor diagrams can be found in section 4.1 (box “How to read a Taylor diagram”).

Taylor diagrams are plotted for the light extinction coefficient and dissolved inorganic nitrogen (DIN) in Figure 5-1, and for chlorophyll a and DO in Figure 5-2. These parameters were selected because they are key drivers of ecosystem functioning. Statistics for the period 2012-2016 are plotted on the left side and statistics for 2021 on the right side. For reference, the 2017 simulation report (Deltares, 2022a) provides, in its Appendix A, similar diagrams for the individual years 2012 to 2016. The plots show statistics for three clusters of monitoring stations: Northern Bay stations (F22, N01, N04, N07, F10, N18, F15, F13 and F23), Southern Bay and Cape Cod stations (F06, F29, F01 and F02), and harbor stations (024, 140, 142, 139 and 124) (see Figure 2-4 for station locations).

Extinction skill metrics (Figure 5-1) for 2021 show similar unbiased RMSE errors and variability compared to the calibration period 2012-2016. Correlation coefficients are in the range of those from the validation period (individual years 2012-2016). As discussed in section 5.2.1, the light extinction coefficients for both model and data are generally low and fall within a narrow range overall, and even small deviations can cause larger scatter, resulting in poor correlation coefficients. Therefore, this is not an issue of concern regarding the skill of the model.

Skill metrics for DIN (Figure 5-1) include smaller dimensionless unbiased RMSE errors than 2012-2016 for most stations. Correlations for surface concentrations are better than 2012-2016. Variability of surface and bottom concentrations for 2021 is largely similar to 2012-2016.

Skill metrics for chlorophyll a (Figure 5-2) in 2021 are more scattered than for previous years (2017-2020), especially in terms of variability. Correlations are weak or negative, and near-surface chlorophyll a variability is largely similar to 2012-2016.

DO skill metrics (Figure 5-2) are similar to 2012-2016. The model performs very well for surface concentrations at Northern and Southern stations. Variability is overall underestimated by the model near the seabed but still comparable to 2012-2016 and previous years (2017-2020).

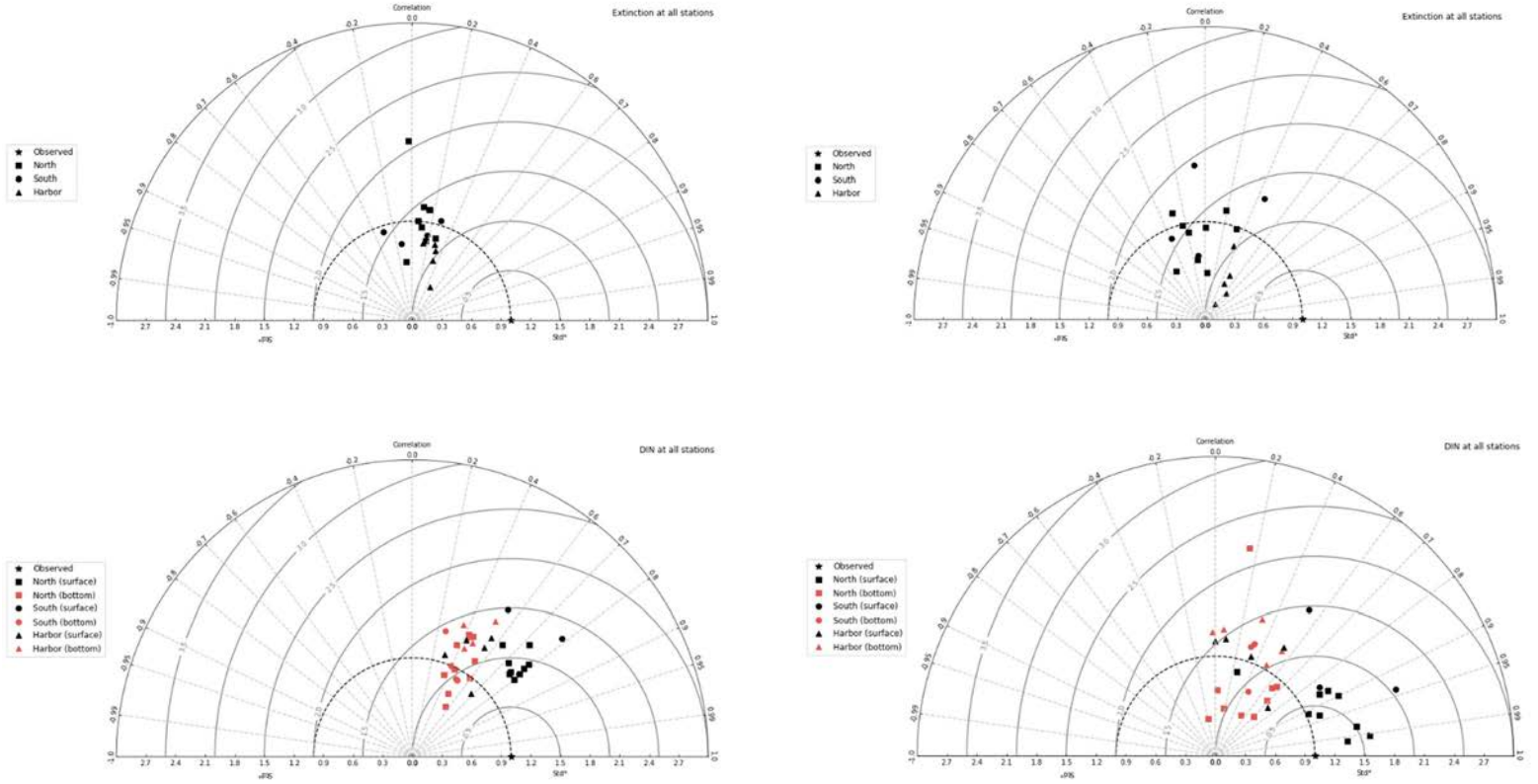

Figure 5-1 Taylor diagrams for MWRA vessel-based survey observations. Top panels show the parameter Extinction and bottom panels Dissolved Inorganic Nitrogen. Left panels show results for the simulation period 2012-2016 and right panels for the year 2021.

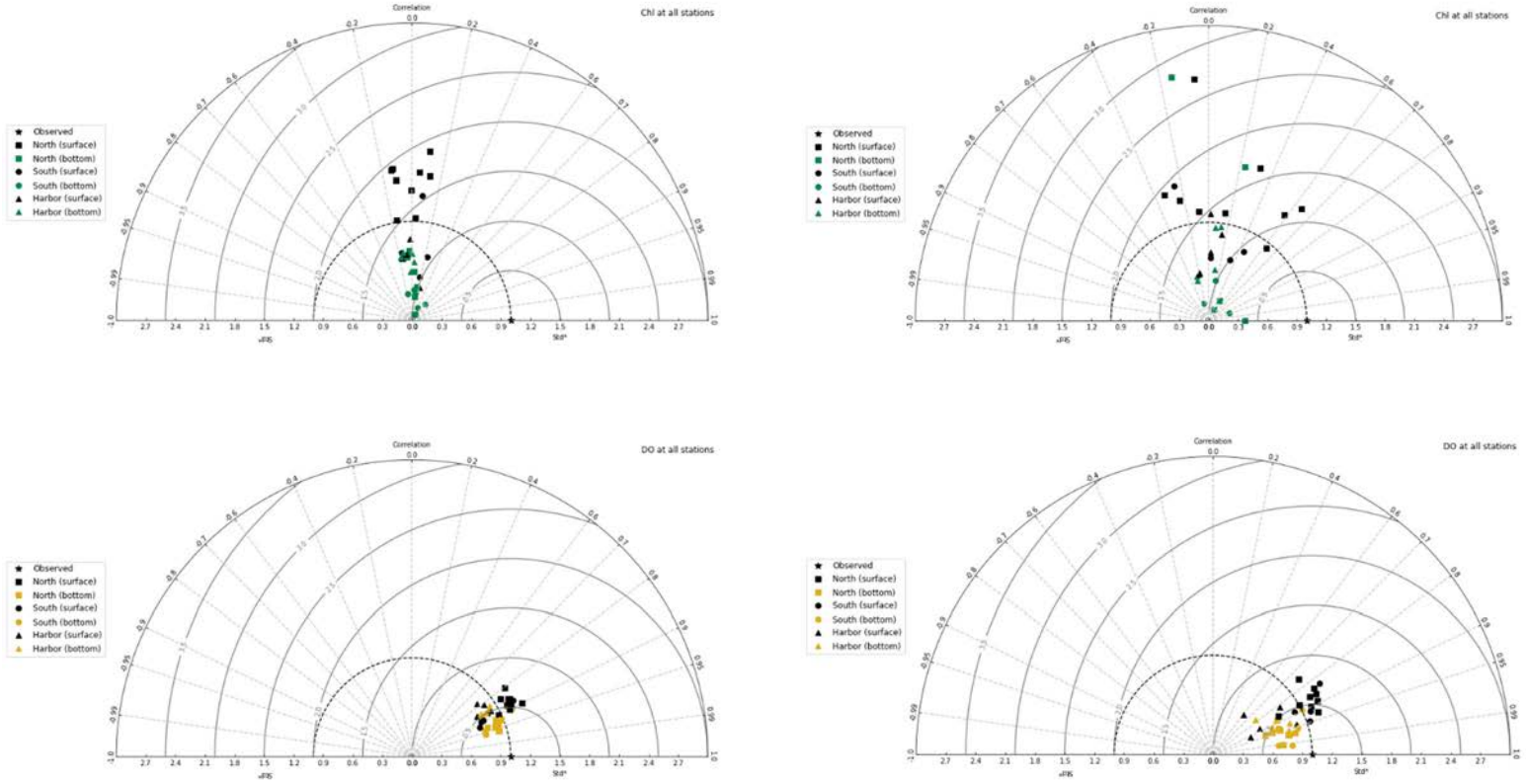

Figure 5-2 Taylor diagrams for MWRA vessel-based survey observations. Top panels show the parameter Chlorophyll a and bottom panels Dissolved Oxygen. Left panels show results for the simulation period 2012-2016 and right panels for the year 2021.

5.2 Model-observation comparisons

In this section model-observation comparisons in the same format as for the hydrodynamic model (Section 4) are provided. For time series plots, a 3-day moving average is applied to the model outputs to smooth high-frequency variability.

To assess the simulation spatially, vertical transects have been plotted along North-South and West-East transects (Figure 2-4). Model results in these figures are 5-day averages centered around the sampling date indicated in each plot.

5.2.1 Light extinction

Measured extinction for the year 2021 (Figure 5-3) ranged from 0.1 to 0.5 per m at all stations, except at F23, near the harbor, where it ranged between 0.3 and 0.7. This was similar to previous years for which higher and more variable extinction was observed at harbor stations (e.g. Zhao et al., 2017). The model reproduced the extinction range and variability well at most stations. The relatively narrow range of light extinction coefficients indicates that light penetration is generally high (approximately 10 m or greater, when Kd is lower than 0.5 per m). Conditions near the harbor tend to be more variable, likely influenced by both wind-induced resuspension and suspended sediments loading from freshwater inflows. The model does a reasonable job of capturing these events. For example, the higher light extinction coefficient observations at F13 and F23 around Day 300 are reproduced well by the model. This period follows a period of sustained wind gust (see Figure 4-12), and higher extinction therefore most likely resulted from a wind-induced resuspension event.

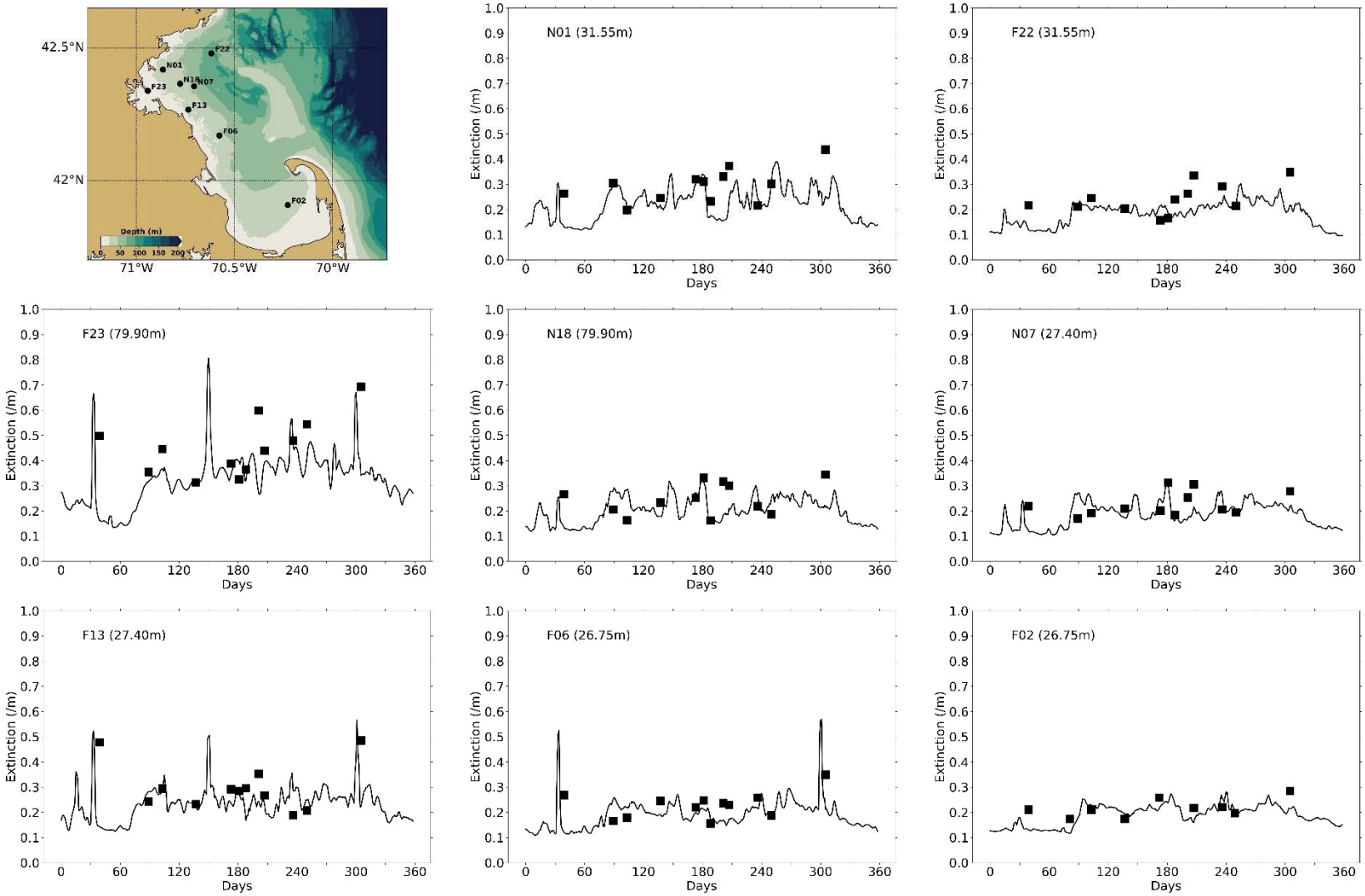

Figure 5-3 Extinction time series, model-observation comparison for 2021. Model: lines. MWRA vessel-based survey observations: symbols.

5.2.2 Dissolved inorganic nitrogen

Seasonal variations of surface and bottom DIN concentrations in 2021 were similar to those observed and simulated for previous years (Figure 5-4). Surface and bottom concentrations were similar in winter, when the water column was well mixed. Surface DIN concentrations declined at the end of winter and were depleted from April to October, before increasing again mid-fall. Bottom concentrations remained around winter levels in the locations farther offshore (F22, N07), but nearshore locations (F23) followed a similar pattern as the surface concentrations. The model generally reproduced these observed seasonal variations and vertical differences. Bottom DIN concentrations in Cape Cod Bay (F02) were however slightly overestimated, which could be linked to the underestimation of phytoplankton (lower simulated uptake in the model). Observed variations at intermediate depths in the water column were generally well reproduced by the model except for at N18 where the model underestimated a few deeper observations of higher DIN concentrations (Figure 5-5).

The model reproduced the year-round outfall DIN signature that was evident in the data, which showed elevated concentrations at depth near the outfall during the stratified months of April/May through October (Figure 5-6). During the other months, higher DIN concentrations were evident throughout the water column in vicinity of the outfall (station N21). This was similar to observations and simulations from previous years. In the model during stratified periods, the highest concentrations at N21 (directly over the outfall) were always simulated at the bottom of the water column, while the highest measured concentrations were sometimes higher up in the water column (e.g., May 18th, June 23rd, July 27th, August 25th and September 8th). This aspect of the model directly over the outfall was discussed by Deltares (2021).

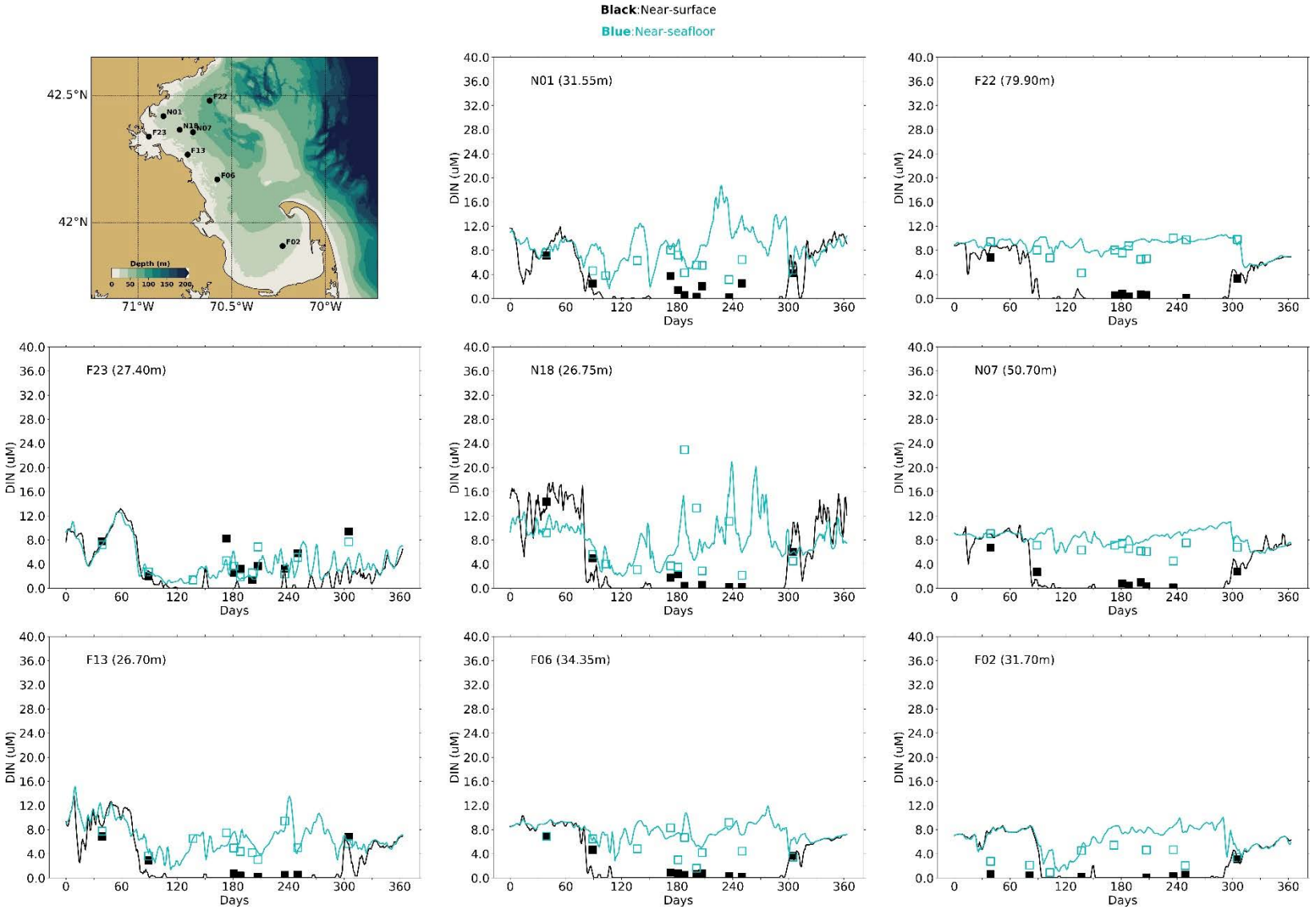

Figure 5-4 Dissolved Inorganic Nitrogen time series, model-observation comparison near surface (black) and seafloor (cyan). Model results: lines. MWRA vessel-based survey observations: symbols.

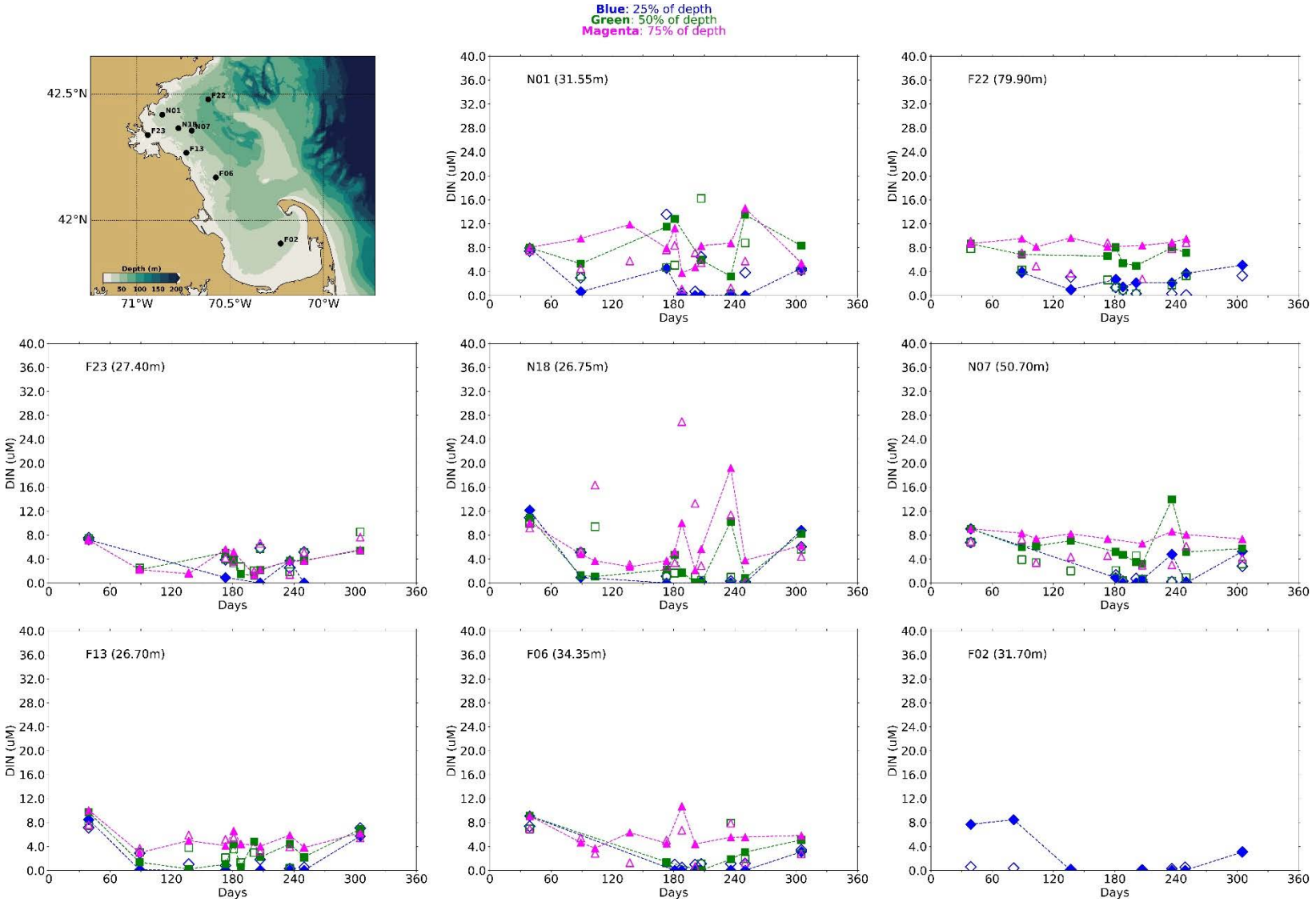

Figure 5-5 Dissolved Inorganic Nitrogen time series, model-observation comparison within water column (between surface and seafloor). Model results: lines and full symbols. MWRA vessel-based survey observations: open symbols.

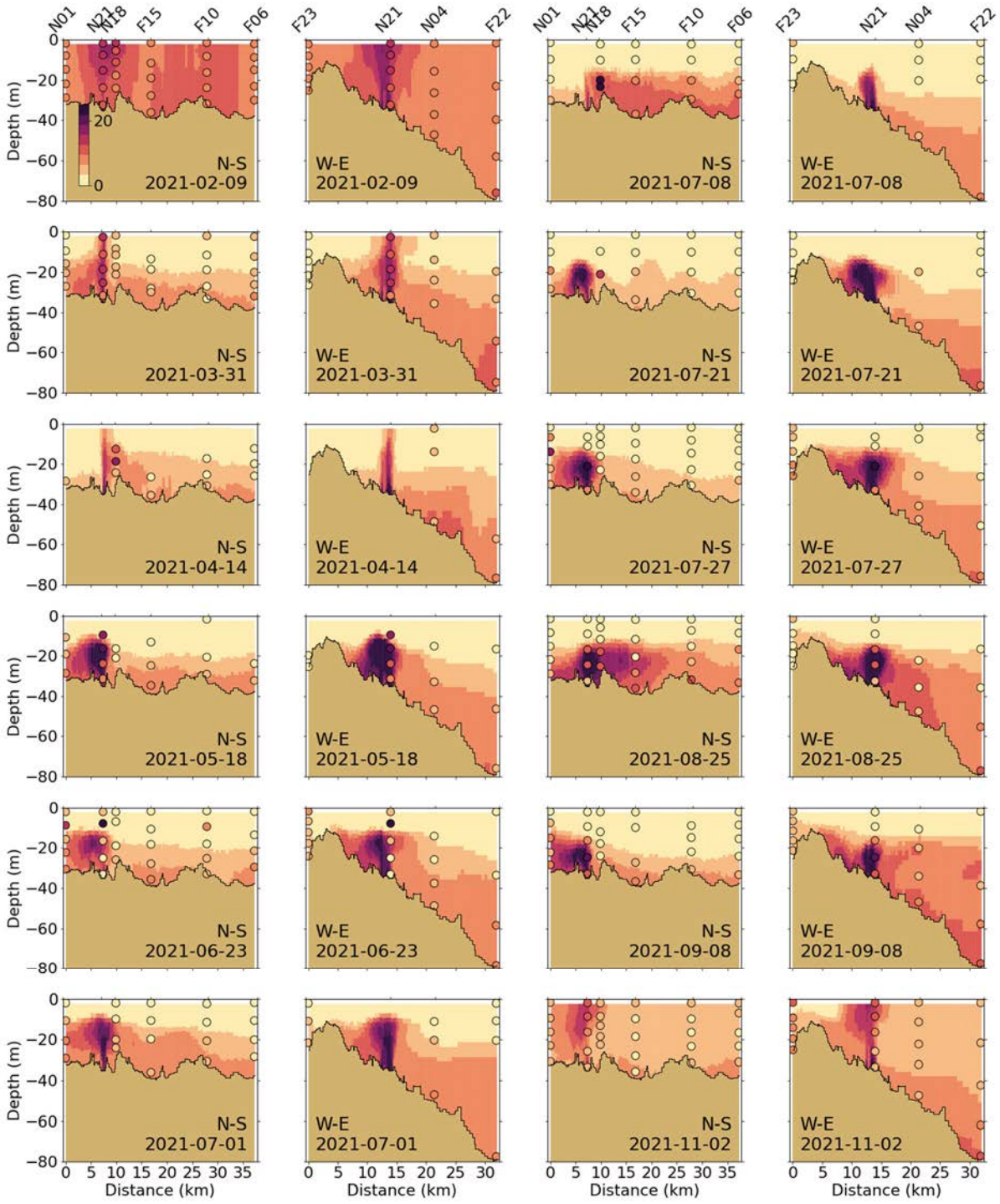

Figure 5-6 Dissolved Inorganic Nitrogen (µM) for 2021 along North-South (N-S) and West-East (W-E) transects (Figure 2-4). MWRA measurements are plotted with round symbols. Model results are 5-day averages around sampling date.

5.2.3 Chlorophyll a

Seasonal variations of chlorophyll a observations in 2021 showed two distinct peaks in chlorophyll a at most locations, one centered around late March and another in mid-July (e.g. stations F13, F22, F23, and N07 see Figure 5-7). In the spring months, biomass production is evident throughout the water column in the nearshore locations and extends deeper than 20 m farther offshore (see Figures 5-8 and 5-9). These are consistent with the observations of the photic depth discussed earlier with the light extinction coefficient (see Section 5.2.1). Once stratification sets in around late spring to early summer, the top 10 to 15 m are devoid of nutrients because of the spring production. Therefore, biomass production in summer months is largely limited to the lower edge of the photic zone where DIN still diffuses up from the lower portions of the water column (compare Figures 5-6 and 5-9).

The model simulated the higher observed chlorophyll a peaks in late winter/early spring and at the end of summer (e.g., stations N01, F22, and N18), but did not fully capture the observed mid-summer chlorophyll a peak (e.g., stations N01, F22, F06, and N07) (Figure 5-7). As observed already in 2019 and 2020, this end-of-summer-bloom is dominated by dinoflagellates. Figure 5-20 shows that the model does simulate a peak of dinoflagellate biomass in the end of summer (Figure 5-20), but most likely underestimates the mid-summer biomass from a *Alexandrium catenella* bloom that occurred in late June and July, or the corresponding chlorophyll a concentration (chlorophyll-to-carbon ratio for dinoflagellates in the model is 30% lower than for diatoms in the model). As for previous years, near-surface simulated concentrations were usually in the same range as observations. Bottom chlorophyll a measurements appear similar to previous years. In Cape Cod Bay (station F02), the surface concentrations also exceeded the bottom concentrations for most of the year in the model, while some observed bottom concentrations in summer were higher than near the surface. As in the simulations for previous years, simulated bottom chlorophyll a was underestimated. Chlorophyll a concentrations in summer and fall were slightly underestimated at the observation stations at intermediate depths as well (Figure 5-7 and Figure 5-8).

Simulated chlorophyll a concentrations decreased eastward from the coast (Figure 5-9). Early spring increase (March 31) occurred throughout the water column as it was relatively well mixed. During the months in which stratification occurred, simulated bottom chlorophyll a remained low and highest values occurred in the subsurface, near the bottom edge of the photic depth. This is consistent with the depth of highest measured concentrations in this period (e.g., June 23rd).

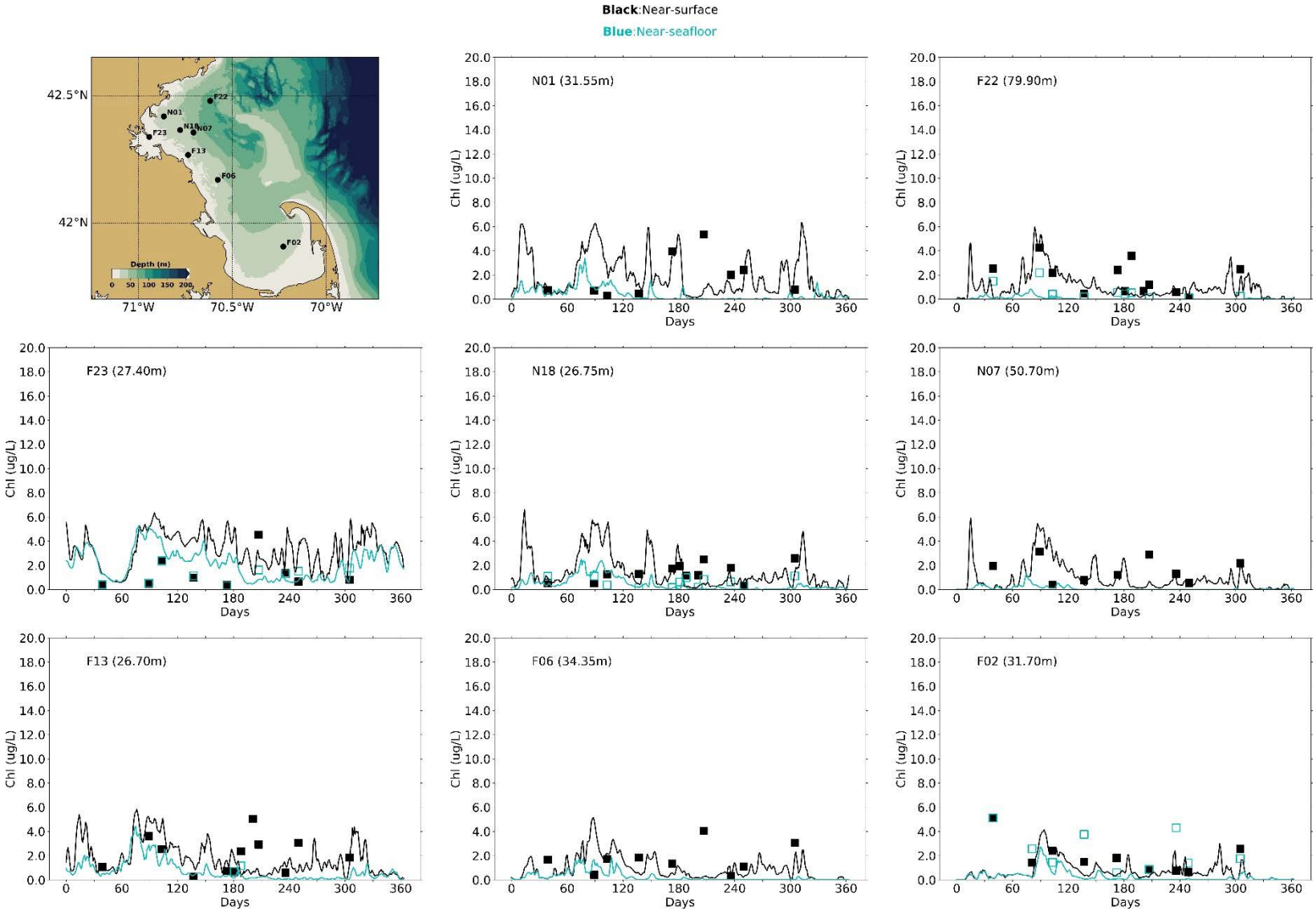

Figure 5-7 Chlorophyll a time series, model-observation comparison near surface and seafloor. Model results: lines. MWRA vessel-based survey observations: symbols.

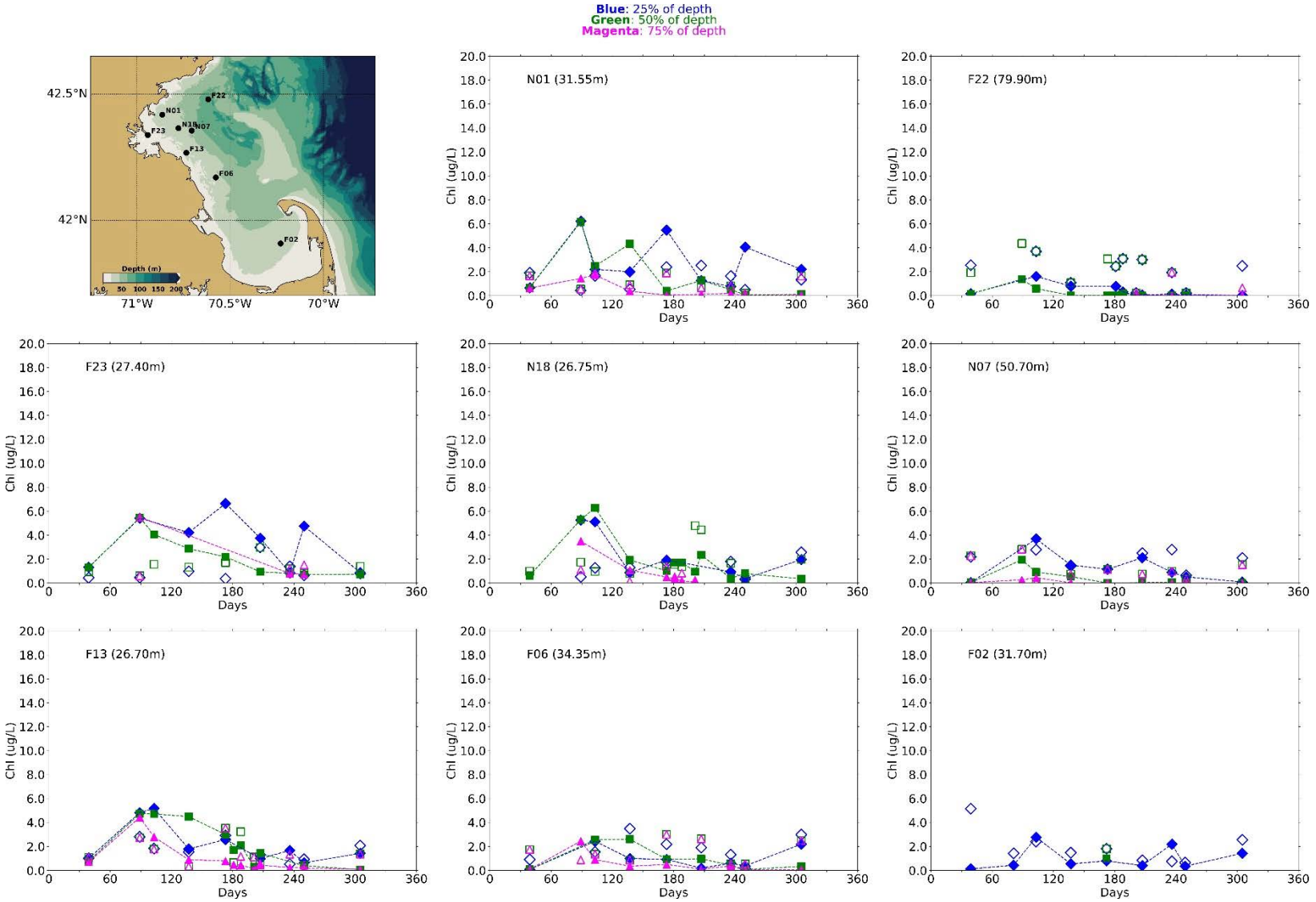

Figure 5-8 Chlorophyll a time series, model-observation comparison within water column (between surface and seafloor). Model results: lines and full symbols. MWRA vessel-based survey observations: empty symbols.

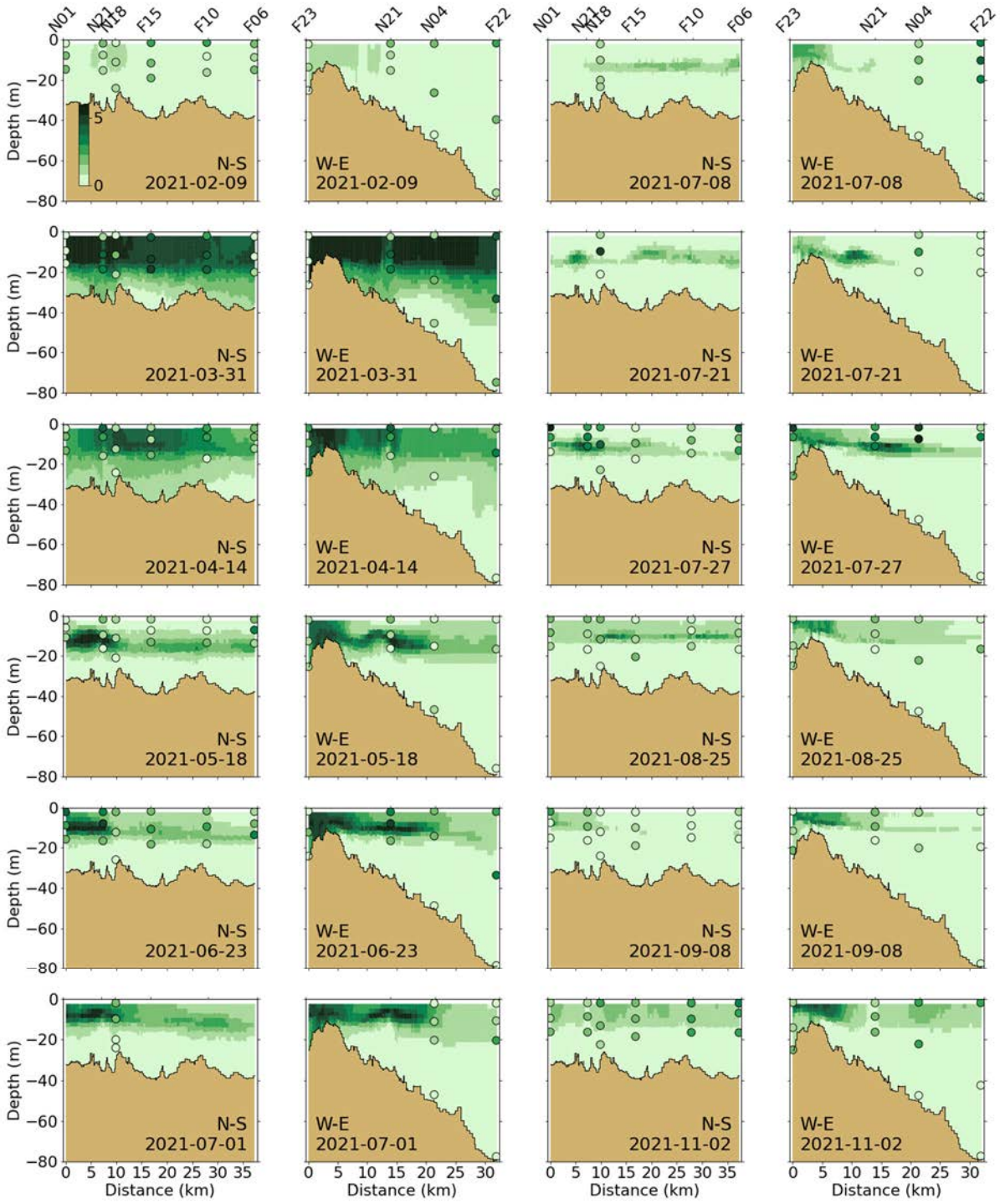

Figure 5-9 Chlorophyll a (µg/L) for 2021 along North-South (N-S) and West-East (W-E) transects (Figure 2-4). MWRA measurements are plotted with round symbols. Model results are 5-day averages around the sampling date.

5.2.4 Particulate organic carbon

POC observations showed higher concentrations in summer months with the upper layers exhibiting higher concentrations than the bottom (Figures 5-10 through 5-12). POC peaks are consistent with the timing of the runoff events and the biomass production discussed in the previous section.

The model seemed to generally capture POC concentration ranges and vertical gradients at the plotted locations (Figure 5-10 and Figure 5-11). As for previous years, POC concentrations were overestimated at F23, closer to the harbor. The model moreover does not capture the observed peak end of July at stations F22, N18, N07 and F06. This is consistent with the discussion in Section 5.2.3 about the model potentially missing or underestimating the phytoplankton peak in that period.

Model predicted POC concentrations decreased from the coast eastward (Figure 5-12). The signature of the outfall was not visible along either the North-South or the West-East transects. This was consistent with the fact that the MWRA outfall only represented a small part of the total non-oceanic OC inputs to the study area (Figure 3-6). Highest simulated concentrations occurred in July and August in the Northwest. In deeper areas, during periods of stratification, concentrations are higher in the subsurface, most likely due to higher phytoplankton biomass.

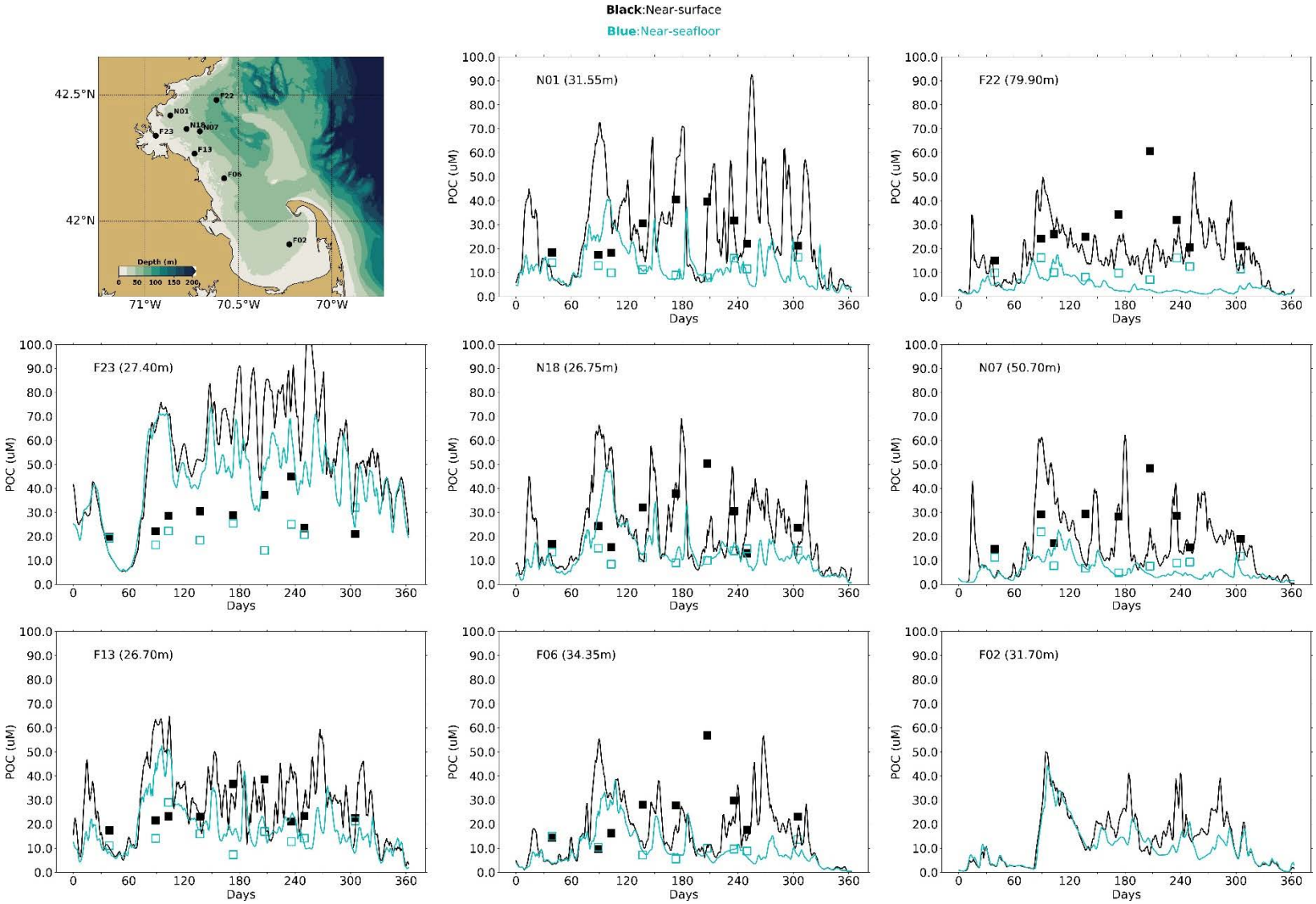

Figure 5-10 Particulate Organic Carbon time series, model-observation comparison near surface and seafloor. Model results: lines. MWRA vessel-based survey observations: symbols.

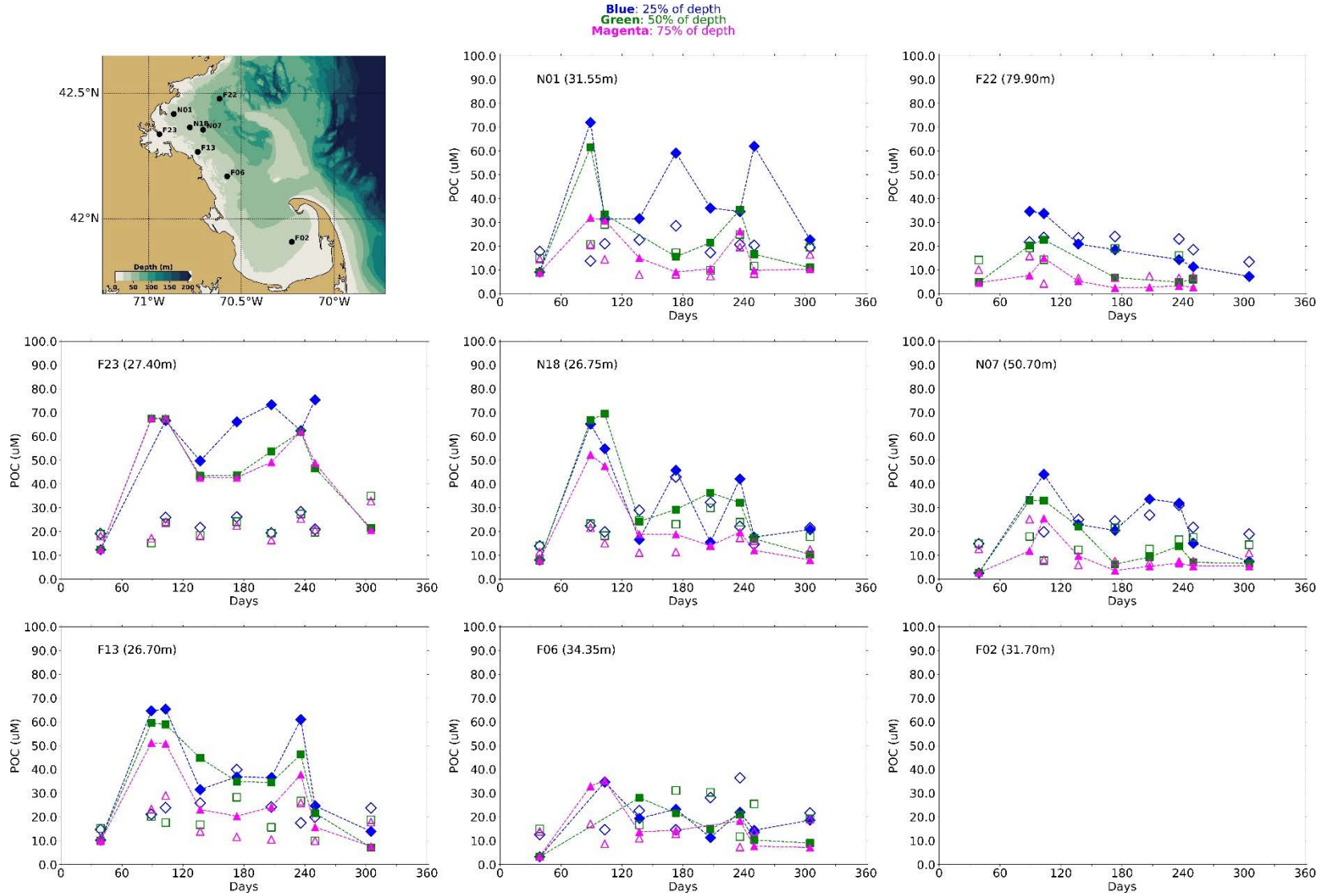

Figure 5-11 Particulate Organic Carbon time series, model-observation comparison within water column (between surface and seafloor). Model results: lines and full symbols. MWRA vessel-based survey observations: empty symbols.

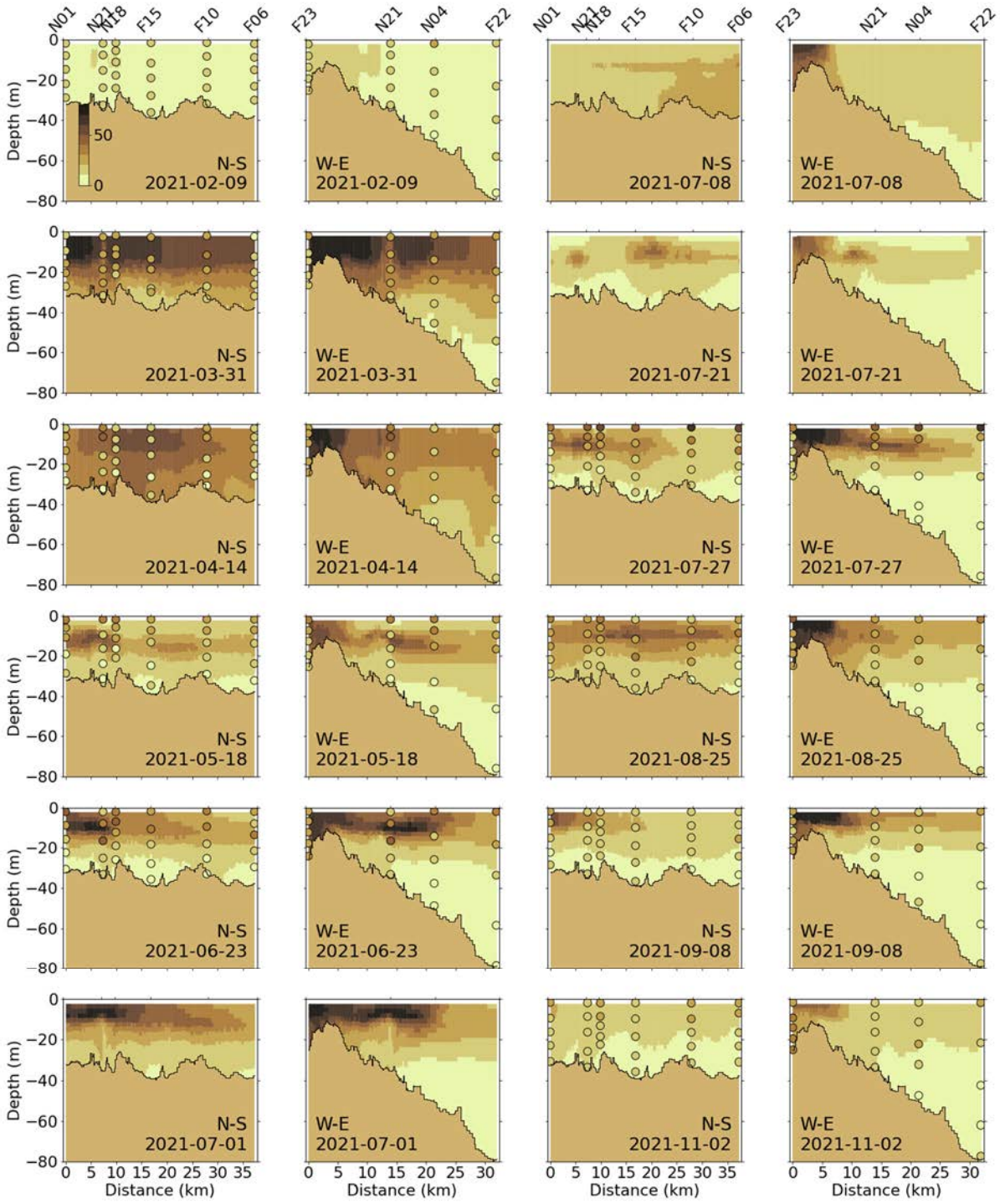

Figure 5-12 Particulate Organic Carbon (µM) for 2021 along North-South (N-S) and West-East (W-E) transects (Figure 2-4). MWRA measurements are plotted with round symbols. Model results are 5-day averages around the sampling date.

5.2.5 Dissolved oxygen

The 2021 seasonal variations of near-surface DO concentrations were well reproduced, with maximum concentrations observed at the end of winter or beginning of spring and decreasing until the end of summer before rising again (Figure 5-13). While winter concentrations at the surface and the bottom were comparable, bottom concentrations dropped lower at the end of the summer and beginning of fall. Differences between top and bottom concentrations reached about 2 mg L^{-1} at the end of October at several stations. Field measurements reported historic minima of DO at many stations in the summer. The field measurements included unusually low bottom DO concentrations at stations N01, F22, N07 and F13 at the end of the summer (more than 2 mg L^{-1} lower than at the surface). The model does not capture these lowest concentrations at the plotted stations. The model-observation comparison at intermediate water depths showed similar behavior. However, in summer, the model slightly overestimated concentrations, and in fall, the decrease in DO throughout the water column was underestimated (Figure 5-14).

At the A01 mooring station, the model reproduced the general seasonal pattern in the observed DO well, although it overestimated the end-of-fall minimum by about 1.5 mg L^{-1} (Figure 5-15).

As for previous years, the North-South and West-East cross-section plots show that DO generally had weak vertical gradients (Figure 5-16). Concentrations were higher at the end of winter and beginning of spring and decreased until fall. The model reproduced the elevated DO observations in the subsurface, where phytoplankton biomass was present, at the end of spring or early summer. Several low DO observations (about 6 mg L^{-1}) in deep water were not fully captured by the model (for example, see N01, F22 and N07). The overestimation of DO in late summer and fall may reflect the model's underprediction of summer dinoflagellate bloom event in the offshore locations when the bloom termination and subsequent detrital decomposition in the water column likely caused the lower observed DO.

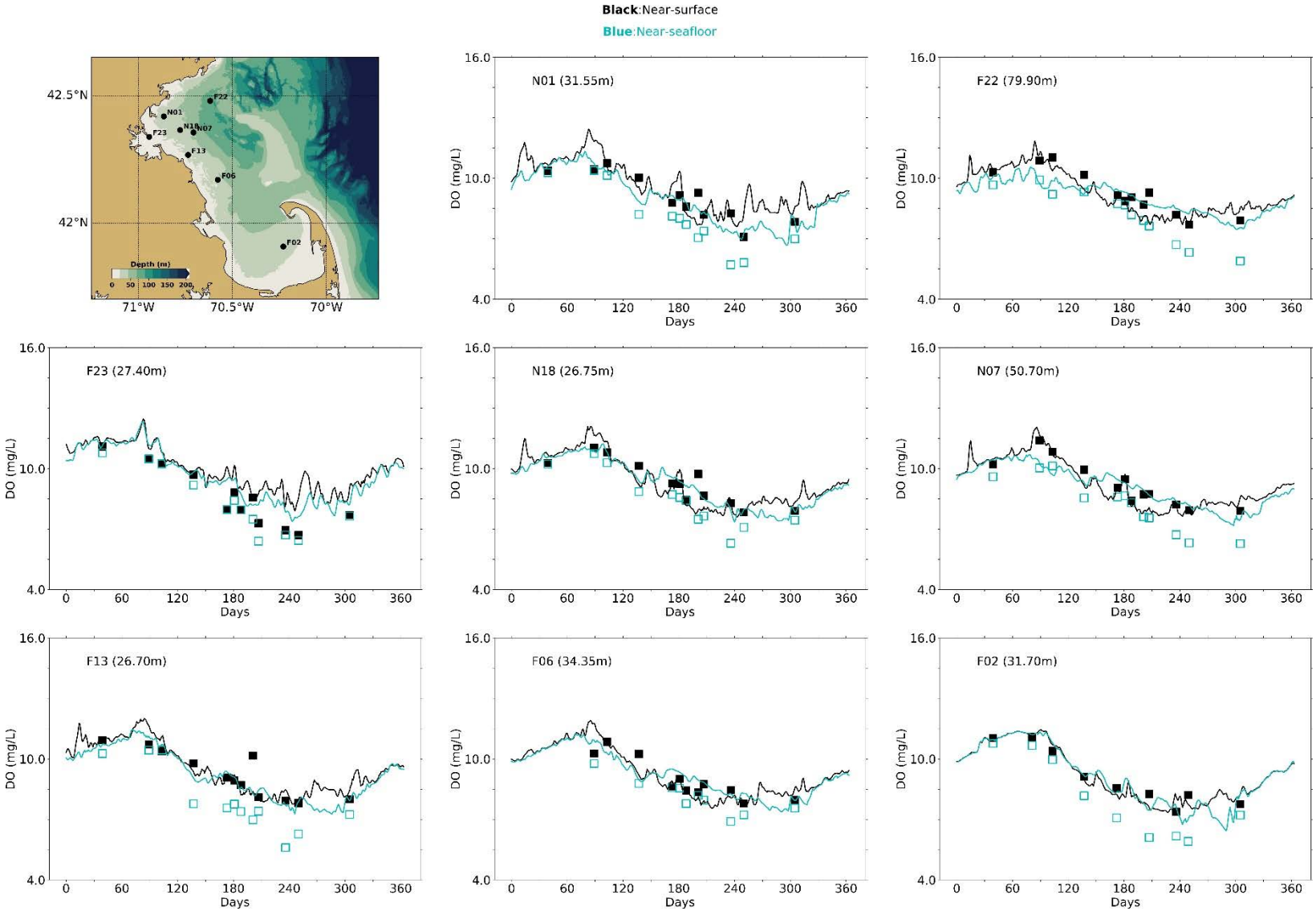

Figure 5-13 Dissolved Oxygen time series, model-observation comparison near surface and seafloor. Model results: lines. MWRA vessel-based survey observations: symbols.

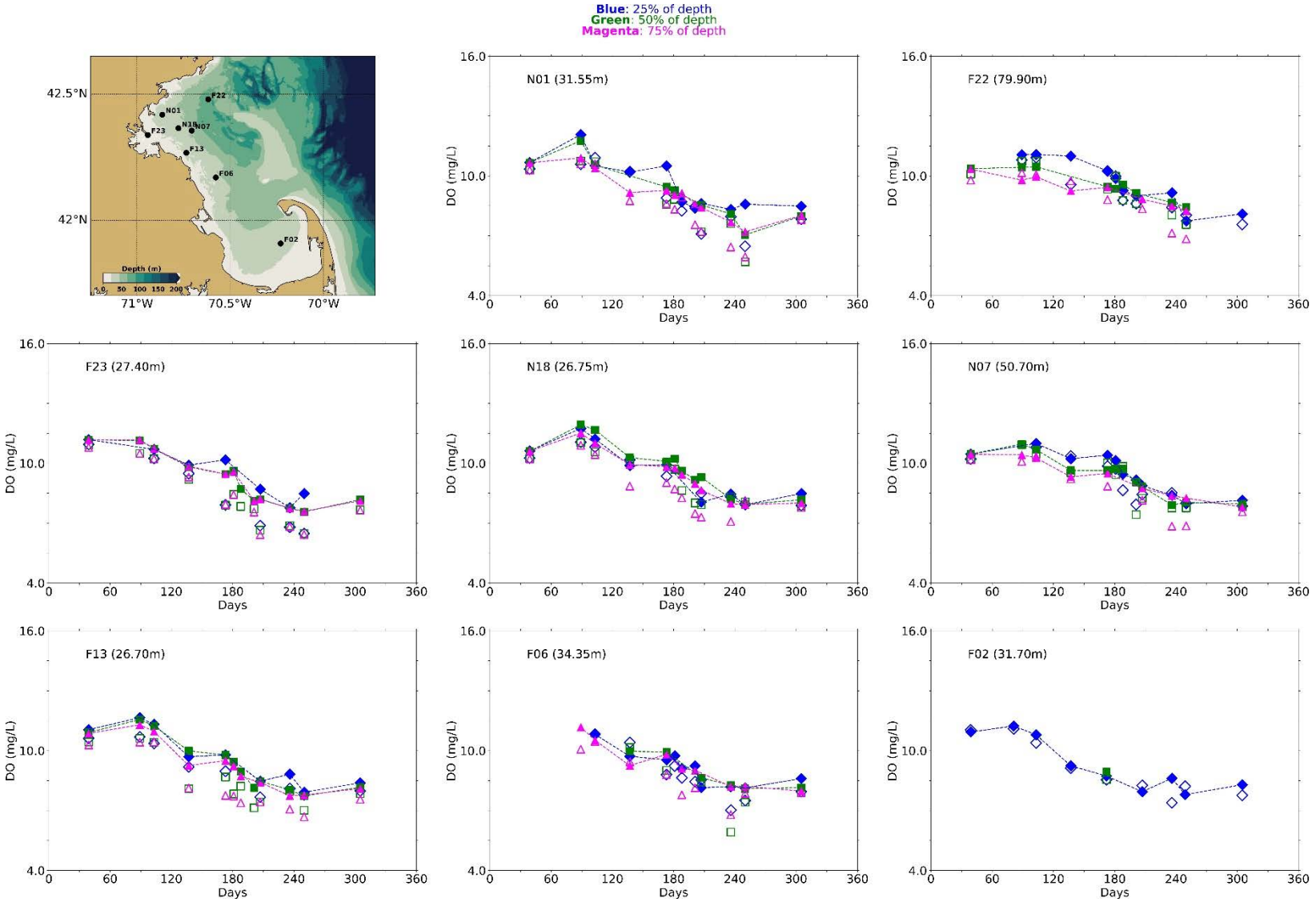

Figure 5-14 Dissolved Oxygen time series, model-observation comparison in water column. Model results: lines and full symbols. MWRA vessel-based survey observations: open symbols.

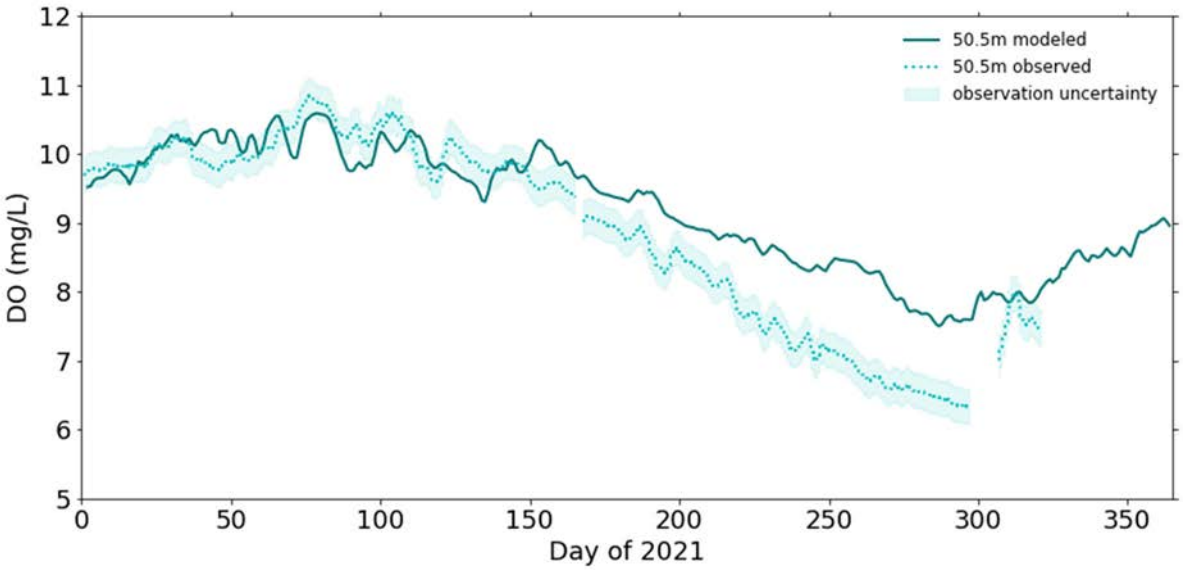

Figure 5-15 Dissolved Oxygen time series 50.5m deep at A01 mooring site, model-observation comparison for 2021.

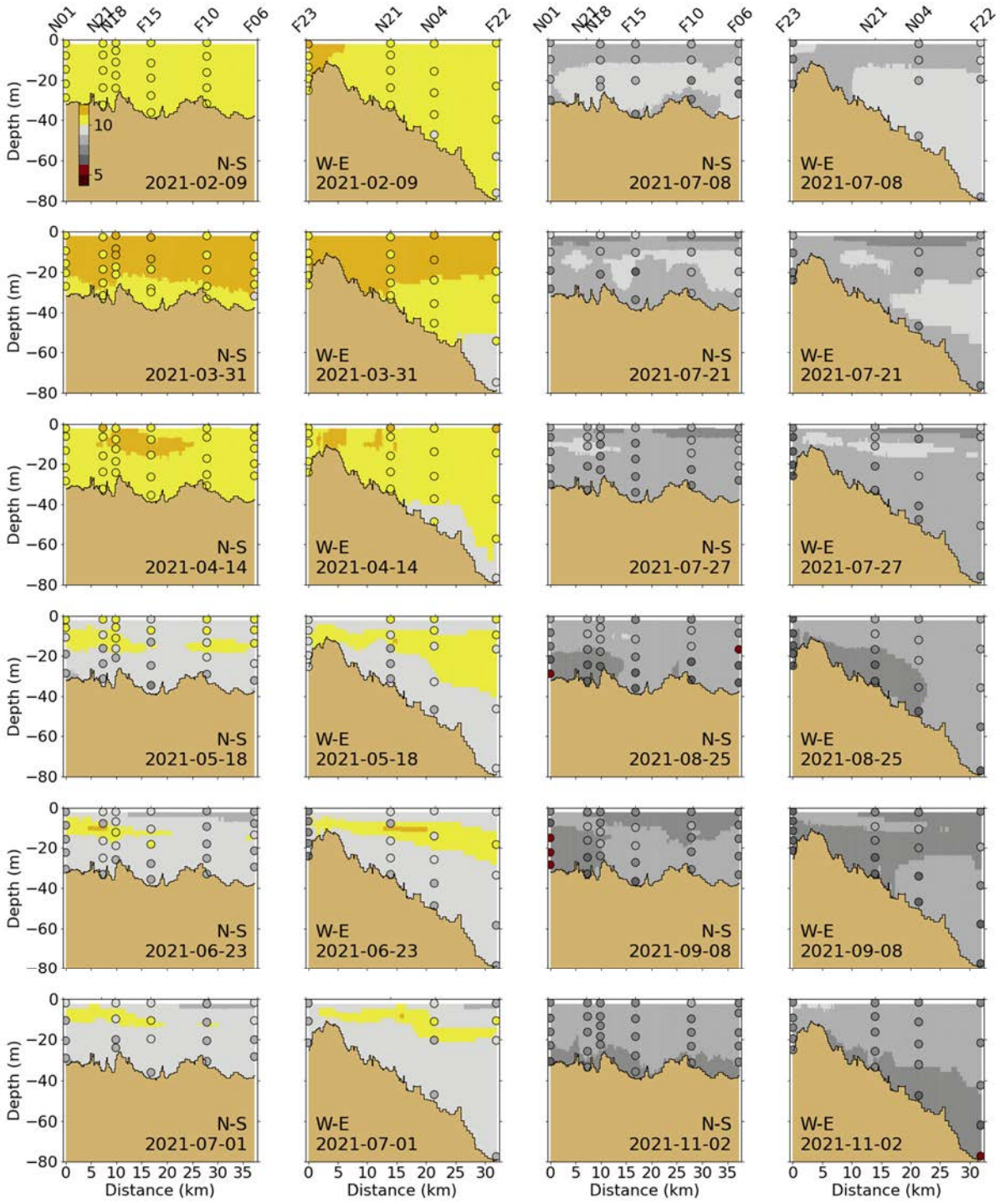

Figure 5-16 Dissolved Oxygen (mg/L) for 2021 along North-South (N-S) and West-East (W-E) transects (Figure 2-4). MWRA measurements are plotted with round symbols. Model results are 5-day averages around the sampling date.

5.2.6 Primary production

Simulated primary production was compared to historical measurements at three monitoring locations (Figure 5-17). Box whiskers represent the 9th, 25th, 50th, 75th, and 91st percentiles of primary productions observations over the period 1995-2010 (Keay et al., 2012). Primary production was in the range of historical measurements for the entire year 2021 at all three stations. Highest simulated primary production at F23 occurred in September, slightly later than for previous years.

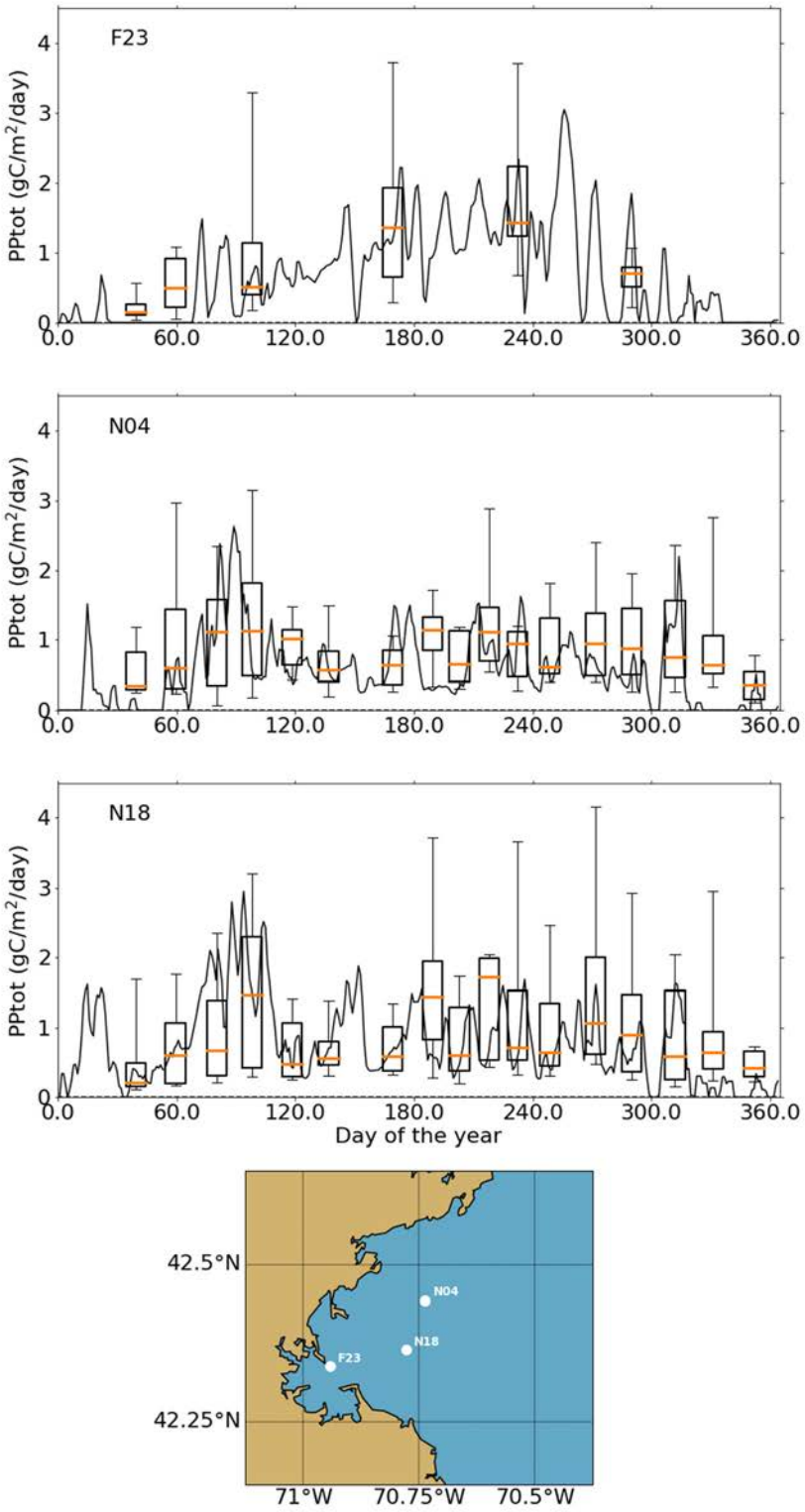

Figure 5-17 Simulated (lines; 2021) and observed (box-whiskers; 1995-2010) primary production.

5.2.7 Sediment fluxes

Sediment NH4 fluxes (Figure 5-18) and sediment oxygen demand (Figure 5-19) outputs from the model were compared to measurements from the 2001-2010 period from Tucker et al. (2010) at stations located in Boston Harbor and Massachusetts Bay using plots in the same format as Figure 5-17.

Simulated sediment fluxes were low in winter and peaked in the summer due to higher temperatures favorable to biogeochemical activity, which mineralizes organic matter in the sediment. Sediment fluxes were higher in the harbor area than in Massachusetts Bay, which was captured by the model. Results for the year 2021 were similar to those from the individual years 2012 to 2016. These were mostly in the range of historical measurements, except for NH_4 sediment fluxes at the Mass Bay stations (MB01, MB03 and MB05). This discrepancy is related to the simplified representation of sediment biogeochemical processes (see Deltares, 2021).

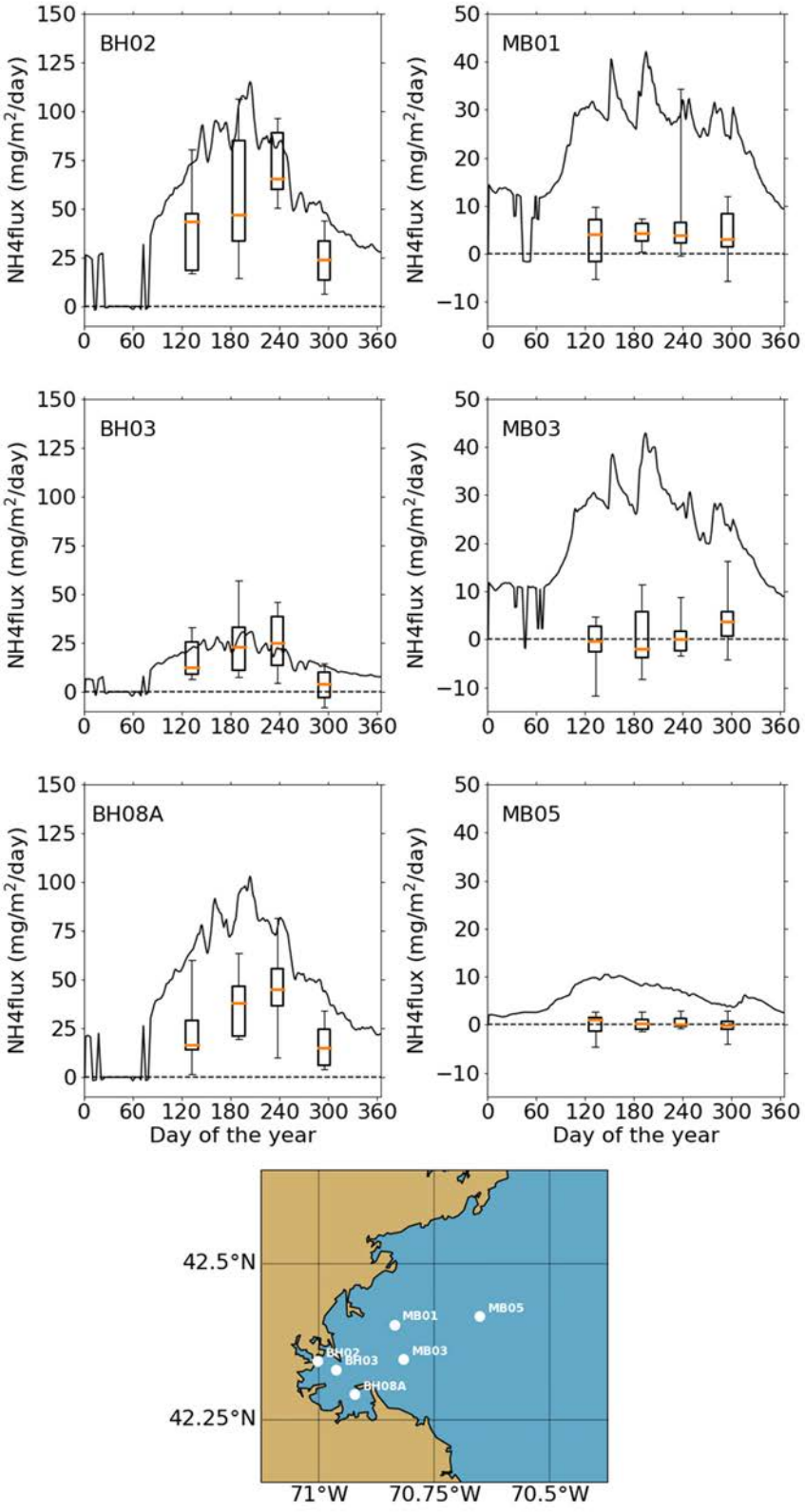

Figure 5-18 Simulated (line; 2021) and observed (box-whiskers; 2001-2010) sediment flux of ammonium. Note change of scale between the Boston Harbor stations (left) and Mass Bay stations (right).

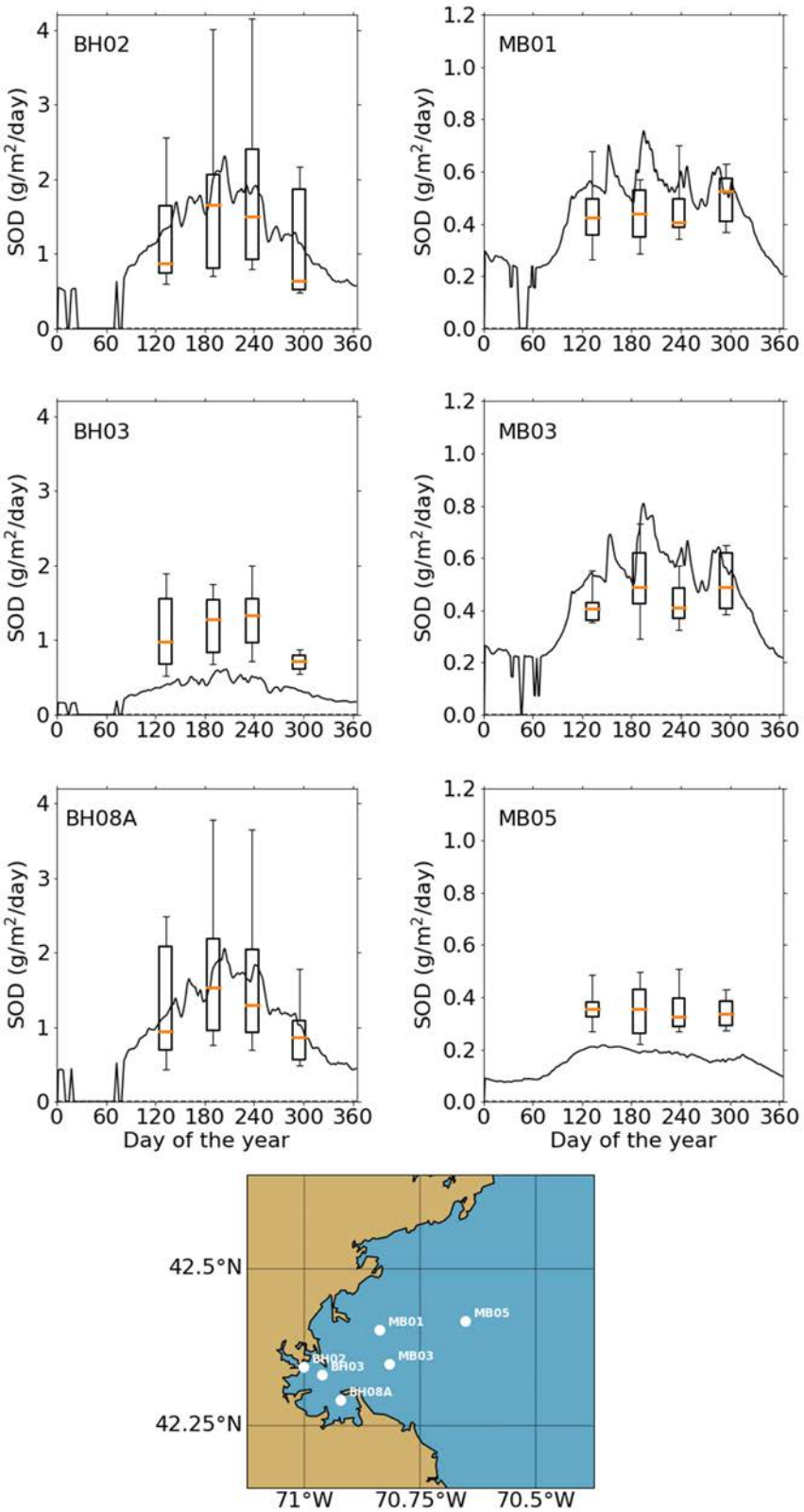

Figure 5-19 Simulated (line; 2021) and observed (box-whiskers; 2001-2010) sediment oxygen demand. Note change of scale between the Boston Harbor stations (left) and Mass Bay stations (right).

5.3 Phytoplankton community composition

Model phytoplankton community/species composition was not validated against field observations during model setup and calibration/validation. However, it is of interest to verify that its main characteristics in the model are not inconsistent with general patterns known to characterize the bays, based on monitoring observations.

The phytoplankton sub-module (BLOOM) simulated the dynamics of 4 functional groups and their adaptation to changing environmental conditions (i.e., light and nutrient limitation). BLOOM simulates the rapid shifts in phytoplankton communities due to these changes, using linear programming to optimize whole-community net primary production (Los, 2009). Simulated phytoplankton groups include: diatoms, dinoflagellates, other marine flagellates, and *Phaeocystis*. Their parameterization was initially based on that used in the North Sea eutrophication model (Blauw et al., 2009) and tuned during the BEM calibration process to better represent chlorophyll a as well as observed PON:POC ratios at MWRA monitoring locations (see Appendix B of Deltares, 2021).

Figure 5-20 shows the share of the different simulated phytoplankton groups in the total phytoplankton biomass near the water surface. Although total phytoplankton biomass temporal dynamics differed from station to station for the year 2021, phytoplankton composition showed similar temporal patterns. Marine diatoms dominated in the winter period and were succeeded in spring by marine flagellates. Dinoflagellates clearly dominated from June to October. This is similar to the simulated successions in communities for the previous years (2017-2020).

In 2021 increases in spring chlorophyll was observed, which along with changes in nutrient concentrations, suggests a possible *Phaeocystis* bloom, though the *Phaeocystic* abundances were relatively low (Libby et al., 2022). The simulated *Phaeocystis* biomass in the model showed noticeable levels during the spring flagellate bloom period (April-May), at all stations except for F23, near the harbor.

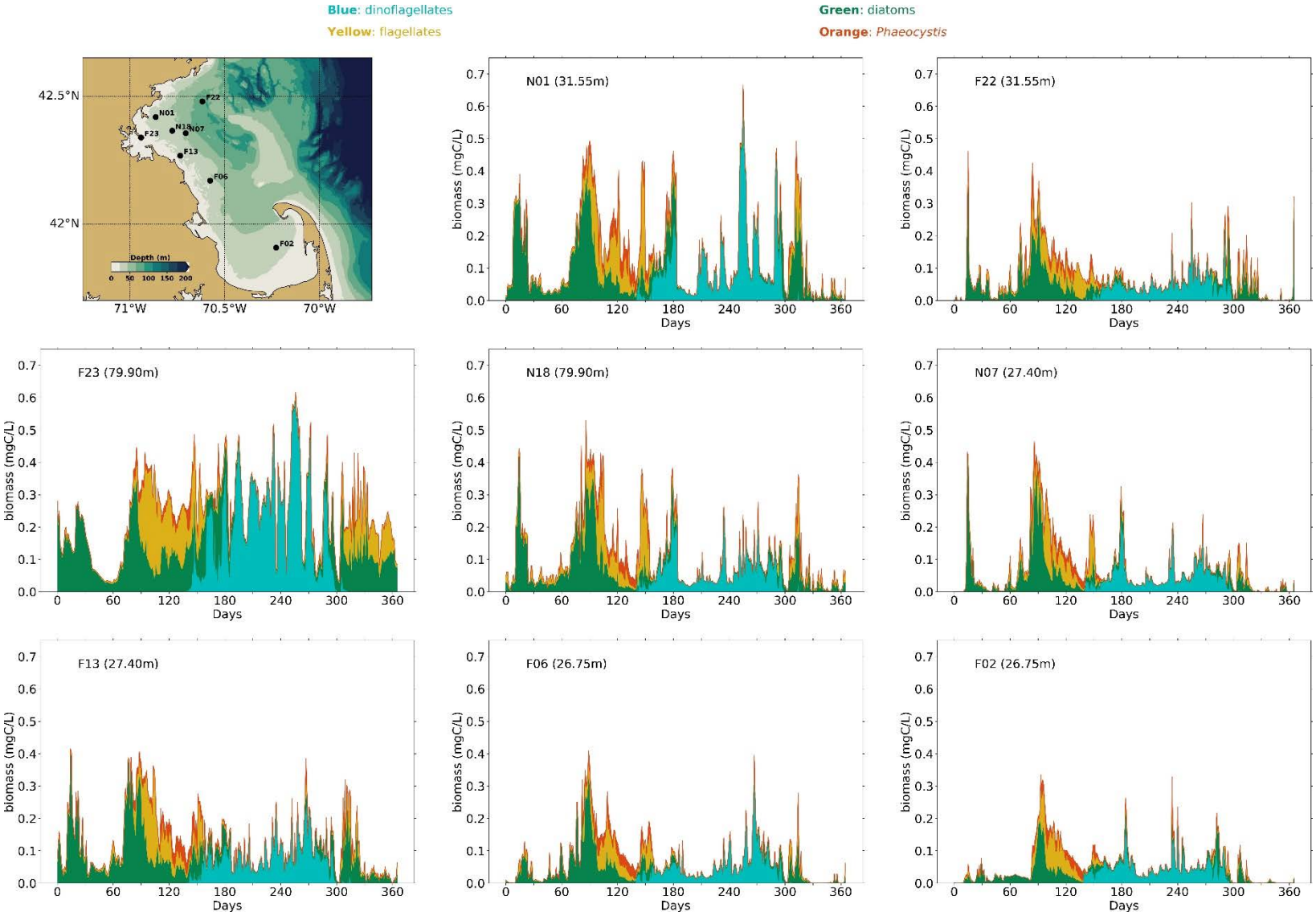

Figure 5-20 Simulated phytoplankton biomass time-series. Biomasses of the 4 simulated species groups (dinoflagellates, other flagellates, diatoms and Phaeocystis) are stacked.

5.4 Conditions on West-East transect through outfall

The signature of the outfall in terms of DIN concentrations was visible all year round, with increased concentrations up to a distance of about 10 km (Figure 5-21). The increased DIN was trapped in the lower layers of the water column in the period of stratification (April/May-October). During the other months, the effluent led to an increase in surface DIN concentrations. These temporal patterns were similar to those observed in previous years.

All year round, chlorophyll a concentrations were higher nearshore (Figure 5-22). This was most likely due to the nutrient inputs from rivers to the harbor area, promoting algal growth. Further offshore, highest chlorophyll a concentrations were simulated in late winter/early spring near the surface. In summer months, maximum chlorophyll a concentrations occurred at a depth of ~15 m, approximately at the edge of the photic depth and consistent with the availability of DIN limited predominantly to the bottom waters under stratified conditions. These patterns were mostly similar to those simulated for previous years. Any effect of the outfall on chlorophyll a concentrations was difficult to detect in the plotted cross section.

The vertical cross-sections of DO concentrations for 2021 showed similar temporal and spatial patterns as for previous years, but slightly shifted in time (Figure 5-23). The highest concentrations occurred near the surface between January and April, similar to 2020. The highest concentrations occurred slightly under the surface between May and July, which corresponded to the depths at which chlorophyll a was the highest. Similar to chlorophyll a, no effect of the outfall on DO concentrations was visible in the plotted cross sections.

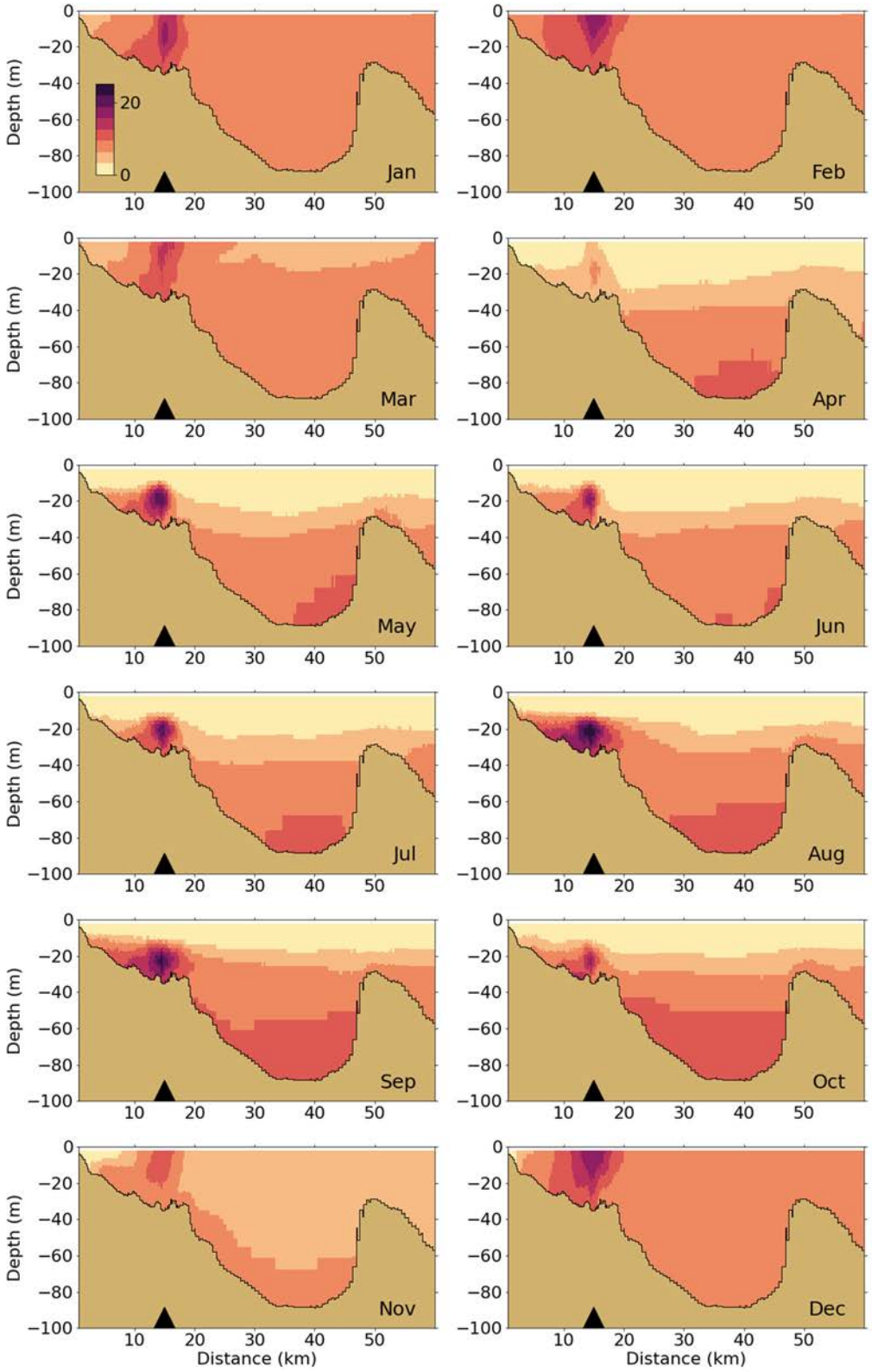

Figure 5-21 Dissolved Inorganic Nitrogen (µM) for 2021 along west-east transect (Figure 2-4). Horizontal axis is distance eastward from coast; black triangle indicates the location of the outfall on the seafloor.

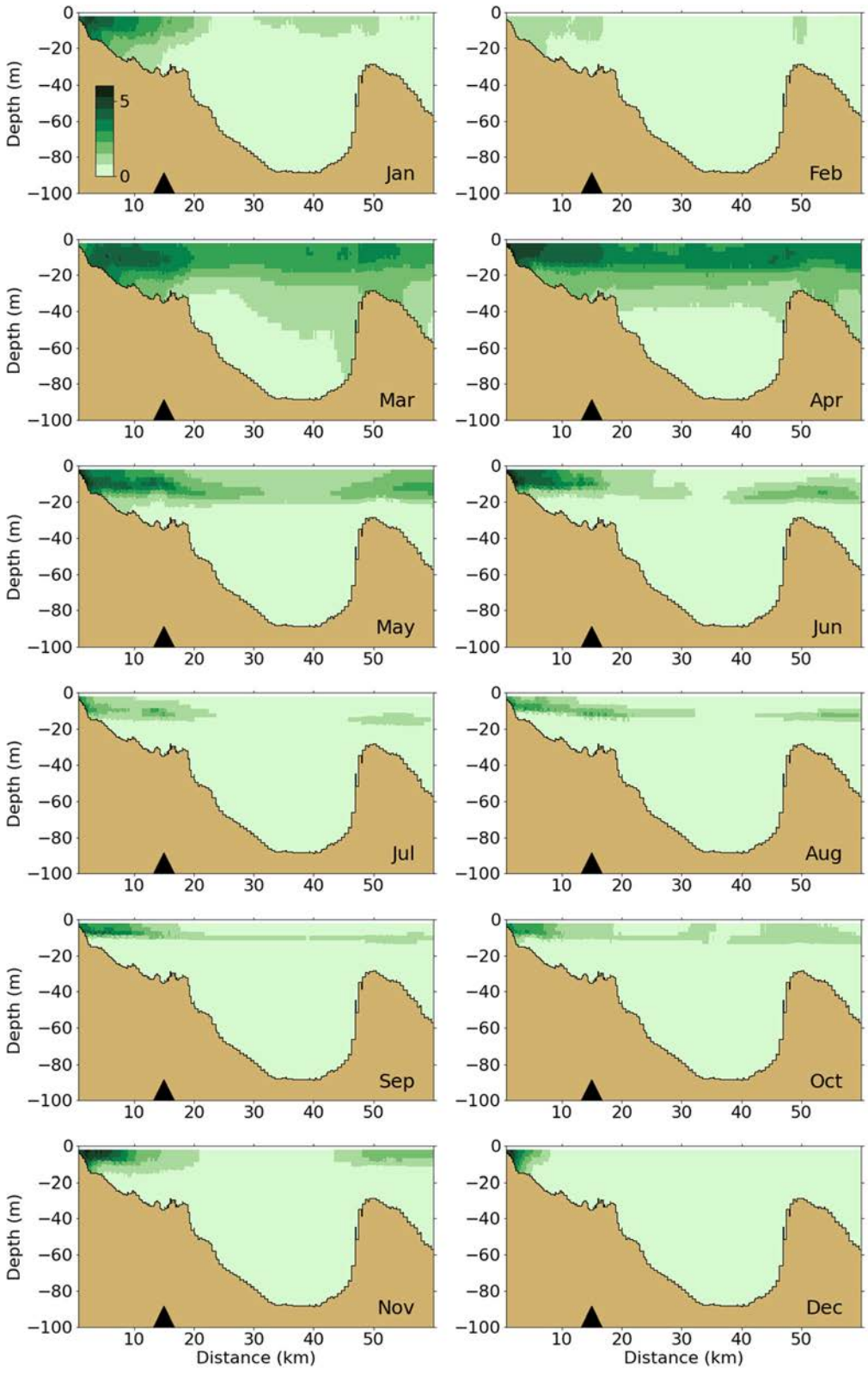

Figure 5-22 Chlorophyll a (µg/L) for 2021 along west-east transect (Figure 2-4). Horizontal axis is distance eastward from coast; black triangle indicates the location of the outfall on the seafloor

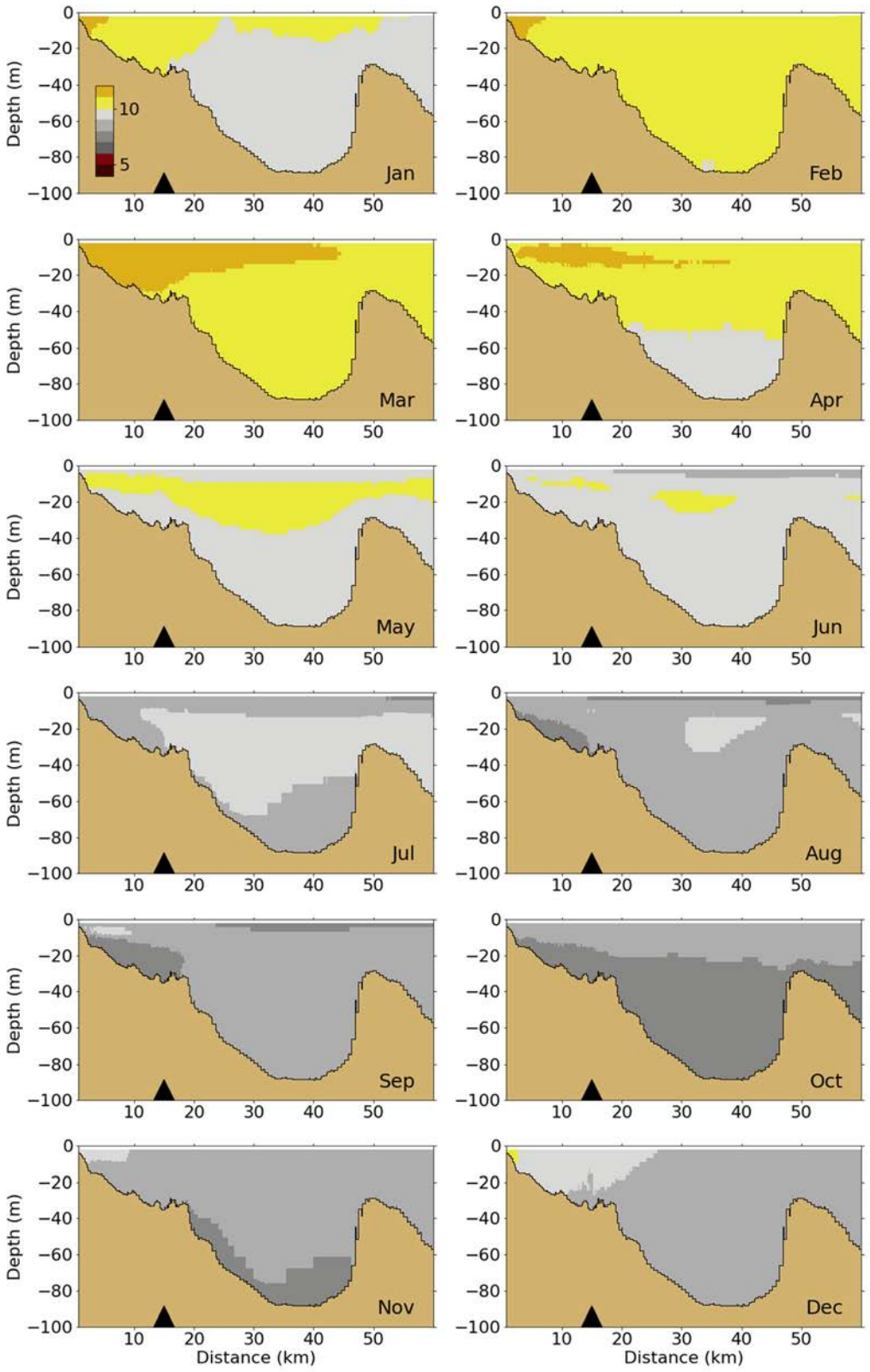

Figure 5-23 Dissolved Oxygen for 2021 along west-east transect (Figure 2-4). Horizontal axis is distance eastward from coast; black triangle indicates the location of the outfall on the seafloor.

6 Synthesis/Application

There are no synthesis/application simulations focused on the year 2021.

7 Conclusion

The performance of the hydrodynamic model was comparable to previous years. Temperatures were reproduced accurately, especially at the surface, even considering that the observed summer surface water temperature warmed to unusually high values in late July and August (Libby et al., 2022). The quality of modeled salinity was comparable to previous years at most stations. At nearshore locations that were influenced by high runoff events in summer 2021, the model overestimated salinities.

At most stations, temperature stratification was present from April until late-October with its maximum in July and August. This is in agreement with the observation of unusually high temperature stratification in July and August compared to previous years. Salinity stratification in summer 2021 was also unusually high due to the low surface salinity in response to the larger river flow (Libby et al., 2022). Salinity stratification during the rest of the year was relatively small compared to previous years, due to the low river flow in winter and spring.

Modeled non-tidal current patterns were similar to observations, but the magnitudes near the surface, and the temporal variability, were slightly smaller. At the bays-wide scale, the expected circulation pattern driven by the Western Maine Coastal Current was visible in the model. In general, the agreement between the hydrodynamic model and the observations was sufficient to conclude that the representation of processes was adequate to support water quality modeling.

In the water quality model, light extinction for the year 2021 was similar to previous years and the model reproduced the extinction range and variability well at most stations. Seasonal variations of surface and bottom DIN concentrations in 2021 were similar to those observed and simulated for previous years. Surface and bottom were comparable in winter, when the water column was well mixed. Surface DIN concentrations declined at the end of winter and were depleted from April to October, before increasing again mid-fall. Bottom concentrations remained stable or declined to a much lesser degree than surface concentrations, in spring and summer. The model generally reproduced these observed seasonal variations and vertical differences throughout the water column.

Seasonal variations of chlorophyll a observations in 2021 were similar to previous years though with a notable *Alexandrium catenella* bloom in late June and July in Massachusetts Bay. The model simulated the higher chlorophyll a peaks at the end of winter and early spring and in late fall, and some smaller peaks in the summer. As for previous years, near surface simulated concentrations were in the same range as observations. Temporal variability was generally reproduced except for the summer peaks when the *Alexandrium catenella* bloom occurred. The latter bloom was captured by the model but corresponding chlorophyll a concentrations were underestimated, due to an underestimation of the phytoplankton biomass and/or of the community's chlorophyll-to-carbon ratio. Simulated chlorophyll a concentrations decreased eastward from the coast. Early spring increases occurred throughout the relatively well-mixed water column. During the more stratified months, simulated bottom chlorophyll a remained low and highest values occurred near surface in the nearshore locations, and at the subsurface at the edge of the photic zone farther offshore where nutrients were depleted near the surface.

Particulate organic carbon (POC) concentrations at the observation stations showed generally higher levels in summer months and were generally consistent with biomass production at the offshore locations. Measured POC concentrations were highest closer to the harbor, likely due to the high river

POC inputs. Concentrations were significantly lower near the bottom than at the surface. The model generally captured these POC concentration ranges, variability and vertical gradients. However, at stations closer to the harbor the model POC concentrations were higher than observed. As for chlorophyll a, simulated POC concentrations decreased from the coast eastward.

The vertical cross-sections of DO concentrations for 2021 showed similar temporal and spatial patterns as for previous years, with the highest concentrations occurring near the surface between January and April. The 2021 seasonal variations of DO concentrations were overall well reproduced in the model, with maximum concentrations observed at the end of winter or early spring and decreasing until fall before rising again. While winter concentrations at the surface and the bottom were comparable, bottom concentrations dropped lower at the end of the summer and beginning of fall. For 2021, the model tended to overestimate summer bottom concentrations. Some of this may be attributed to the fact that the field measurement campaign observed historic minima of DO at many stations by May and some unusually low DO concentrations in deep waters in late summer. The model-observation comparison at intermediate water depths showed similar behavior: in fall, the decrease in DO throughout the water column was slightly underestimated. The North-South and West-East cross-section plots show that DO generally had weak vertical gradients. Concentrations were higher at the end of winter and early spring and decreased until fall. Slightly higher concentrations were observed and simulated in the subsurface, where phytoplankton biomass is located, at the end of spring or early summer. The observed vertical gradients in DO concentrations were well captured by the model.

Although total phytoplankton biomass temporal dynamics differed from station to station, phytoplankton composition showed similar temporal patterns across stations. Diatoms dominated in the winter period and were succeeded in spring by flagellates. Dinoflagellates clearly dominated from June to the end of October. These were typical characteristics of community composition seen in monitoring observations. Simulated *Phaeocystis* biomass in the model showed noticeable levels during the spring flagellate bloom period (April-May), at all stations except for F23, near the harbor. This is similar to the timing of a possible *Phaeocystis* bloom as suggested by observed chlorophyll increases and changes in nutrient concentrations (e.g. nitrogen to silica ratio, Libby et al., 2022).

The signature of the MWRA outfall in terms of DIN concentrations was visible all year round, with increased concentrations up to a distance of about 10 km. The increased DIN concentrations were trapped in the lower layers of the water column during the period of stratification (April/May-October). During the other months, the effluent led to an increase in surface DIN concentrations as well. These temporal patterns were similar to those observed in previous years. All year round, chlorophyll a concentrations were higher nearshore. This was most likely due to the nutrient inputs from rivers to the harbor area, promoting algal growth. In the plotted model results for chlorophyll a, no effect of the outfall on chlorophyll a concentrations can visibly be detected. Any effect of the outfall on chlorophyll a concentrations appears to be limited. Similar to chlorophyll a, based on the presented model outputs, there was no direct apparent effect of the outfall on DO concentrations in the nearshore areas.

References

Alessi, Carol A., Beardsley, Robert C., Limeburner, Richard, Rosenfeld, Leslie K., Lentz, Steven J., Send, Uwe, Winant, Clinton D., Allen, John S., Halliwell, George R., Brown, Wendell S., Irish, James D.,1985. "CODE-2: moored array and large-scale data report", Woods Hole Oceanographic Institution Technical Report 85-35, DOI:10.1575/1912/1641. (https://hdl.handle.net/1912/1641)

Blauw AN, HFJ Los, M Bokhorst and PLA Erftemeijer, 2009. GEM: a Generic Ecological Model for estuaries and coastal waters. Hydrobiologia 618: 175-198.

Deltares, 2019a. D-Flow Flexible Mesh, Technical Reference Manual. Released for: Delft3D FM Suite 2020. Version: 1.1.0 SVN Revision: 63652. December 4, 2019.

Deltares. 2019b. Delft3D Flexible Mesh Suite, D-Flow FM in Delta Shell, User Manual, Version 1.5.0, December 5, 2019 (https://content.oss.deltares.nl/delft3d/manuals/DFlow_FM_User_Manual.pdf)

Deltares, 2021. Demonstration of the updated Bays Eutrophication Model. Boston: Massachusetts Water Resources Authority. Report 2021-02. 138 p. plus appendices. (www.mwra.com/harbor/enquad/pdf/2021-02.pdf)

Deltares, 2022a. Simulations of 2017 Hydrodynamics and Water Quality in the Massachusetts Bay System using the Bays Eutrophication Model. Boston: Massachusetts Water Resources Authority. Report 2021-12. 107 p. https://www.mwra.com/harbor/enquad/pdf/2021-12.pdf

Deltares, 2022b. Simulations of 2020 Hydrodynamics and Water Quality in the Massachusetts Bay System using the Bays Eutrophication Model. Boston: Massachusetts Water Resources Authority. Report 2022-08. 90 p. https://www.mwra.com/harbor/enquad/pdf/2022-08.pdf

Hunt CD, RK Kropp, JJ Fitzpatrick, P Yodzis, and RE Ulanowicz, 1999. A Review of Issues Related to the Development of a Food Web Model for Important Prey of Endangered Species in Massachusetts and Cape Cod Bays. Boston: Massachusetts Water Resources Authority. Report ENQUAD 99-14. 62 p. (http://www.mwra.state.ma.us/harbor/enquad/pdf/1999-14.pdf)

Keay KE, WS Leo, and PS Libby, 2012. Comparisons of Model-Predicted and Measured Productivity in Massachusetts Bay. Boston: Massachusetts Water Resources Authority. Report 2012-03. 11 p. plus Appendix. (http://www.mwra.state.ma.us/harbor/enquad/pdf/2012-03.pdf)

Libby PS, Borkman DG, Geyer WR, Turner JT, Costa AS, Taylor DI, Wang J, Codiga DL. 2022. 2021 Water column monitoring results. Boston: Massachusetts Water Resources Authority. Report 2022-13. 61 p. http://www.mwra.com/harbor/enquad/pdf/2022-13.pdf

Los, FJ, 2009. Eco-hydrodynamic modeling of primary production in coastal waters and lakes using BLOOM. Ph.D. Thesis, Wageningen University, 2009.

Scully, M. E., Geyer, W. R., Borkman, D., Pugh, T. L., Costa, A., and Nichols, O. C.: Unprecedented Summer Hypoxia in Southern Cape Cod Bay: An Ecological Response to Regional Climate Change?, Biogeosciences Discuss. [preprint], https://doi.org/10.5194/bg-2022-48, in review, 2022.

Tucker J, S Kelsey, and AE Giblin, 2010. 2009 benthic nutrient flux annual report. Boston: Massachusetts Water Resources Authority. Report 2010-10. 27 p. (http://www.mwra.state.ma.us/harbor/enquad/pdf/2010-10.pdf)

Xue, P, C Chen, J Qi, RC Beardsley, R Tian, L Zhao, and H Lin, 2014. Mechanism studies of seasonal variability of dissolved oxygen in Mass Bay: A multi-scale FVCOM/UG-RCA application. Journal of Marine Systems. 131, 102-119.

Zhao L, Beardsley RC, Chen C, Codiga DL, Wang L, 2017. Simulations of 2016 Hydrodynamics and Water Quality in the Massachusetts Bay System using the Bays Eutrophication Model. Boston: Massachusetts Water Resources Authority. Report 2017-13. 111p. (https://www.mwra.com/harbor/enquad/pdf/2017-13.pdf)

Massachusetts Water Resources Authority
Deer Island
33 Tafts Avenue • Boston, MA 02128
www.mwra.com
617-242-6000